Synthesis and Characterization of Semiconductor Diamond Films

（半導体ダイヤモンド薄膜の作製とその評価）

1996

Yusuke Mori

森 勇介

Synthesis and Characterization of Semiconductor Diamond Films

（半導体ダイヤモンド薄膜の作製とその評価）

1996

Yusuke Mori

森 勇介

ABSTRACT

Diamond has great potential for device applications, as cold cathode for vacuum electronics and as high-frequency and high-power transistors operating under extreme conditions. With an exiting development of diamond synthesis from vapor phase, diamond films have gained considerable interest in this decade. However, there are a lot of issues, including the high quality film fabrication, doping of diamond and formation of Schottky and ohmic contacts, which have to be investigated and overcome before the diamond devices are a reality. The purpose of the author's work reported in this thesis is to investigate the synthesis of semiconductor diamond films and the metal-diamond interfaces. The following seven chapters institute this thesis.

Chapter 1.

The general introduction of diamond, its applications and the research objectives are described.

Chapter 2.

The crystallinity and electrical properties of homoepitaxial diamond films grown from carbon monoxide have been investigated. The films were grown on high-pressure high-temperature (HPHT) synthesized diamond (100) and (111) substrates by μ-wave plasma chemical vapor deposition (CVD), and were characterized by means of atomic force microscopy, reflection high-energy electron diffraction, cathodoluminescence (CL), secondary electron microscopy and Hall effect measurement. Doping has been performed as growth proceeds by using B_2H_6 for p-type dopant and $(CH_3O)_3P$ for n-type dopant, respectively. The B doping of diamond could realize p-type conductivity with low resistivity of 7.26 Ohm.cm and high mobility of 451 cm/Vsec at room temperature in the case of the homoepiaxial (100) film. On the other hand, P-doped diamond films showed the high resistivity of ~10^7 Ohm.cm.

Chapter 3.

The characteristics of the diamond surface and its graphitization have been investigated mainly by electron energy loss spectroscopy (EELS). No surface states in the band gap has been observed for the as-grown CVD diamond surface. A feature appear in the band gap region of the energy loss spectra after a high vacuum anneal at ~900°C. On the other hand, graphitization of the as-grown diamond surface is found to be induced when annealed at ~900°C under the low vacuum condition. It is also found that the graphitization can be restrained by the CrO_3 surface treatment.

A remarkable ambient effect on the resistance of CVD diamond during cooling after deposition has been observed. The diamond films that were cooled slowly down to room temperature in the 10^{-3} Torr range after deposition showed relatively low resistances in the range of 10^6~10^7 Ohm. On the other hand, high resistances over 10^{13} Ohm were observed for diamond films that were cooled down to room temperature in an oxygen or an air ambient at atmospheric pressure. Among these surfaces a substantial difference was observed in the electronic structure as studied by EELS.

Chapter 4.

The electronic structure formed by submonolayer coverages of Au, Ti and Ni on CVD diamond surfaces has been studied. There is no chemical reaction with the CVD diamond surface even at 850°C in the case of Au films. In contrast, TiC_x formation has been observed at Ti-CVD diamond interface immediately after deposition at room temperature. After Ni deposition on CVD diamond at RT, the electronic structure of the surface changes to carbidic and graphitic phases because of the solvent and catalytic nature of Ni.

Electrical properties of the interface between metal and semiconducting CVD diamond have been investigated. A high breakdown voltage (>200 V) and a high rectification ratio (10^5) are observed at the evaporated Al-diamond interfaces. In the point contact interfaces, where the metal-carbon reaction is not expected at room temperature, the rectifying and ohmic property depends on the electronegativity of metals. The surface oxidation treatments

change the interfacial properties from ohmic to Schottky. Electroluminescence from metal-diamond film interface has been observed for the first time and found to be due to the same luminescence center as that of CL.

Chapter 5.

Radiation damage and electrical properties produced by ion implantation of diamond produced by CVD and HPHT were studied, Electron energy loss spectroscopy and CL were used to investigate implantation damage. New technique was developed to anneal out this damage, a hydrogen plasma treatment. Graphitization of ion-implanted CVD diamond was observed after subsequent thermal annealing under vacuum. However, an EELS spectrum similar to that of as-grown diamond was obtained from ion-implanted CVD diamond after hydrogen plasma treatment. Another substantial advantage of the hydrogen plasma treatment concerns the electrical properties of implanted diamond; the graphitic phase which influences the resistivity was not present in either the CVD or HPHT synthesized diamond.

Chapter 6.

Diffusion of oxygen atoms into diamond can be introduced by CrO_3 treatment followed by an exposure to a hydrogen plasma. From characterization using Rutherford backscattering spectrometry, it is found that the depth distribution of the doped oxygen in the diamond is homogeneous from the surface where its concentration is about 10^{20} atoms/cm^3. The doped oxygen can form CL centers yielding luminescence peaks at 3.75 and 4.64 eV at room temperature. After the diffusion of oxygen atoms, damages in the diamond cannot be detected by Raman scattering spectroscopy.

Clater 7.

The conclusions of the study are duscussed.

ACKNOWLEDGMENTS

I would like to express my sincere gratitude to my supervisor Professor Akio Hiraki for giving me the opportunity to investigate diamond films at Hiraki laboratory, Department of Electrical Engineering, Osaka University, and for his instructive direction, support, encouragement and great assistance both in public and private.

I would like to thank my co-supervisor Professor Takatomo Sasaki for his continued support, encouragement and serving on my reading committee.

I would like to thank Professor Junji Shirafuji for serving on my reading committee and helpful suggestion.

I am greatly indebted to Professor Toshimichi Ito and Dr. Akimitsu Hatta of Hiraki laboratory for their supports, fruitful discussions and helpful suggestions throughout this work. I am also deeply greatful to Professor Hiroshi Kawarada of Wasada University and Dr. Jing Shing Ma of Chemical Abstracts, the former staffs at Hiraki laboratory, for their supports and kind advices.

I wish to express my appreciation to Professors R. Aoki, K. Matsuura, S. Kumagai, K. Tsuji, S. Komaki, E. Kuroda, T. Yamanaka, Y. Kato and H. Nakashima of Osaka University for their kindness, guidance and advice.

I would like to thank Emeritus Professor K. Ogino of Osaka University and his group members for the instruction of AFM and useful discussion.

I would like to thank Professor T. Sugino, Dr. R. Hattori and group members of Shirafuji laboratory for fabrication of Ti electrode on homoepitaxial diamond films and kind suggestion.

Many thanks are given to Professor T. Izumi and Mr. Y. Show of Tokai University for ESR measurement and helpful discussion.

I would like to thank Dr. K. Nishimura of Kitakyusyu Politechnic College for supplying HPHT synthesized diamond substrates, useful research support and discussion.

I would like to thank Dr. T. Hirao at Matsushita Technoresearch Inc., and Dr. M. Kitabatake and Dr. M. Deguchi at Matsushita Electric Industrial Co., Ltd. for collaboration in the ion implantation research presented in this dissertation. I could not have achieved this work without their help.

I would like to thank Dr. H. Ohnishi and Mr. T. Sogi at Osaka Gas Co., Ltd. for their kind cooperation concerning the measurement of Hall effect of boron-doped and ion-implanted homoepitaxial diamond films. I learned immensely from a collaboration with them.

I would like to thank Mr. M. Yuasa at Sekisui Chemical Co., Ltd. for the instructions of XPS and FT-IR, and also for useful suggestion and companionship.

Many thanks are given to my former co-workers Dr. Y. Yokota, Dr. J. Wei, Dr. T. Yara, Mr. O. Arakaki and Dr. J. Moon, who have graduated Hiraki laboratory, for their kindness, efficient cooperation, helpful discussion and support. I would also like to thank present co-workers Messrs. H. Yagyu, N. Eimori, H. Yagi and K. Bekku at Hiraki laboratory for their efficient cooperation, kind help, and fruitful discussion.

I would like to thank visiting scientist at Hiraki laboratory, Dr. J. Suzuki at Shimadzu Co., Ltd., Messrs. A. Tomiyama at Kyocera Co., Ltd., H. Matsuyama at Fuji Electric Co., Ltd. and K. Mishyuku at Gunze Co., Ltd. and Mrs. F. R. Sivazlian from North Carolina State University, Dr. J. G. Lee at Samsung Electronics Co., Ltd. and Dr. M. Marinelli of the II

University of Rome for their cooperations and helpful discussions in this work.

It is my pleasure to express my deep gratitude to the secretaries Miss. K. Kasukawa at Hiraki laboratory and Mrs. H. Shirai at Sasaki laboratory, and all the members of Hiraki laboratory and Sasaki laboratory for their support and kindness.

I would like to thank Sumitomo Electric Industries, Ltd., Kobe Steel Co., Ltd. and Idemitsu Petrochemical Inc. for their great support and kind help for this work.

Finally, I thank my father Yuzo and my mother Fusa and my wife Satoko and my daughter Midori and my brother Eisuke and my sister Mika for their support and advice. They have cheered me up constantly. This gratitude can never be expressed.

TABLE OF CONTENTS

LIST OF TABLES

LIST OF FIGURES

Ch. 1. INTRODUCTION

Ch. 2. GROWTH OF DIAMOND FILMS

1. INTRODUCTION

1.1 Properties and Applications of Diamond

Diamond has been well known from ancient times. The long-established and the most important use of natural diamonds has been for gemstones. Diamond is the hardest material and this has made it pre-eminent as abrasives and cutting tools. Then various unique properties of diamond other than hardness have been pointed out up to date. The value of characteristics property associated with diamond is almost always represent an extremist position among all materials considered for that property. Table 1.1-1 provides a listing of the material properties that render diamond so useful across many fields of science and technology. The hardest material and the premier thermal conductor at room temperature, diamond resists heat, acid and radiation, is a good electrical insulator but can be doped to form p-type semiconductor, and has the highest figure of merit for power semiconductor applications. Additionally, the wide gap, 5.45 eV, should make diamond an attractive material for optoelectronic from blue to ultraviolet light region. The one of the most interesting electronic application of diamond is considered to be a cold cathode by virtue of its negative electron affinity.

1.2 History of Synthesized Diamond

Though long recognized, most of the superior properties of diamond mentioned above have remained largely unexploited because natural diamond did not exist in a form suitable for many applications.

I. Newton was the first to determine diamond to be of organic origin, then A. L. Lavoisier was the first to determine that its product of combustion was carbon dioxide. W. H. Bragg and W. L. Bragg have determined that carbon allotropies were diamond, graphite and amorphous. With this information, C. Cagniard, J. B. Henney and H. Moisson have begun to try to synthesize diamond. Unfortunately, the results of their works are disputed to this day. In 1955, first man-made diamond by a high-pressure, high-temperature (HPHT) processes was reported by General Electric. The successful HPHT synthesized diamond, however,

resulted in products no better than those available with natural diamond and could be used only as a replacement for uses already established for natural diamond.

The new vision of diamond derives from the success of chemical vapor deposition (CVD) of diamond, which can remove the limitations in size and control of properties which restricted the use of diamond to a few specialized applications. The vapor-phase synthesis of diamond has facilitated serious interest in the development of diamond applications for mechanical and optical coatings, heat sink, tools and electronic devices.

1.3 Objective of This Work

The synthesis of diamond under vapor phase has made great progress. The serious two problems, however, still remain to achieve semiconductor devices in diamond. Although the process allows diamond films to be laid down over large area, single-crystalline diamond films on non-diamond substrates has not been obtained. There is a substantial difficulty in doping of diamond. Boron doping gives rise to p-type semiconductivity with sufficiently low resistivity. In the case of n-type doping, however, the resistivity of diamond is too high to be the practical use.

The author has aimed to develop semiconductor diamond films. There are two main objectives in this work. The first objective is to investigate the synthesis semiconductor diamond films because doping capability is critical to achieve semiconductor devices in diamond. The author has grown diamond films on both HPHT synthesized diamond and Si substrates and has employed various methods to dope diamond films. In deposited diamond, doping was performed as growth proceeds by using B_2H_6 for p-type dopant and $(CH_3O)_3P$ for n-type dopant, respectively. Ion implantation was attempted as a means of forcing the desired impurities into the diamond in which the solubility of the most elements are extremely small. Since process of the annealing out the implantation damage and the dopant activation in diamond are complicated and difficult compared with Si, the author developed a hydrogen plasma treatment instead of commonly used thermal annealing method. Concerning impurity diffusion process, the author found that hydrogen plasma can enhance oxygen diffusion in

diamond despite the extremely low diffusivity of most elements in diamond.

The second objective is to investigate and control the diamond surface and the metal-diamond interface. Although diamond surface is chemically inert, diamond surface tends to reconstruct to graphite phase. Additionally, diamond CVD differs from other crystal growth processes in that the bulk material deposited is a metastable phase of carbon, so that other phases of carbon, which may affect electrical property, can grow and can result from breaking off the grown diamond during deposition. Therefore, the investigation of diamond surface is important to obtain ideal surfaces. The surface of as-grown CVD diamond formed from CO has been shown to be hydrogen-terminated and there were no surface states in the band gap. The surface graphitization were investigated and the surface treatment was found to restrain the graphitization. The author found a remarkable ambient effect on the resistance of CVD diamond during cooling after deposition. Insulating CVD diamond film, which, by analogy to SiO_2 in Si device technology, is important for fabrication of diamond-based electronic devices, could be obtained by cooling in an oxygen ambient after deposition. Formation and control of metal-diamond interfaces are one of the most important subjects in order to realize semiconductor devices in diamond because of the inability to obtain practical n-type diamond at present. Investigation of the initial stage of metal-CVD diamond interface formations by using Au, Ti and Ni was carried out and revealed the difference in reaction between the CVD diamond surface with Au, Ti and Ni. It was found that Ti is the most available element for the stable electrode due to the formation of a stable TiC_x layer. The properties of metal-diamond interfaces was investigated in order to fabricate Schottky and ohmic contacts. It was shown that the interfacial properties depend on the electronegativity of the contact metal and the surface treatment affects the properties. Electroluminescence due to the Schottky diode was obtained at metal-diamond interfaces in the boron-doped polycrystalline diamond.

1.4 Reference

Synthetic Diamond, Edited by K.E.Spear and J.P.Dismukes, John Wiley & Sons, Inc. 1994.

Table 1.1-1. Properties of diamond

Property	Value	Units
Hardness	1.0×10^4	kg/mm^2
Strength, tensile	>1.2	GPa
Strength, compressive	>110	GPa
Coefficient of friction (Dynamic)	0.03	
Sound velocity	1.8×10^4	m/s
Density	3.52	g/cm^3
Young's modulus	1.22	GPa
Poisson's ratio	0.2	
Thermal expansion coefficient	1.1×10^{-6}	K^{-1}
Thermal conductivity	20.0	W/cm-K
Thermal shock parameter	3.0×10^8	W/m
Debye temperature	2200	K
Optical index of refraction (at 591 nm)	2.41	
Optical transmissivity (from nm to far IR)	225	
Loss tangent at 40 Hz	6.0×10^{-4}	
Dielectric constant	5.7	
Dielectric strength	1.0×10^7	V/cm
Electron mobility	2200	$cm^2/V\text{-}s$
Hole mobility	1600	$cm^2/V\text{-}s$
Electron saturated velocity	2.7×10^7	cm/s
Hole saturated velocity	1.0×10^7	cm/s
Work function	Negative	On [111] surface
Bandgap	5.45	eV
Resistivity	10^{13}–10^{16}	Ω-cm

2. GROWTH OF DIAMOND FILMS

2.1 Introduction

The growth of pure diamond films from the vapor phase on both diamond and nondiamond substrates at practical rates has been accomplished with the development of thermal- and plasma-enhanced chemical vapor deposition (CVD) methods, in which a hydrocarbon gas mixed at low concentrations with H_2 is energized thermally or in a plasma prior to contact with a heated substrate [1]. The selective deposition of diamond from carbon containing species in the presence of atomic hydrogen is based on the realization that diamond is more stable toward atomic hydrogen than graphite. The roles of atomic hydrogen are considered to be that atomic hydrogen can etch graphite selectively, and hydrogen in reaction with carbon induces sp^3-configuration preventing the surface reconstruction into graphitic sp^2 or carbynic sp structures [2].

The first of enhanced CVD methods was the chemical transport reaction synthesis [1]. Then the developments have been done on the variety of methods including hot filament CVD [3], electron-assisted CVD [4], laser-assisted CVD [5], RF-plasma CVD [6], μ-wave plasma CVD [7] and magnet-active plasma CVD [8]. Among these methods, μ-wave plasma CVD methods have been used much more extensively for the growth of diamond films because μ-wave deposition, being a electrodeless process, avoids contamination of the films due to electrode erosion. The μ-wave discharge at 2.45 GHz, being a higher frequency process than the RF discharges at 13.5 MHz, can product higher plasma density with high energy electrons, resulting in higher concentrations of atomic hydrogen and hydrocarbon radicals. A schematic of a deposition system the author has used is shown in Figure 2.1-1 and typical deposition parameters employed for the growth of diamond films are shown in Table 2.1-1.

Diamond films can be grown from a variety of carbon-containing species, such as methane and alcohol, mixed in certain concentrations with other reactive and inert gases. In the author's laboratory, carbon monoxide (CO) has been employed as a reaction gas instead

Table 2.2-1. Typical growth condition of CVD diamond

reaction gas	dopant gas	temprerature	pressure	growth period
5~40% CO in H_2 0.5~2% CH_4 in H_2	B_2H_6 $(CH_3O)_3P$	850~900°C	25~35 Torr	2~8 hours

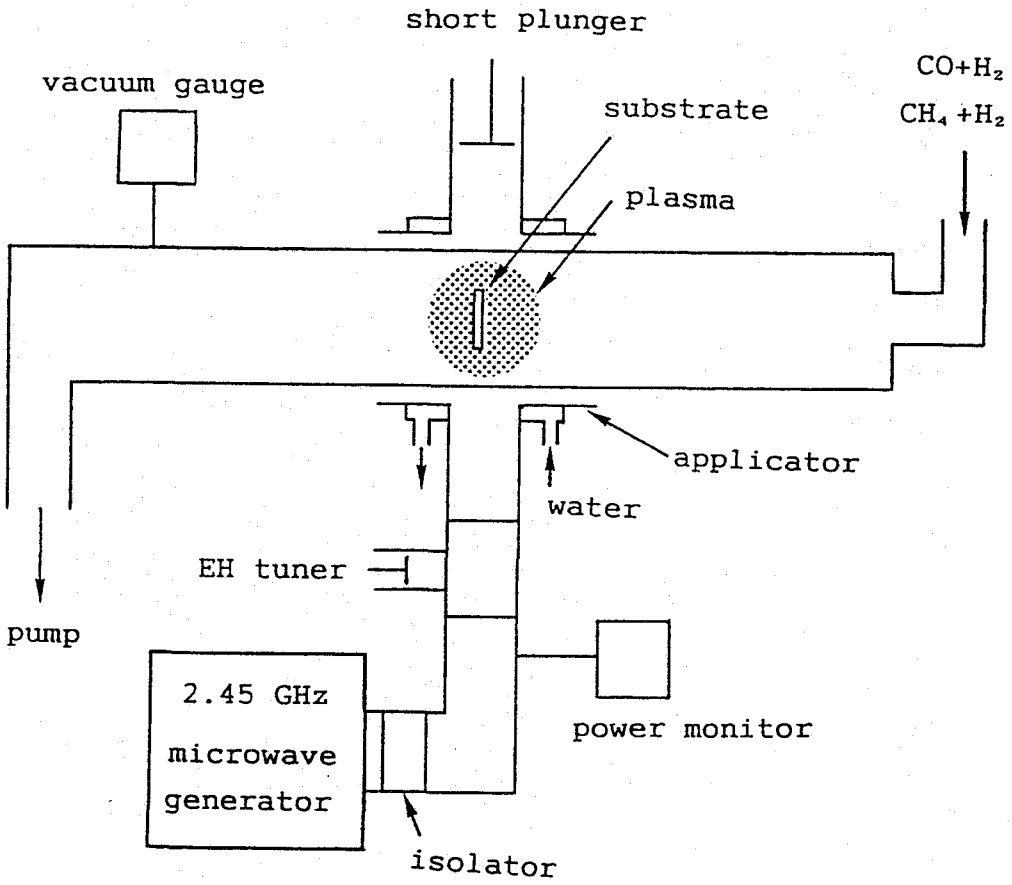

Figure 2.1-1. Schematic illustration of μ-wave plasma CVD apparatus used for the diamond growth.

of commonly used methane because the presence of oxygen can improve the quality and sometimes the growth rate of CVD diamond films [9]. The role of oxygen in diamond deposition is to act as a strong etchant of nondiamond carbon. It should be pointed out that there is a dependence of the effect of oxygen on the reaction gases. The added oxygen atoms etches diamond strongly in the $CH_4 + O_2$ case and no diamond can grow for higher oxygen concentration. Therefore, difficulty in controlling the growth rate and film quality of diamond remains for case of the oxygen addition in $CH_4 + H_2$ plasma, whereas it is relatively easy to obtain high quality diamond from CO/H_2 system. The author believes that CO is one of the most suitable reaction gas for CVD diamond growth.

In this chapter, the growth of homoepitaxial diamond films from CO by using μ-wave plasma CVD method and their characterization have been investigated. Electrical properties of B- and P-doped CVD diamonds are also reported.

2.2 Homoepitaxy of Diamond Films

Much effort has been focused on fabrication of single-crystal thin films over large areas in order to utilize diamond's exceptional electronic properties. Although heteroepitaxial growth of diamond has been reported on cubic-boron nitride (cBN) [10], it is presently extremely difficult to grow cBN in large single-crystal form. Therefore, studies of homoepitaxial diamond films are of the most interest for optical and electronic device applications and also promise to be useful in improving the basic understanding of diamond growth mechanism. Diamond homoepitaxy has been achieved using methane, acetone and acetylene via various CVD methods up to date [11-13]. It has been reported that the morphology of homoepitaxial films depends on the growth condition, such as methane concentration versus hydrogen concentration, and substrate orientations [14-16]. There have also been some suggestions as to the diamond growth mechanism in reference to observed morphologies [11,15,16]. Most growth mechanisms reported concern only the chemical reaction between carbon and hydrogen, although oxygen can have a marked influence on the deposition process [9]. Recent C-H-O phase diagram has indicated that the CO/H_2 system can help in developing new models of the

surface processes and growth species needed for diamond deposition [17]. Therefore, studies of homoepitaxial diamond growth from the CO/H_2 system have become important for understanding the diamond growth mechanism.

In this section, the author has characterized the (100)- and (111)-oriented homoepitaxial diamond films grown from CO in H_2. The differences in the crystallinity among the substrate orientations and growth mechanisms are reported.

2.2.1 Growth and Characterization of Homoepitaxial Diamond Films

Homoepitaxial diamond films have been grown on high-pressure high-temperature (HPHT) synthesized diamond (100) and (111) substrates, 3 x 3 x 1 mm^3 in dimensions, by means of microwave plasma CVD. The process parameters used were as follows: 2.45 GHz, 200 W microwave source, 900°C substrate temperature (as determined by an optical pyrometer), 30 Torr pressure, 5~40 % CO in H_2, and 100 sccm gas flow. A dilute B_2H_6 gas was used to synthesize semiconducting diamond to prevent charging of the specimens during electron microscopy measurements.

The morphologies of the films grown on the (111)- and (100)-oriented substrates exhibited significant differences. SEM images of diamond films grown for 2 hours on (111)- and (100)-oriented substrates are shown in Figures 2.2.1-1~3. The (111) films shown in Figures. 2.2.1-1 (a)-(c) were grown from 5%, 10% and 20% CO in H_2 at substrate temperature of 900°C, respectively. In the 5 and 10% cases, clear triangular microstructures textured with (111) faces parallel to the (111) substrate indicated a multinucleation homoepitaxial growth. On the other hand, the (100) films grown at substrate temperature of 900°C shown in Figures 2.2.1-2 (a)-(d) are very smooth and show little difference in morphology for various carbon ratios. Although these (100) films also show the growth steps and square microstructures textured with (100) faces as shown in Figure 2.2.1-3, the square patterns on the (100) film are ten times larger and appeared much less frequently than the triangular patterns on the (111) film. This indicates single-nucleation homoepitaxial growth of the (100) surface. A (2 x 1) reconstruction appeared clearly on the RHEED pattern for the (100) surface as shown in

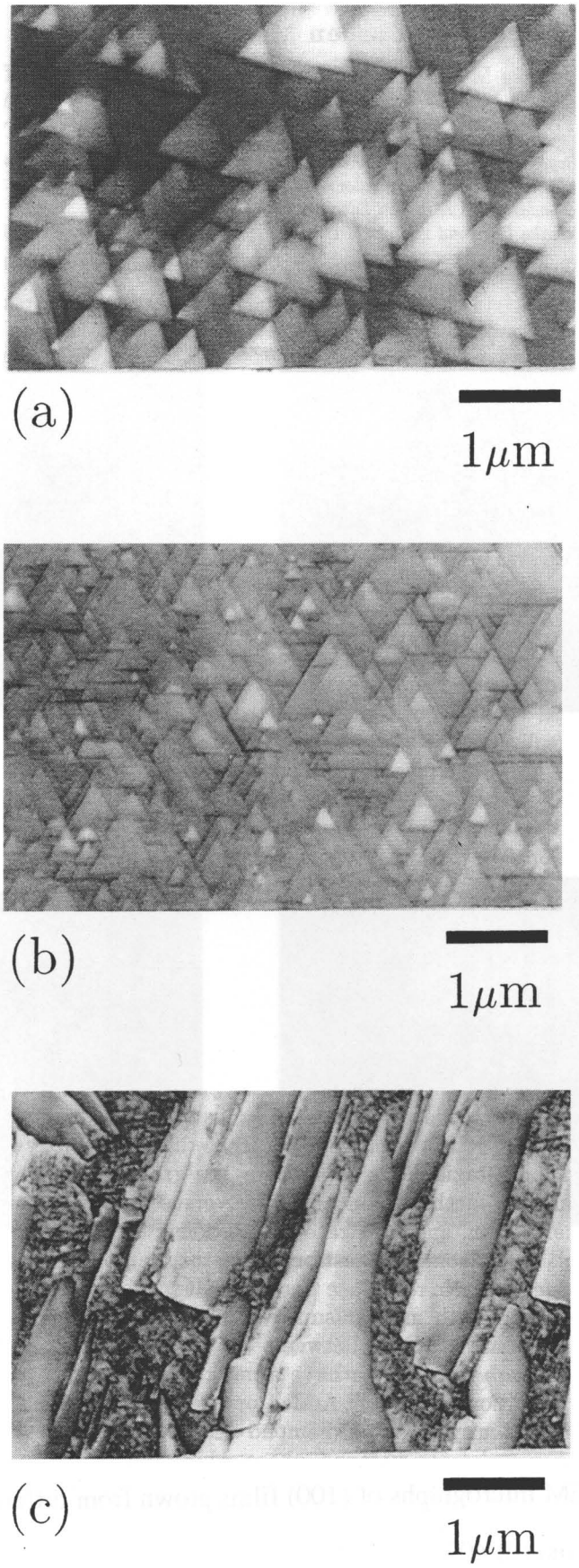

Figure 2.2.1-1. SEM micrographs of (111) films grown from different CO/H_2 ratios. (a) 5%, (b) 10% and (c) 20%.

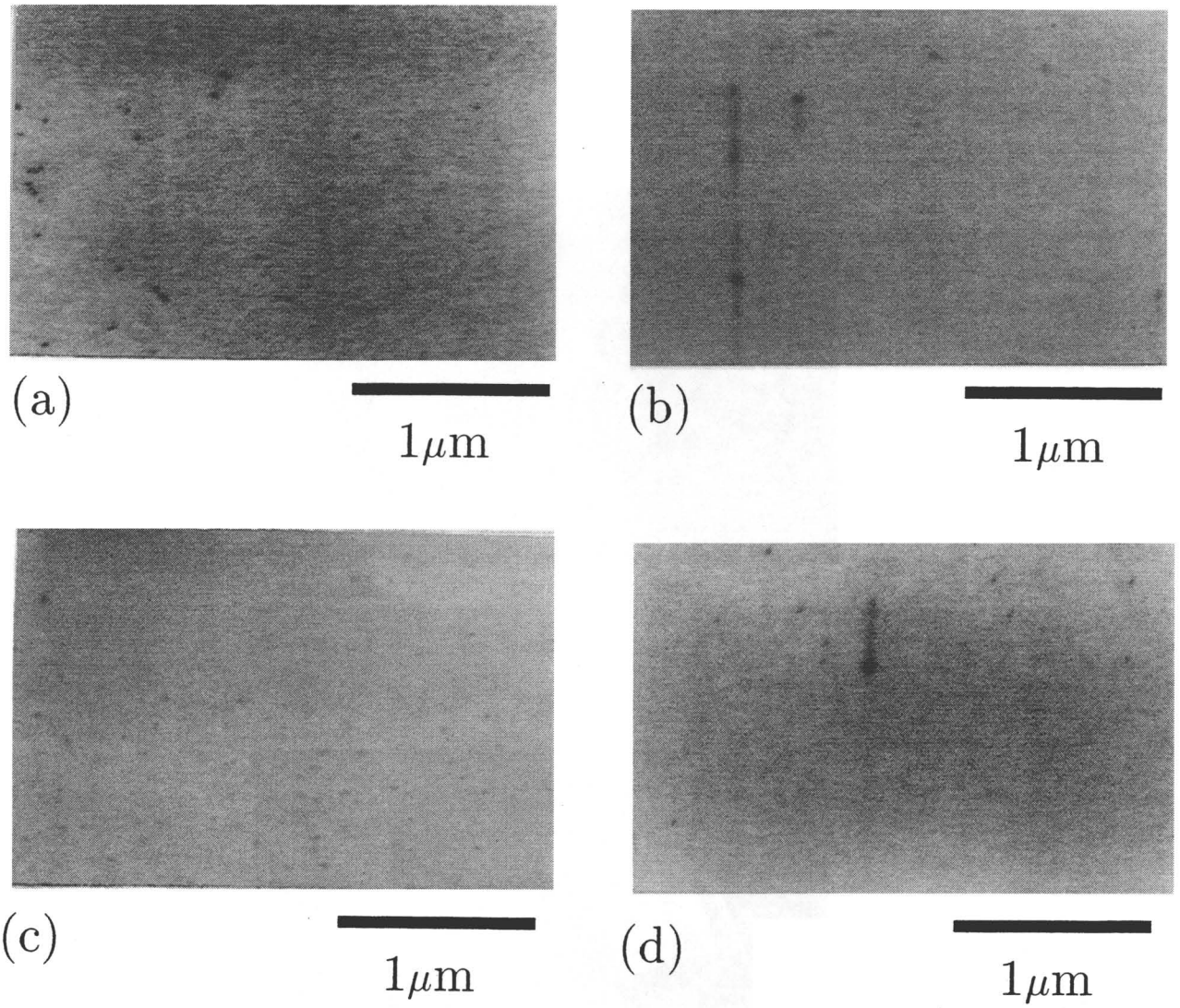

Figure 2.2.1-2. SEM micrographs of (100) films grown from different CO/H_2 ratios. (a) 5%, (b) 10%, (c) 20% and (d) 40%.

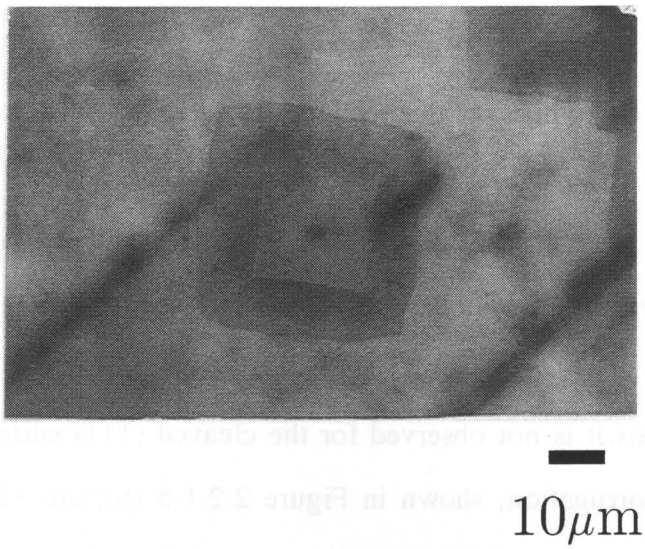

Figure 2.2.1-3. SEM micrograph of the (100) film grown with 5% CO.

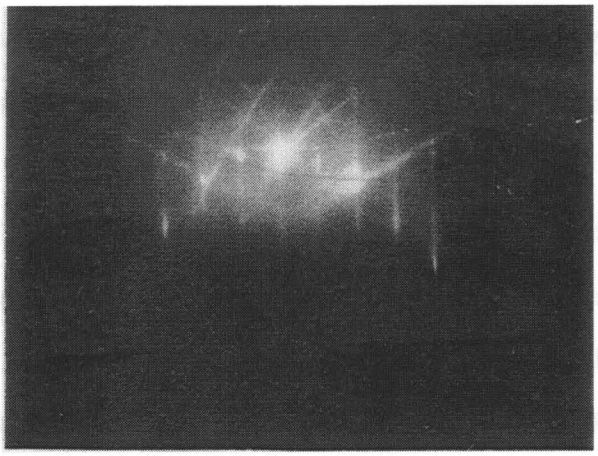

Figure 2.2.1-4. RHEED pattern of the (100) 2 x 1 surface with [110] incidence, grown with 5% CO. Accelerating voltage is 20 keV.

Figure 2.2.1-4. The clear streaks provide direct support for single-nucleation homoepitaxy. On the other hand, the RHEED pattern for the (111) surface showed spots. This indicates that the (111) surface was rougher, compared with the (100) surface, due to multinucleation homoepitaxy.

The atomic-level smoothness of diamond film surfaces is critical to electronic, optical, and tribological applications, and AFM is more suited for characterization of homoepitaxial films on the nanometer scale than SEM is. Figures 2.2.1-5 (a) and (b) show AFM images of the (111) and (100) substrates used in the present study. Scan areas are 800 nm x 800 nm for both pictures. A large surface corrugation amplitude is clearly visible for the highly polished (100) substrate, whereas it is not observed for the cleaved (111) surface. The width and height of individual corrugation, shown in Figure 2.2.1-5 (b), are ~20 nm and ~3 nm, respectively. Obviously, a fine polishing treatment caused these ridges on the (100) surface. Figures 2.2.1-6 (a) and (b) show AFM images of the (111) and (100) films grown from 10% CO in H_2 at substrate temperature of 900°C. Scan areas are 200 nm x 200 nm for both pictures. On the nanometer scale the (111) film in Figure 2.2.1-6 (a) is extremely rough and covered with hillocks due to the multinucleation growth as mentioned above. The hillocks are typically 50-100 nm wide and 10-20 nm high. The (100) film shown in Figure 2.2.1-6 (b), by contrast, is extremely flat among these AFM images. This suggests that diamond growth on the (100) surface occurs predominantly at steps, ledges or kinks, leading to layer-by-layer growth.

Cathodoluminescence spectroscopy is a powerful technique for characterizing the defects present in diamond. Figure 2.2.1-7 shows typical CL spectra acquired from homoepitaxial diamond films: (a) 5 % CO in H_2 on (111) substrate; (b) 5 % CO in H_2 on (100) substrate; (c) 20 % CO in H_2 on (100) substrate. The vertical scale of each spectrum in Figure 2.2.1-7 was adjusted to best display the spectral features; hence they were not scaled uniformly. Band A, which is the most commonly observed CL emission from natural and CVD diamond [18,19], with a peak around 425 nm was observed in spectra (a) and (b). Although the origin of this center remains unclear at present, it seems to be dislocations or

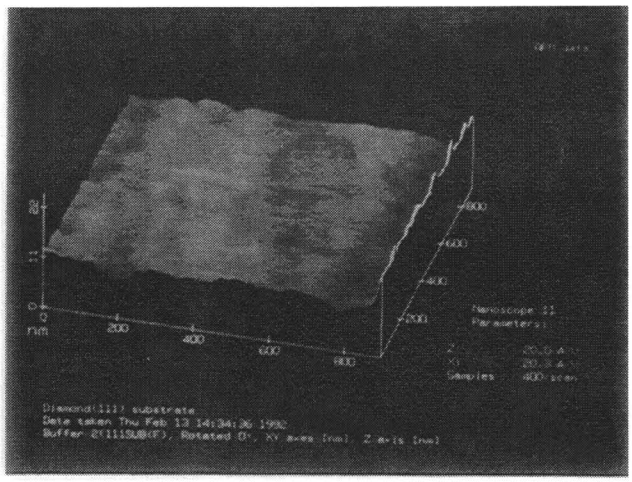

(a)

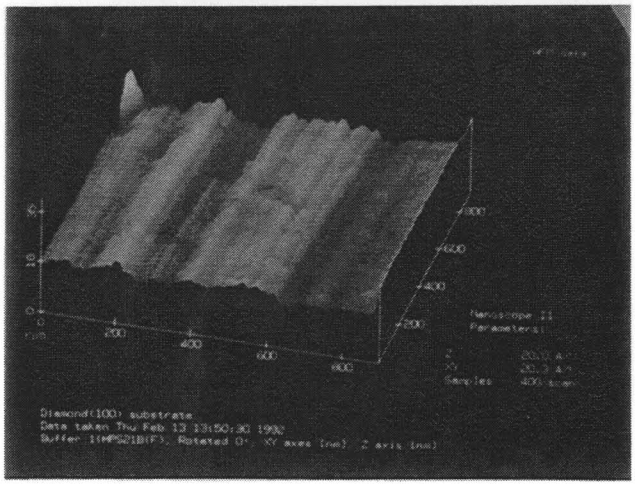

(b)

Figure 2.2.1-5. AFM images of HPS diamond substrates: (a) cleaved (111); (b) polished (100). Z = 20.0 A/V, XY = 20.3 A/V. Scan area = 800 x 800 nm

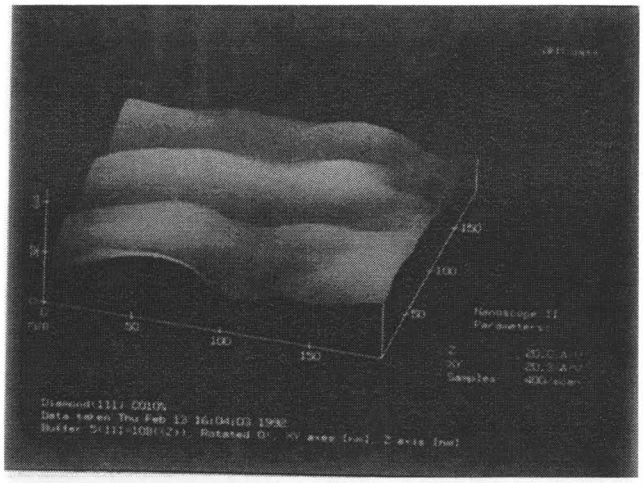

(a)

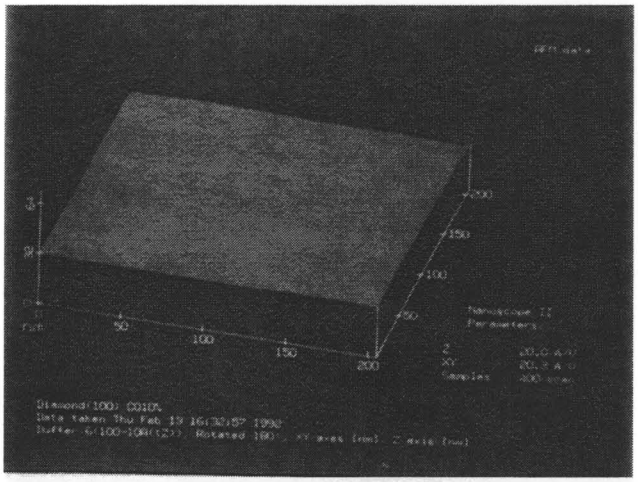

(b)

Figure 2.2.1-6. AFM images of homoepitaxial diamond films grown with 5% CO on (a) (111) and (b) (100) HPS diamond substrates.Z = 20.0 A/V, XY = 20.3 A/V. Scan area = 200 x 200 nm

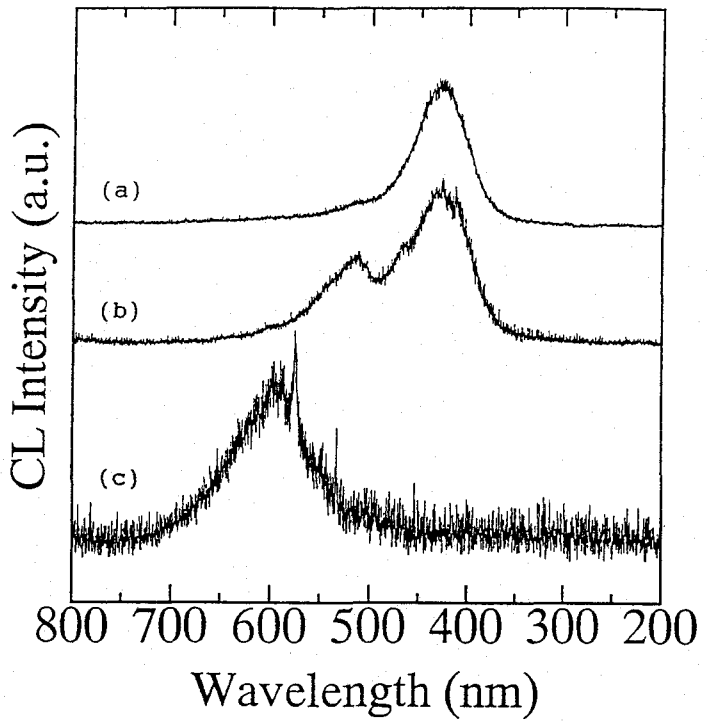

Figure 2.2.1-7. CL spectra of diamond films grown from different CO/H_2 ratios: (a) 5% CO on (111) substrate; (b) 5% CO on (100) substrate; (c) 20% on (100) substrate.

donor-acceptor pair recombinations [18,20]. The 510 nm peak in spectrum (b) is from HPHT synthesized diamond substrate [18]. It is curious that the (100) film grown from 20 % CO in H_2 shows the 575 nm system as shown in spectrum (c), whereas the (111) film grown from 20 % CO in H_2 does not. Following radiation damage and annealing, most diamonds exhibit some CL in a system with a zero-phonon line at 575 nm, and this optical center has concluded that it is comprised of a single nitrogen atom and a vacancy [18]. The 575 nm center has been reported in epitaxial films grown on (131) and (141) [21]. In contrast to the epitaxial films grown from 20% CO in H_2, we have observed the 575 nm in the {111} growth sectors of the CVD diamond particles after neutron irradiation followed by subsequent annealing, whereas not in the {100} growth sectors [22]. The reason of this difference is not clarified at present. Besides the defect structure in [111] growth, the strong band A emission appeared in the present (111) films, whereas the 575 nm system could not be observed. This indicates that defects formed in [111] growth seem to concern dislocations, and that there is a correlation of defect formation with growth mechanism.

Additionally, the CL study can make a rough estimate of thickness of epitaxial films, because the CL substrate signal of HPHT synthesized diamond is distinguishable from the CVD diamond signal. The penetration depth D (μm) of an electron whose incident energy is E (keV) can be written to a 0.1 μm accuracy

$$D = 0.018 \times E^{1.825} \qquad (1)$$

for $5 < E < 70$ keV [23]. CL spectra from the HPHT synthesized substrate and the (111) films for 2 hours growth of various carbon ratios are shown in Figures 2.2.1-8. The 510 nm peak is from HPHT synthesized diamond, and the 425 nm peak is from CVD diamond. The thickness of CVD diamond was estimated roughly by comparing these two intensities using equation (1). About 2 micron has been estimated for the 10% case. The dependence of relative growth rate on CO fraction on (111) and (100) substrate orientations is shown in Figure 2.2.1-9. The growth rate on (111) substrate is about one order of magnitude greater than that on (100) substrate. The ratio of [111] and [100] growth rates is much larger than the value of 1 ~1.3 reported for the diamond grown from CH_4 by hot-filament CVD [24]. This

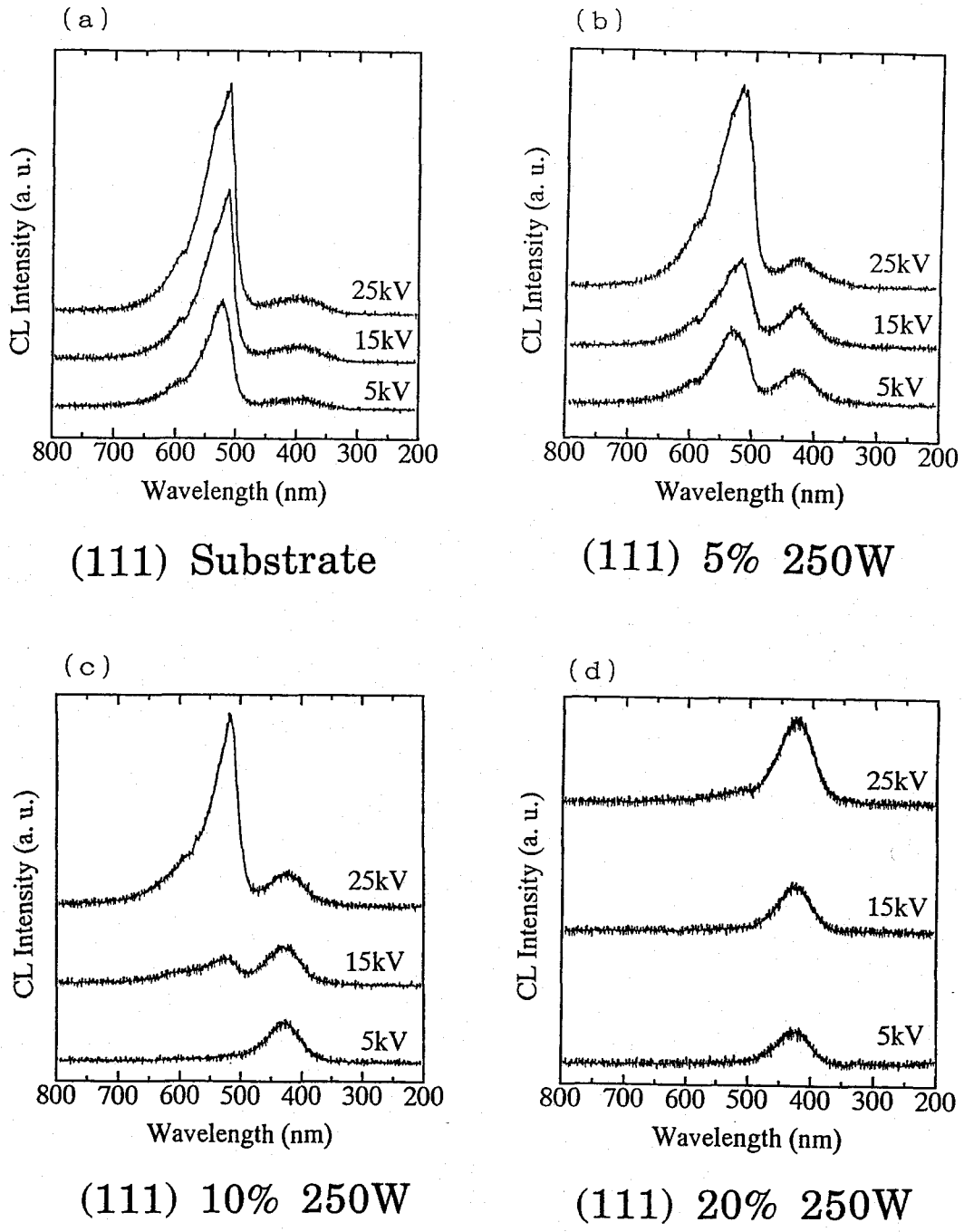

Figure 2.2.1-8. CL spectra of HPHT synthesized and (111)-oriented homoepitaxial diamond films grown with different carbon ratios, obtained at electron-beam energies of 5, 15 and 25 eV: (a) HPS diamond; (b) 5% CO; (c) 10% CO; (d) 20% CO.

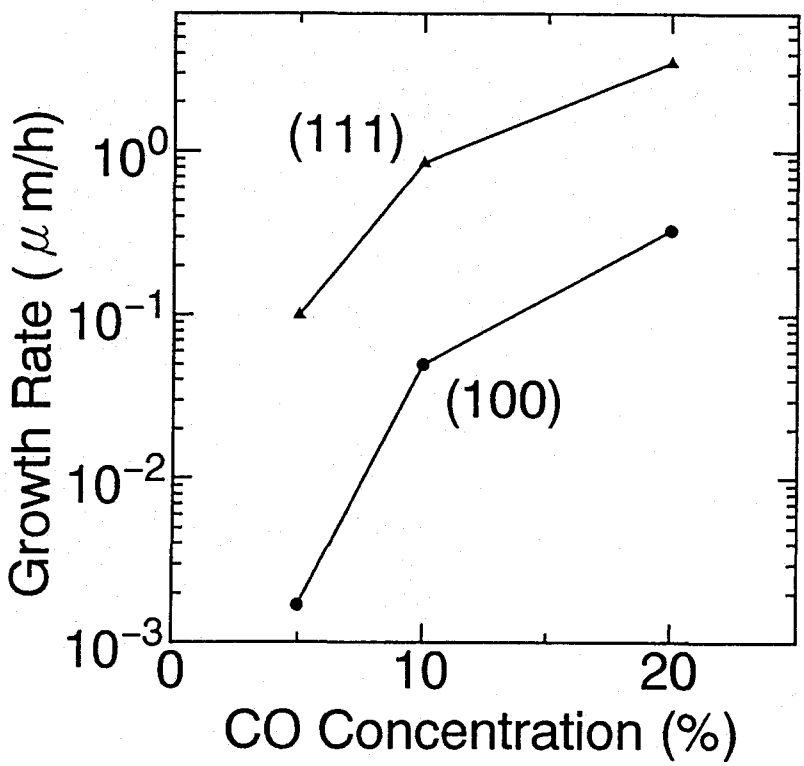

Figure 2.2.1-9. Dependence of homoepitaxial growth rate on CO mole fraction at a substrate temperature of 900°C for growth on (111) and (100) orientations.

result implies that oxygen affect the surface reaction mechanism and the effect of oxygen on the diamond growth is different for substrate orientations.

2.3 Doping of Diamond Films

Diamond has very attractive basic properties as an advanced electronic material. Doping capability is critical to achieve semiconductor devices in diamond. In deposited diamond, doping can be performed as growth proceeds and this may be the most practical method for doping of diamond at present. Because of the low diffusivity of most elements in diamond, conventional diffusion processing is not practical (see chapter 6). Although ion implantation can achieve active doping (see chapter 5), process of the annealing out the implantation damage and the dopant activation in diamond are complicated and difficult compared with Si and GaAs. A wide variety of dopants, reaction gases and methods of incorporation have been investigated, for example B_2H_6 in CH_4 by μ-wave plasma CVD and B_2O_3 in CH_3OH by hot filament CVD for p-type, and PH_3 in CH_4 by μ-wave plasma CVD and P_2O_5 in CH_3OH by hot filament CVD for n-type [25,26]. The boron doping of diamond can realize p-type conductivity. On the other hand, no satisfactory n-type conduction has been obtained. For n-type doping, phosphorous is still one of the most available impurities due to the theoretical analysis by Kajihara which indicates that P would form the donor level at 0.2 eV below the conduction band minimum [27]. It is, however, necessary to increase an amount of P in the growth ambient to increase P concentration in diamond because of its small solubility in diamond. It has been reported that the P addition leads growth ambient away from optimal conditions when PH_3 was used as a doping gas [28]. The diamond crystal quality is impaired by P addition. Therefore, development of new dopant source of P, which can allow diamond to grow in the ambient with very high P concentration, are requested.

In this section, the electrical properties of B-doped homoepitxial diamond films have been investigated. There has been no report on doping of CVD diamond grown from CO, though CO can provide the high quality diamond films as shown in section 2.2.1.An attempt to introduce P in diamond by using a liquid source triethyl phosphate $(CH_3O)_3P$ for heavy

doping are also shown.

2.3.1 Fabrication of Semiconducting Diamond Films by gas doping

Diamond films have been grown on HPHT synthesized diamond (100) and (111) substrates, 3 x 3 x 1 mm^3 in dimensions, and Si substrate by means of microwave plasma CVD. The process parameters used were as follows: 2.45 GHz, 200 W microwave source, 900°C substrate temperature (as determined by an optical pyrometer), 30 Torr pressure, 10 % CO in H_2, and 100 sccm gas flow. A dilute B_2H_6 gas was used to synthesize p-type semiconducting diamond. $(CH_3O)_3P$ was used for n-type dopant and kept at 0°C in iced water in order to yield constant vapor pressure. Vaporized $(CH_3O)_3P$ was mixed with CO gas before reaction. The P/C ratio was approximately 2000~2400 ppm. The Hall effect measurement has also been carried out in magnetic fields up to 5 Tesla in the present study. For resistivity measurement, surface conductive layers of the specimens were etched off by reaction with oxygen during cooling after deposition [29]. Electrical contacts to the samples were made by evaporation of Ti dots.

2.3.2 Electrical Properties of Semiconducting Diamond Films

The resistivity ρ, Hall mobility μ and carrier density N of the B-doped (100) and (111) films, measured as a function of temperature, are shown in Figure 2.3.2-1. Using these results, ρ and μ are plotted as a function of N in Figure 2.3.2-2. The respective thickness of the (100) and (111) films were determined by CL measurement, and were about 1 and 10 μm. The films are much thicker than the surface corrugation amplitude of the (100)-oritented substrate and the roughness of the (111) films. So, they are thick enough for the Hall measurement. Although the ratio of B to C in the reactant gas was 100 ppm for both specimens, the (100) film showed resistivity of 0.151 Ohm.cm at 500 K, which is one order of magnitude lower than that of the (111) film, as shown in Figure 2.3.2-1 (a). The (100) film exhibited a high μ of 451 cm/Vsec at room temperature (RT) which decreased monotonically with increasing temperature. The (111) film, on the other hand, showed a low value of 4.8

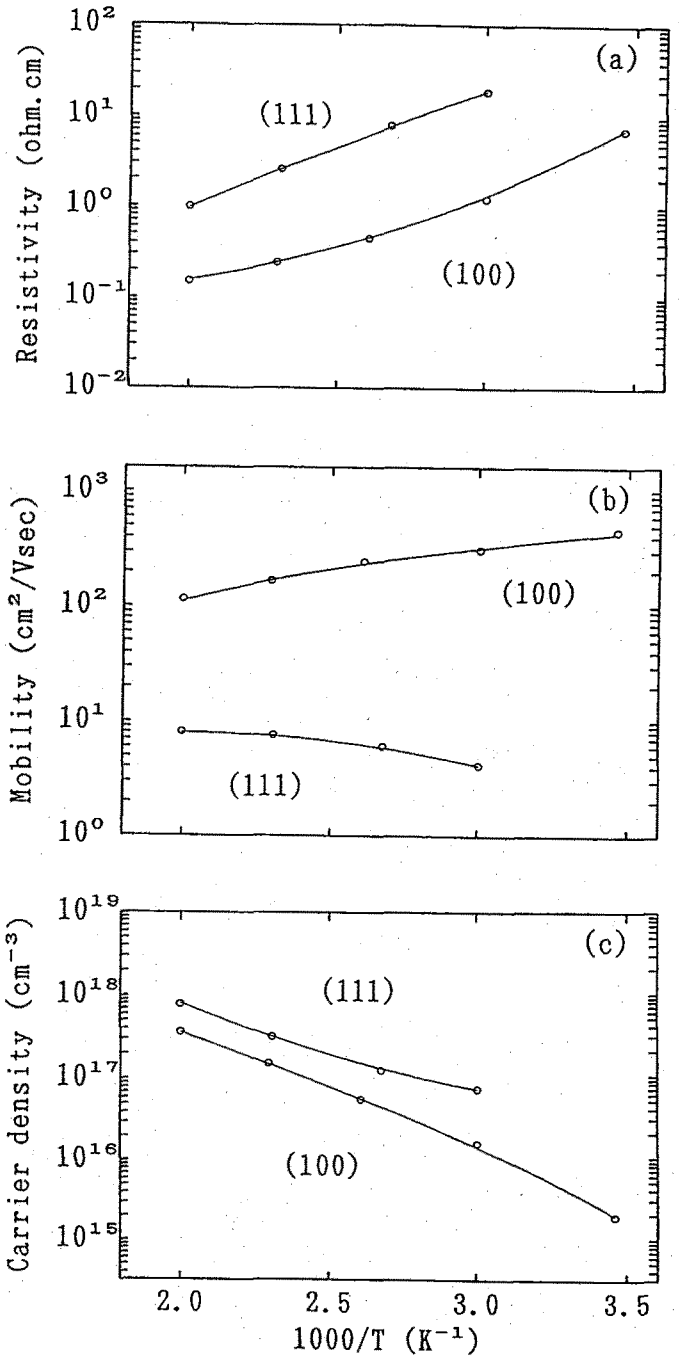

Figure 2.3.2-1. (a) Resistivity, (b) Hall mobility and (c) carrier density vs temperature characteristics for B doped (100) and (111)-oriented homoepitaxial diamond films. The ratio of B to C in the reactant gas was 100 ppm for both cases.

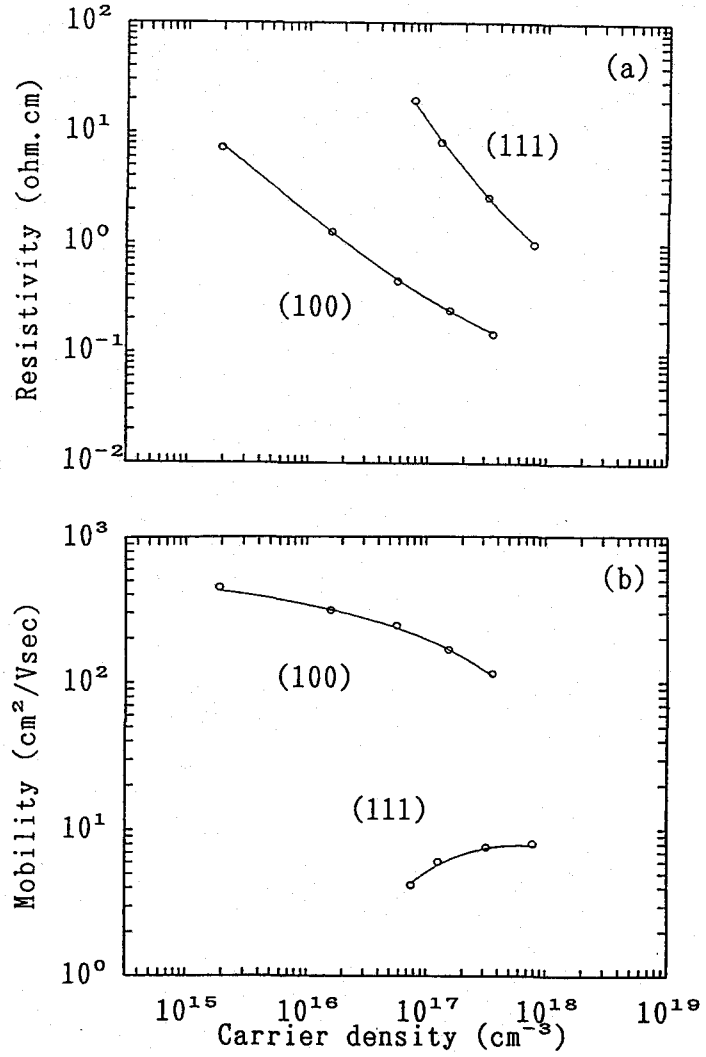

Figure 2.3.2-2. (a) Resistivity and (b) Hall mobility measured as a function of carrier density.

cm/Vsec. This may be due to the strong influence of scattering at the defects and/or grain boundaries present in the (111) films. Additionally, in contrast to the (100) film, the (111) film increased in μ with raising temperature, as shown in Figure 2.3.2-1 (b). Although the reason for this phenomenon remains unclear, it appears to be inferior crystallinity of the (111) film. Thus, these results directly support the results of defect structures in [111] growth, and are consistent with the present SEM and AFM investigations. The slopes in Figure 2.3.2-1 (c) give B activation energies of 0.38~0.28 eV and 0.21~0.28 eV for the (100) and (111) films, respectively.

Magnetoresistance measurement gives a guide to the structure of, for example, the valence band and defecs. We have observed transverse magnetoresistance, which is understood to be the quantity $\Delta\rho/\rho 0$, where $\Delta\rho$ is the resistivity change and $\rho 0$ is the zero-field resistivity, of CVD diamond for the first time. Figure 2.3.2-3 shows the magnetoresistance as a function of the magnetic field for the (100) film for sample current in the [110] direction and magnetic field in the [100] direction. The present specimens had the similar dimensions with the natural diamond used in the previous work so that we can neglect the size-effect of the present sample. Measurements were taken at RT for forward and reverse directions of magnetic field and current to reduce spurious effects. The magnetoresistance is proportional to the square of the magnetic field, and we observed the value of 0.2 at 5 Tesla, which is close to the reported value of ~0.35 for natural semiconducting diamond [30]. This study shows the crystallinity of the (100) film to be of the same level as that of natural semiconducting diamond. The temperature dependence of magnetoresistance is shown in Figure 2.3.2-4. From RT to about 333 K, the magnetoresistance decreased rapidly down to 0.08 with increasing temperature and the slope starts to change gradually above about 385 K. At 500 K, the magnetoresistance of about 0.02 can be still observed, indicating a possibility of high temperature operating Hall device application for CVD diamond.

For P doping, diamond films have been successfully grown on Si substrate. On the other hand, it was difficult to grow homoepitaxial heavy P-doped diamond in this work. Figure 2.3.2-5 shows a Raman spectrum over the energy range from 1200 to 1800 cm^{-1}

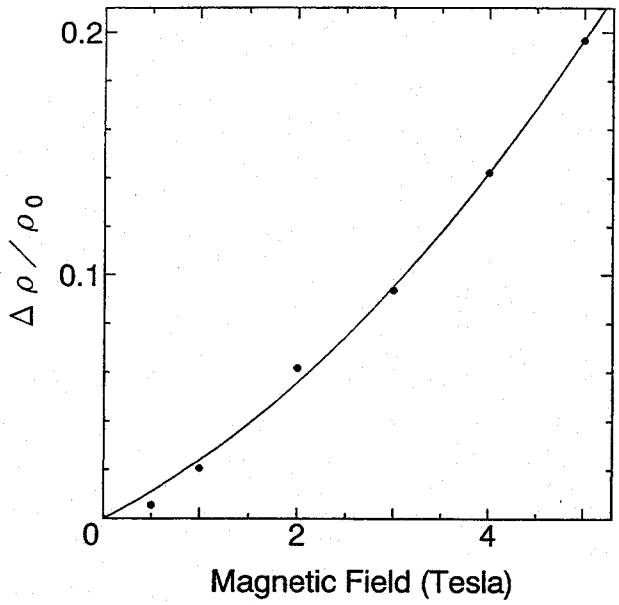

Figure 2.3.2-3. Field dependence of transverse magnetoresistance for B doped (100)-oriented homoepitaxial film.

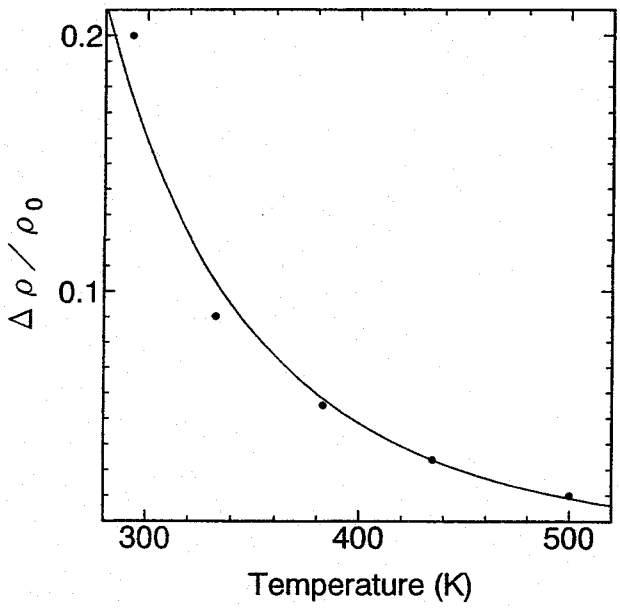

Figure 2.3.2-4. Temperature behavior of transverse magnetoresistance for B doped (100) film.

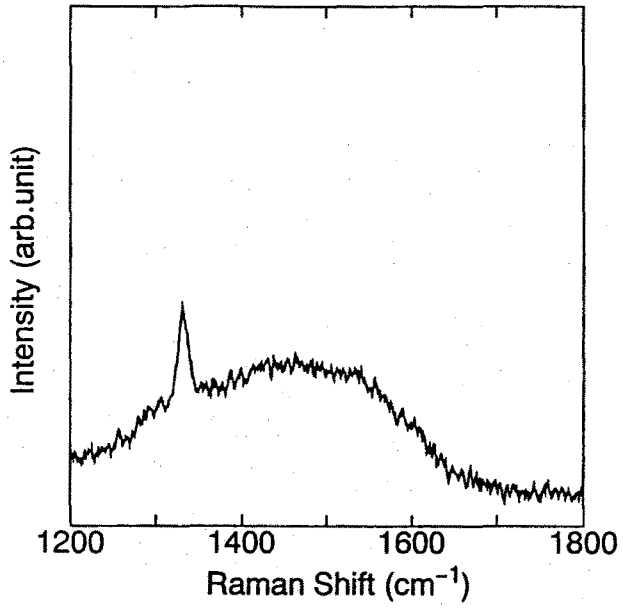

Figure 2.3.2-5. A typical Raman spectrum obtained for the P-doped diamond film.

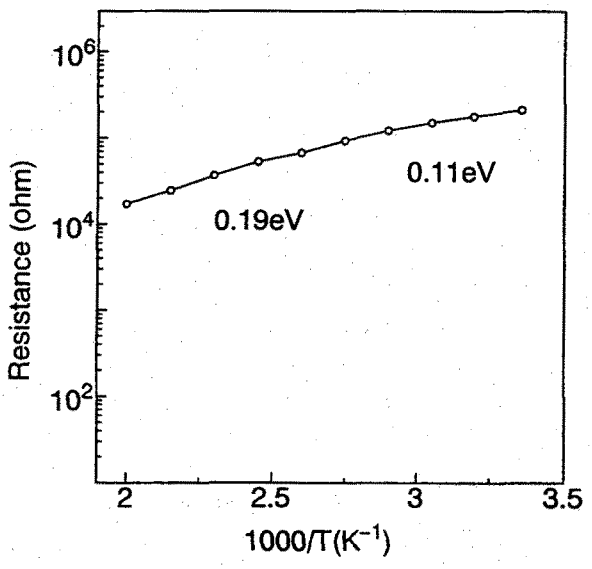

Figure 2.3.2-6. Electrical resistance of the P-doped diamond film as a function inverse absolute temperature

obtained for P-doped polycrysatlline diamond film. A sharp peak at 1332 cm^{-1} originating from diamond and a broad peak of graphite at 1550 cm^{-1} were observed, indicating that this diamond film contained a graphite phase. Large amount of P addition makes diamond growth difficult, so that it is hard to obtain high quality P-doped diamond. Figure 2.3.2-6 shows the temperature dependence of the resistivity of the sample. The activation energy (Ea) of P doped films was deduced from the slope of the R-1/T curve. The Ea of 0.19 eV obtained for high temperature region shows good agreement with calculated value of 0.2 eV. The resistivity of this sample is about 10^7 Ohm.cm at RT. Although doped P might be attributable to this electrical conduction, this resistivity is too high for the practical use.

2.4 Summary

Homoepitaxial diamond films grown from CO by using μ-wave plasma CVD have been characterized. The (100) 2 x 1 surface was smooth, whereas the (111) surface was rough with triangular microstructures. The growth rate on the (111) substrate was about one order of magnitude greater than that on the (100) substrate.

The resistivity, Hall mobility and corresponding B activation energy measured for the B-doped (100) film were 7.26 Ohm.cm, 451 cm/Vsec and 0.38 eV at RT, respectively. The transverse magnetoresistance has been observed to be 0.2 at 5 Tesla at RT. The P-doped CVD diamond films have grown on Si substrate by using $(CH_3O)_3P$ as a dopant. These films showed the high resistivity of ~10^7 Ohm.cm at RT.

2.5 References

[1] B.V.Spitsyn, L.L.Bouilov, and B.V.Derjaguin: J. Cryst. Growth 52 (1981) 219.

[2] B.B.Pate: Surf.Sci. 165 (1986) 83.

[3] S.Matsumoto, Y.Sato, M.Kamo and N.Setaka: Jpn. J. Appl. Phys. 21 (1982) L183.

[4] A.Sawabe and T.Inuzuka: Appl. Phys. Lett. 46 (1985) 146.

[5] K.Kitahama, K.Hirata, H.Nakamatsu, S.Kawai, N.Fujimori, T.Imai, H.Yoshino and A.Doi: Appl. Phys. Lett. 49 (1986) 634.

[6] S.Matsumoto: J. Mater. Sci. Lett. 4 (1985) 600.

[7] M.Kamo, Y.Sato, S.Matsumoto and N.Setaka: J. Cryst. Growth 62 (1983) 642.

[8] H.Kawarada, K.S.Mar and A.Hiraki: Jpn. J. Appl. Phys. 26 (1987) L1032.

[9] M.Frenklach and H.Wang: Phys. Rev. B43 (1991) 1520.

[10] S.Koizumi, T.Murakami, T.Inuzuka, K.Suzuki: Appl. Phys. Lett. 57 (1990) 563.

[11] N.Fujimori, T.Imai, H.Nakahata, H.Shiomi and Y.Nishibayashi: Mater. Res. Soc. Proc. 162 (1990) 23.

[12] M.W.Geis: Mater. Res. Soc. Proc. 162 (1990) 15.

[13] K.A.Snail, J.A.Freitas, C.L.Vold and L.M.Hanssen: Proc. 2nd Int. Symp. Diamond Materials 91-8 (1991) 81.

[14] T.Tsuno, T.Imai, Y.Nishibayashi, K.Hamada and N.Fujimori: Jpn. J. Appl. Phys. 30 (1991) 1063.

[16] H.G.Maguire, M.Kamo, H.P.Lang, E.Meyer, K.Weissendanger and H.J.Guntherodt: Diamond and Related Mater. 1 (1992) 634.

[16] L.F.Sutcu, M.S.Thompson, C.J.Chu, R.H.Hauge, J.L.Margrave and M.P.D'Evelyn: Appl. Phys. Lett. 60 (1992) 1685.

[17] P.K.Backmann, D.Leers and H.Lydtin: Diamond and Related Mater. 1 (1991) 1.

[18] A.T.Collins: Diamond and Related Mater. 1 (1992) 457.

[19] Y.Yokota, H.Kotsuka, T.Sogi, J.S.Ma, A.Hiraki, H.Kawarada, K.Matsuda and M.Hatada: Diamond and Related Mater. 1 (1992) 470.

[20] N.Yamamoto, J.C.H.Spence and D.Fathy: Philos. Mag. B49 (1984) 609.

[21] S.Katsumata: Jpn. J. Appl. Phys. 31 (1992) 3594.

[22] Y.Yokota, H.Kawarada and A.Hiraki: Jpn. J. Appl. Phys. 29 (1990) L2232.

[23] J.E.Field: The Properties of Diamond (Academic Press, New York, 1979).

[24] C.J.Chu, R.H.Hauge, J.L.Margrave and M.P.D'Evelyn: Appl. Phys. Lett. 61 (1992) 1393.

[25] N.Fujimori, H.Nakahata and T.Imai: Jpn. J. Appl. Phys. 29 (1990) 824.

[26] K.Okano, H.Kiyota, T.Iwasaki, T.Kurosu, M.Iida and T.Nakamura: Appl. Phys. Lett. 58

(1991) 840.

[27] S.A.Kajihara, A.Antonelli, J.Bernholc and R.Car: Phys. Rev. Lett. 66 (1991) 2010.

[28] S.Bohr, R.Haubner and B.Lux: Diamond and Related Mater. 4 (1995) 133.

[29] Y.Mori, A.Hatta, T.Ito and A.Hiraki: Jpn. J. Appl. Phys. 31 (1992) L1718.

[30] K.J.Russel and W.J.Levio: Phys. Rev. B6 (1972) 4588.

3. SURFACE OF CVD DIAMOND FILMS

3.1 Introduction

Diamond belonging to group IV in the periodic table has some very special characteristics which make it an interesting material for theoretical and experimental studies of surface, compared with other group IV semiconductors such as Si and Ge. Diamond surfaces are chemically inert and no stable native oxides are usually observed. There are, however, unfavorable characteristics of diamond surface. Diamond surface tends to reconstruct to graphite phase. Because diamond CVD differs from other crystal growth processes in that the bulk material deposited is a metastable phase of carbon, other phases of carbon can grow and can result from breaking off the grown diamond during deposition. In particular, there have been some reports of the existence of impure diamond layer at the surfaces and/or grain boundaries [1-3]. Of course, the presence of impure diamond surfaces depends on the growth condition. Characterization of CVD diamond surface is important in three respects. First, it is necessary to check the presence of impure diamond layers, identify them and assess their impact on the electrical properties of the diamonds. Second, it is desirable to understand and control the formation of these layers so that an insulating CVD diamond film can be obtained without any additional surface treatment. Third, studies of as-grown surface promise to be useful in improving the basic understanding of diamond growth mechanism.

In this chapter, the CVD diamond surface and its graphitization, effect of surface treatment on graphitization, and the surface conductive diamond layers have been investigated.

3.2 As-Grown CVD Diamond Surface

The diamond films used in the present study were polycrystalline as shown in Figure 3.2-1. Figure 3.2-2 shows typical electron energy loss spectroscopy (EELS) spectra presented as the negative second derivative of the electron energy distribution scattered from an as-grown CVD polycrystalline diamond film using incident electrons of 300 eV. These spectra are similar to those of as-polished natural diamond [4]: The structure is mainly characterized by

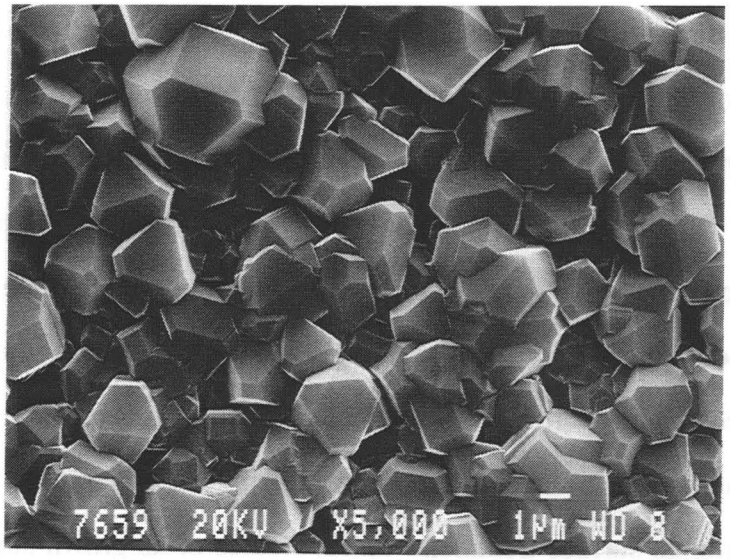

Figure 3.2-1. SEM image of polycrystalline diamond film.

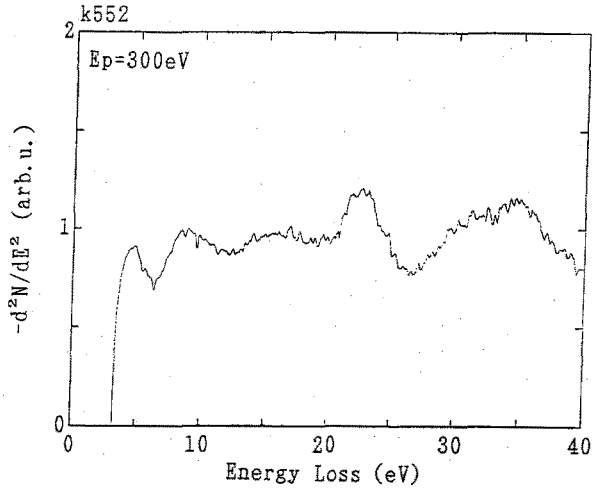

Figure 3.2-2. Negative second derivative EELS spectrum by valence band excitation at E_p=300 eV for as-grown CVD diamond surface which is covered with hydrogen.

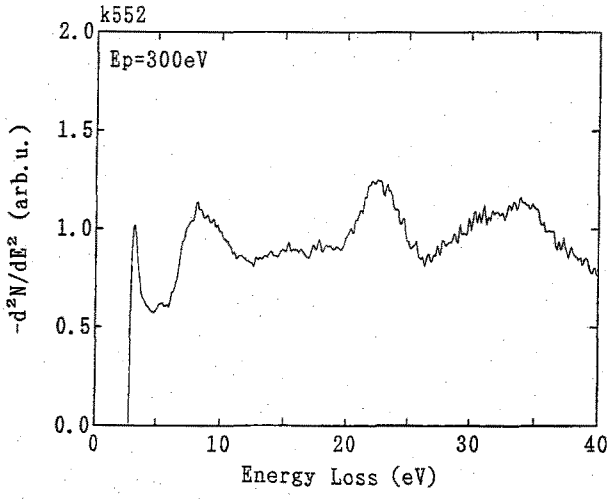

Figure 3.2-3. Negative second derivative EELS spectrum by valence band excitation at E_p=300 eV for CVD diamond surfaces after heating at 900°C and 10^{-9} Torr.

two losses due to the bulk plasmon excitation near 34 eV and to the surface plasmon excitation near 23 eV. No losses originating from possible surface states in the band gap can appear in the EELS spectra.

Figure 3.2-3 depicts EELS spectra taken from the diamond after heating for 5 min at 900°C under vacuum in the 10^{-9} Torr range. A new energy loss due to surface states in the band gap is observed near 3~4 eV. These states can not be seen either for the as-grown CVD diamond or polished natural diamonds, while theory predicts occupied and empty surface states located in the band gap of ideal diamond [5]. In the case of polished natural diamonds, their surfaces have been reported to be covered with hydrogen atoms [6-8]. The 1 x 1 surface of natural diamond is hydrogen-terminated and there are no intrinsic surface states in the band gap region as predicted by theoretical calculations [5]. After heating at 900°C in a vacuum, the as-polished natural diamond 1 x 1 surface, from which the chemisorbed hydrogen atoms are evolved, is reconstructed to a 2 x 1 / 2 x 2 structure. In contrast the as-polished 1 x 1 surface, intrinsic surface states are observed for the 2 x 2 / 2 x 1 reconstructed surface. Therefore, the results shown in Figures 3.2-2 and -3 strongly suggest that as-grown CVD diamond surfaces are hydrogen-terminated, and that the characteristic loss near 3~4 eV is produced after hydrogen desorption from the surface. The intrinsic surface states originating from dangling bonds appear to be too stable to react with possible contaminants such as oxygen atoms even after exposure to the air at room temperature.

The as-grown surfaces of CVD diamond show a relatively low resistance, in the order of 10^7 Ohm, compared with natural diamond, ~10^{16} Ohm.cm, although the electronic structure of the as-grown CVD diamond is similar to that of natural diamond. The detailed study of this phenomenon is discussed in the next section.

3.3 Surface Conductive Layers

Natural diamond, except type IIb, has been reported to exhibit electrical resistivity on the order of 10^{16} Ohm.cm [9], whereas there have been some reports that undoped CVD diamond shows a relatively low resistance, on the order of 10^4 Ohm [1-3]. The conduction

mechanism of undoped CVD diamond has not been completely clarified so far and several assumptions have been reported. Landstrass et al. suggested that the low resistivity of the undoped CVD diamond films may be due to hydrogen passivation of carrier traps in the films and that thermal annealing causes an increase in the resistivity due to dehydrogenation resulting in the electrical activation of deep traps [1]. On the other hand, it has been reported that a thin conductive surface layer is formed on top of the CVD diamond films and that insulating diamond remains after removal of this layer by chemical cleaning with a CrO_3 solution or by heating in an oxygen ambient [2,3]. In most cases, suitable subsequent treatments after deposition are necessary to obtain an insulating CVD diamond film, which, by analogy to SiO_2 in Si device technology, is important for fabrication of diamond-based electronic devices. Ideally, these excess processes should be omitted in order to obtain clarified diamond surfaces and to simplify device fabrication.

In this section, the author shows the effect of ambient on the resistance of CVD diamond films during cooling after deposition and the capability of obtaining insulating diamond films without any additional surface treatment. Secondly, the electronic structure of these surfaces is discussed with relation to their conductivity.

3.3.1 Effect of Ambient on the Diamond Surface during Cooling after Deposition

After turning-off the input microwave power to stop the diamond growth, various gases (N_2, O_2, H_2, air) were immediately introduced into the reaction tube, up to atmospheric pressure, for cooling specimens. There was a delay of several seconds before introducing gases into the reaction tube after turning-off microwave plasma, and a rapid decrease in temperature of the specimen was observed at one time. However, to measure or to estimate accurate temperatures of the diamond surface just before and after the introduction of gases until reaching atmospheric pressure is difficult.

Electrical contacts to the samples were made by evaporation Ti of dots or using silver epoxy, shown to make ohmic contacts [10,11]. The contact area and the separation distance between electrodes was about ~1 mm and 1~2 mm, respectively. For resistance measurements,

a two-point probe technique was used. The current-voltage characteristics were measured using a Keithley 237 high voltage source measurement unit with computer interface for automatic data collection.

Resistances of the diamond films varied with different ambient during cooling after deposition at 900°C. These results are summarized in Table 3.3.1-1. The diamond films, single- (sample 1) and poly-crystalline (sample 2), cooled slowly until room temperature (RT) in the 10^{-3} Torr range after deposition showed relatively low resistances in the range of 10^{6}~10^{7} Ohm. On the other hand, the high resistances over 10^{13} Ohm were observed for the films (samples 3 and 4) after cooling in an oxygen ambient at atmospheric pressure. Similar results were obtained after cooling in air. Cooling of specimens in other ambient has been carried out to clarify what is essential. The cooling in a nitrogen or a hydrogen ambient at atmospheric pressure increased the resistance of films (samples 5 and 6) up to 10^{7}~10^{8} Ohm, 1~2 orders of magnitude greater compared with that of sample 1. These results indicate that oxygen is indispensable as a cooling ambient to produce highly insulating diamond films. A remarkable increase of the resistance by two orders of magnitude via a cooling in the oxygen-contained ambient was also observed for boron doped specimens (samples 7 and 8).

This investigation reveals clearly that surface conductivity of the undoped CVD diamond films is not due to hydrogen passivation of carrier traps in the films. It is possible to increase the resistivity without additional thermal annealing.

3.3.2 Characterization of Surface Conductive Layers

Rutherford backscattering spectrometry was used to detect surface oxygen on polycrystalline diamond films. By tilting the target with respect to the direction of the incident beam, we obtained an increase in the effective depth resolution for surface analysis. Figure 3.3.2-1 shows the spectra for 2.125-MeV He^{+} ions backscattered from diamond films: (a) as-grown (sample 9) and (b) cooled in an oxygen ambient (sample 10). Sample 9 and 10 return thick target signals whose reading edges are at channel number 105, and sample 10 also shows a peak for the surface oxygen atoms at channel number 150. The amount of

Table 3.3.1-1. Summary of the specimens examined in the present study

Sample	Doping	Substrate	Introduced gases during cooling	Resistance (Ω)
1	no	HPSD(111)	none (10^{-3} Torr)	$\sim 10^{6}$
2	no	SiO_2	none (10^{-3} Torr)	$\sim 10^{7}$
3	no	HPSD(111)	oxygen	$>10^{13}$
4	no	SiO_2	oxygen	$>10^{13}$
5	no	HPSD(111)	hydrogen	$\sim 10^{7}$
6	no	HPSD(111)	nitrogen	$\sim 10^{8}$
7	boron	HPSD(111)	none (10^{-3} Torr)	$\sim 10^{2}$
8	boron	HPSD(111)	oxygen	$\sim 10^{4}$
9	boron	p^+-Si	none (10^{-3} Torr)	—
10	boron	p^+-Si	oxygen	—

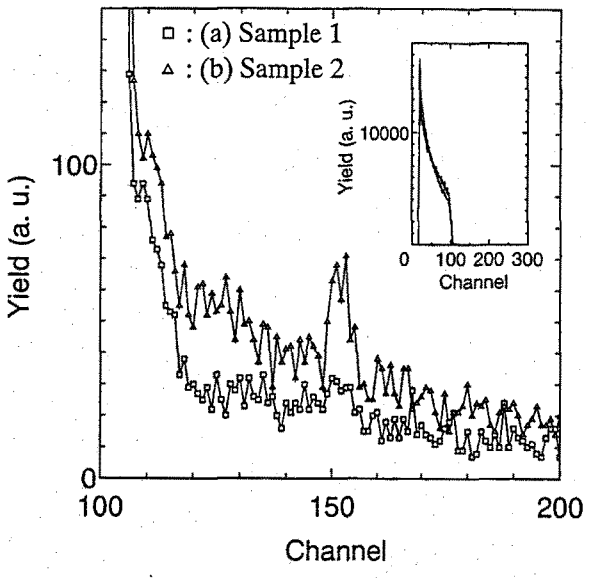

Figure 3.3.2-1. Rutherford backscattering spectra of 2.125 MeV He^+ ions from polycrystalline diamond surfaces: (a) as-grown and (b) cooled in oxygen ambient after deposition.

oxygen per square centimeter can be calculated directly from the RBS data, and is approximately less than 10^{15} atoms/cm^2 for the case of sample 10.

The electronic structure of the above diamond surfaces was investigated using EELS. Figure 3.3.2-2 shows EELS spectra presented as the negative second derivative of the electron energy distribution at primary electron energy E_p of 300 eV for (a) sample 9 and (b) sample 10. The characteristic loss features of spectrum (b) are identical to those of as-polished natural diamond [4]. One can assign the 34-eV feature to bulk plasmon excitation, the 22-eV feature to the surface plasmon excitation, and the 15- and 10-eV features to interband transitions [4]. The peak positions of the dominant loss features, surface and bulk plasmon excitations, of spectrum (a) are similar to those of spectrum (b), whereas there are small differences around the 5- and 15-eV features.

The other differences between these spectra have been found. The loss feature near 22 eV appears to be stronger on spectrum (a) than on (b) and also in spectrum (a), the 22 eV feature is significantly larger than the 34 eV feature. In general, the surface plasmon loss should be less than the bulk plasmon loss [12]. Additionally, bulk plasmon excitations of hydrogenated amorphous carbon (a-C:H) and amorphous carbon (a-C) films have been reported around 21-25 eV, depending on the structure [13,14]. Therefore, the loss feature at 22 eV in spectrum (a) may be associated with both the surface plasmon excitation of diamond and a bulk plasmon loss excitation of a-C:H and/or a-C which may be formed on part of the CVD diamond surface during deposition. So, the disordered diamond, a-C:H component, a-C component or their complex seem to cause the conductivity in the samples. This result is supported by the following measurement.

Figure 3.3.2-3 shows EELS spectra presented as the electron energy distribution at primary electron energy E_p of 300 eV for (a) sample 9 and (b) sample 10. The peak positions of the dominant loss feature are, of course, same with those in natural diamond. The point of these spectra is that there are slight differences around 10 and 24 eV between spectra (a) and (b). The loss feature at 24 eV in spectrum (a) seems to be due to bulk plasmon excitations of a-C:H or a-C as mentioned above. The amount of a-C:H or a-C at the surface is too small to

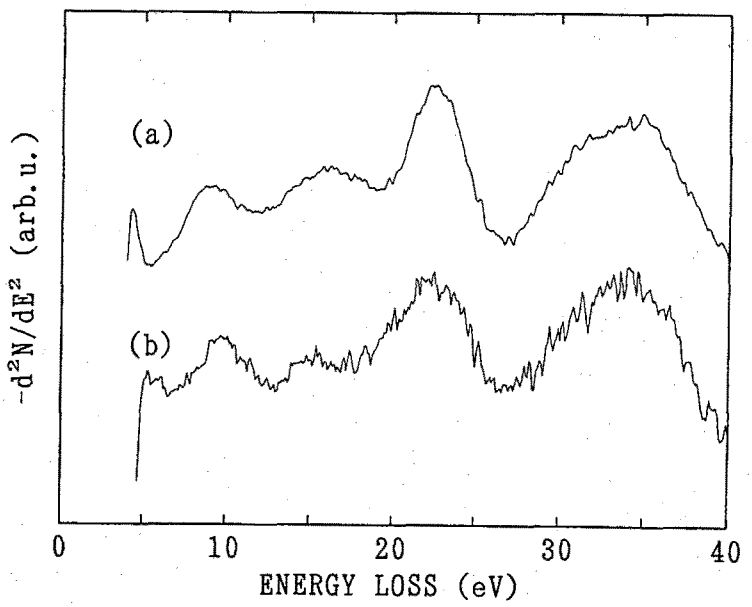

Figure 3.3.2-2. Negative second derivative EELS spectra at E_P=300 eV for various CVD diamond surfaces (a) cooled in the 10^{-3} Torr range and (b) in the oxygen ambient at atomospheric pressure after depositions.

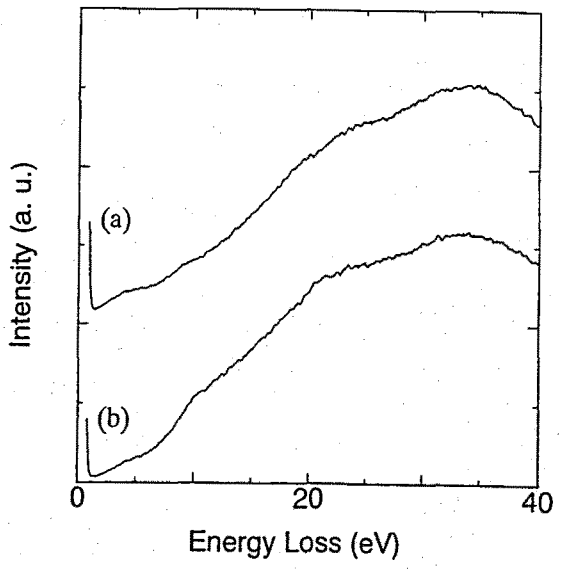

Figure 3.3.2-3. EELS spectra at E_P=300 eV for CVD diamond surfaces (a) cooled in the 10^{-3} Torr range and (b) in the oxygen ambient at atomospheric pressure after depositions.

cover the whole surface. Therefore, the conductivity of the as-grown surface is not attributable to a chain of interpenetrating amorphous region. This result does not disagrees with a recent STM study wherein a 2 x 1 / 2 x 2 reconstructed surfaces were observed for as-grown (100) diamond surfaces. It is hard to detect the very small a-C:H or a-C phase at the surface by STM investigation. The author thinks that this small amount of a-C:H or a-C phase can act as a electrically active p-type dopant in the surface layers, resulting in low surface resistivity. The presence of a-C:H or a-C phase does not always mean the low quality diamond surface. The as-grown surfaces of CVD diamond investigated in this work are considered to be a ideal surface without any surface states.

Such conductive layers can also be created again on insulating diamond surfaces. Insulating HPHT synthesized and CVD diamonds increased in conductivity by an exposure to the μ-wave hydrogen plasma followed by cooling in the 10^{-3} Torr range, whereas it was not observed after cooling in the oxygen ambient. These results indicate that the surface conductive layers of diamond seem to be formed by the hydrogen plasma irradiation during diamond deposition or hydrogenation, and can be removed by reaction with oxygen during cooling. From SEM, a slight difference between the contour of the crystals in sample 9 and 10 was observed and attributed to removal of the conductive layer. Unfortunately, it was difficult to estimate the thickness of this layer from the SEM investigation.

3.4 Graphitization of Diamond Surface

Diamond is a quasi-stable phase under ordinary conditions of room temperature and atmospheric pressure, meaning that surface graphitization may be induced when a sufficient energy is supplied to the diamond surface. If it happens, devices comprising metal-diamond couples will lose their desired functions, because both the diamond-graphite and the graphite-metal interfaces show ohmic behavior [10]. Thus, the investigation on the surface characteristics and transformation of CVD diamonds are important for basic understanding as well as a future technology of the diamond industry.

The surface dynamics, especially the graphitization of the diamond surface, have been

investigated previously, indicating that it is influenced effectively by the extrinsic effects during the heating or the presence of surface adatoms [4,15]. The critical temperature of the diamond graphitization during the heating can be varied widely from 1500°C or more in an ultra high vacuum, to about 600°C in an oxygen ambient [4,15]. With this information, author thought that it is possible to avoid the graphitization by modification of diamond surface.

In this section, the surface of CVD diamond and the controllability of the graphitization using CrO_3 treatment have been investigated.

3.4.1 Effect of Surface Treatment on the graphitization

For the modification of diamond surfaces, two oxidation processes for the diamond surface were employed in the present study: (1) boiling in a saturated solution of CrO_3 in H_2SO_4 at 200°C, followed by a rinse of a hot (90°C) 1:1 solution of H_2O_2 (30%) and NH_4OH (70%) (called chemical treatment: CT); (2) first heating at 900°C in an ultra high vacuum (10^{-9} Torr) to desorb hydrogen atoms initially chemisorbed, followed by a second heating at 400°C in an oxygen ambient (thermal oxidation: TO). CT is commonly used in cleaning diamond surfaces, and the effects of CT on the electrical and interfacial properties under various conditions of metals and surfaces are reported in chapter 4.

From Figure 3.2-3, it is concluded that surface graphitization can not be induced by an ultra high vacuum anneal at ~900°C, because plasmon loss features are still observed near 23 eV and 34 eV. On the other hand, the surface graphitization can be induced after heating of diamond at 900°C in a vacuum in a 10^{-7} Torr range. As is shown in Figure 3.4.1-1, a loss peak due to the π-plasmon loss near 6.7 eV, meaning the presence of the graphite phase [16], appears with a nearly symmetrical shape, whose intensity becomes weaker relative to the bulk transition as E_p is increased. This evidence gives that the graphitization of the CVD diamond films occurs from its surface and penetrates into the bulk since higher energy electrons can probe a deeper bulk region.

The EELS results with E_p=500 eV are shown in Figure 3.4.1-2 (a) for the CVD

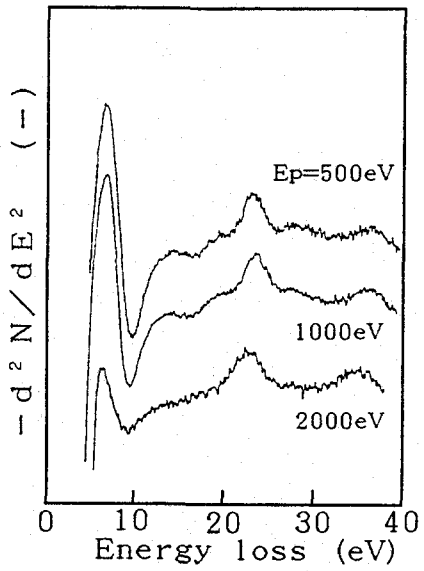

Figure 3.4.1-1. Second-derivative EELS spectra by valence band excitation at E_p=500, 1000, 2000 eV for CVD diamond surfaces after heating to 900°C in a vacuum in the 10^{-7} Torr range.

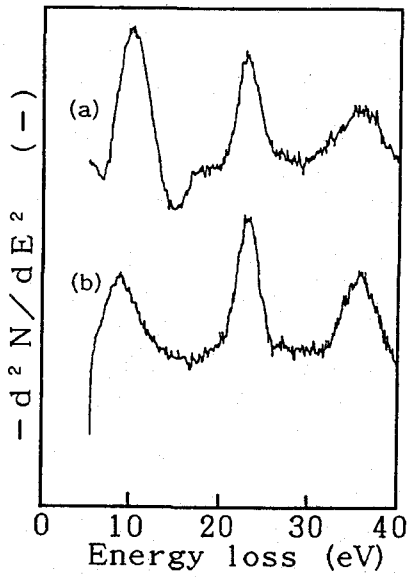

Figure 3-4.1-2. Negative second derivative EELS spectra by valence band excitation at E_p=300 eV for CVD diamond after (a) CrO_3 treatment snd (b) heated to 900°C in a vacuum in the 10^{-7} Torr range after CrO_3 treatment.

diamond after CT and in Figure 3.4.1-2 (b) for the same sample with a subsequent heating at 900°C in a vacuum in the 10^{-7} Torr range. In Figure 3.4.1-2 (a), one can see the same features of the plasmon loss as that of the as-grown CVD diamond with an additional feature near 10 eV related to C-O bonding. Surface graphitization of as-grown CVD diamond covered with hydrogen can be induced by heating to 900°C not in an ultra high, but in the low vacuum range shown in Figure 3.4.1-1. However, it is found that this graphitization can be restrained by the CT shown in Figure 3.4.1-2 (b) since the plasmon loss features of the diamond are still maintained. Oxygen and chromium atoms are still present on the diamond surface even after this heating.

The areal density of the oxygen atoms and the ratio of oxygen/chromium at the surface before and after this heating are determined by RBS measurements to be about 1 x 10^{17} /cm^2, 6 and 3 x 10^{16} /cm^2, 2.8, respectively. These values are much greater than the areal density (7 x 10^{15} /cm^2 of native oxygen on silicon surfaces [17] because the surface area of polycrystalline diamond films is larger than those of single crystals. These results also indicate that the interfacial structure of the metal-CVD diamond after the CrO_3 treatment is like a MIS structure.

However, this restraint effect can not be expected for specimens after TO, because oxygen atoms adsorbed during TO can be thermally desorbed mainly as CO molecules below 900°C, which has been studied by mass spectral analysis. The fact that the desorption of the adsorbed oxygen takes place not as O_2 but as CO molecules, while that of hydrogen as H_2 molecules, may be due to the difference in electronegativities between oxygen (3.5), hydrogen (2.1), and carbon (2.5) [18]. The chemisorbed oxygen, attracting electrons of carbon atoms strongly, can weaken the C-C bonding between the first and second layers of the diamond more than the hydrogen can, due to the decrease in the electron density of the bonding state of the back bonds. Then, one possible explanation for the role of the chemisorbed chromium is that the chromium, with a small electronegativity (1.6), can supply enough electrons to the chemisorbed oxygen atoms so that no significant charge reduction can occur in the bonding states of the diamond. Thus, bond weakening by the oxygen can be restrained when chromium coexists.

3.5 Summary

The surface of as-grown CVD diamond formed from CO has been shown to be hydrogen-terminated and there were no surface states in the band gap. The diamond films cooled slowly until room temperature in the 10^3 Torr range after deposition showed relatively low resistances in the range of 10^6~10^7 Ohm. The EELS study showed that the surfaces of these films seem to contain a small amount of a-C:H and/or a-C phase, which may act as a electrically active p-type dopant in the surface layers. On the other hand, high resistances over 10^{13} Ohm were obtained for the films after cooling in an oxygen or an air ambient at atmospheric pressure.

The characteristics and dynamics of CVD diamond surfaces have been studied mainly by EELS. The graphitization of the as-grown CVD diamond surface is induced by heating at 900°C in a low vacuum (~10^{-7} Torr), while such graphitization can be restrained by the CrO_3 treatment which chemisorb oxygen and chromium atoms onto the diamond surface as a complex to form stable states.

3.6 References

[1] M.I.Landstrass and K.V.Ravi: Appl. Phys. Lett. 55 (1989) 1391.

[2] S.A.Grot, G.Sh.Gildenblat, C.W.Hatfield: C.R.Wronski, A.R.Badzian, T.Badzian, and R.Messier: IEEE Electron Device Lett. 11 (1990) 100.

[3] H.Nakahata, T.Imai and N.Fujimori: Proc.2nd Int.Symp. Dimond Materials, 91-8 (1991) 487.

[4] P.G.Lurie and J.M.Wilson: Surf.Sci. 65 (1977) 476.

[5] J.Ihm, S.G.Louie, and M.L.Cohen: Phys. Rev. B17 (1978) 769.

[6] B.B.Pete, P.M.Stefan, C.Binns, P.J.Jupiter, M.L.Shek, I.Lindau, and W.S.Spicer: J. Vac. Sci. Technol. 19 (1981) 349.

[7] F.J.Himpsel, D.E.Estman, P.Heimann, and J.F.Van der Veen: Phys. Rev. B24 (1981) 7270.

[8] G.D.Kubiak and K.W.Kolasinski: Phys. Rev. B39 (1989) 1381.

[9] J.E.Field: The Properties of Diamond (Academic Press, New York, 1979).

[10] Y.Mori, H.Kawarada and A.Hiraki: Proc. Mater. Res. Soc. 162 (1990) 353.

[11] D.Narducci, J.J.Cuomo, C.R.Guarnieri aand S.J.Whitehair: Proc. Mater. Res. Soc. 162 (1990) 333.

[12] H.G.Maguire: private communication.

[13] E.A.Taft and H.R.Philipp: Phys. Rev. A138 (1965) 197.

[14] F.Richter, K.Bewilogua, H.Kupfer, I.Muhling, B.Rau, B.Rother and D.Schumacher: Proc. 1st Int. Conf. on the Appl. Diamond Films and Related Mater. (1992) 819.

[15] Y.Sato and M.Kamo, Hyomen 19 (1981) 197 in Japanese.

[16] A.Koma, Hyomen Kagaku 7 (1986) 265 in Japanese.

[17] L.C.Feldman, P.J.Silverman, J.S.Williams, T.E.Jackman, and I. Stensgaard: Phys. Rev. Lett. 41 (1978) 1396.

[18] L.Pauling, The nature of the chemical bond (Cornell Univ. press, 1960).

4. FORMATION AND PROPERTIES OF METAL-DIAMOND INTERFACES

4.1 Introduction

Usually the ionic semiconductors and insulators have large band gap, whereas covalent semiconductors have small band gap. Metal-diamond interfaces are of great interest in both basic semiconductor physics and application of diamond-based devices. Diamond may play an important role on basic understanding of metal-semiconductor interface, because the theoretical analysis suggests that the interfacial behaviors would depend on the band gap and ionicity of semiconductor [1,2]. The wide gap and low polarizability of diamond are unique among the homopolar semiconductors, and are useful in understanding the effect of band gap and polarizability on the interfacial reaction and Schottky barrier formation. From the practical point of view, it is important to investigate metal-diamond interfaces because of the lack of pn junction of diamond. Formations of Schottky contact with high breakdown voltage and ohmic contacts with low contact resistance are indispensable to fabricate diodes and field effect transistors.

In this chapter, the formation and properties of metal-diamond interfaces have been investigated.

4.2 Metal-CVD diamond interface formation

The formation of metal-CVD diamond interfaces is indispensable to realize diamond electronic devices. Since diamond is expected for high temperature and high power devices, the stability of electrodes, metal-diamond interfaces, during operation become important issue. Suitable electrodes should be developed before the realization of these devices. There are correlations between interface structure and properties. For example, theoretical analysis has predicted that the interfacial behavior of the ideal Ni-diamond contact system depends strongly on the specific bonding coordination of the Ni atoms at the interface [3,4]. The interfacial reaction can also cause substantial alterations of interfacial properties. Therefore,

it is necessary to study the initial stage of metal-diamond interface formations in order to understand and control interfacial properties.

The author reports an investigation of the initial stage of metal-CVD diamond interface formations by using Au, Ti and Ni as a metal. The author shows the difference in reaction between the CVD diamond surface with Au, Ti and Ni. Metal films were deposited onto a room-temperature (RT) substrate in a vacuum in the 10^{-9} Torr range either by evaporating Au from a tungsten filament or by direct sublimation of twisted Ti and Ni wires through resistive heating. The metal thickness was estimated from Rutherford backscattering spectrometry (RBS) and AES analysis. In-situ AES and EELS measurements were performed using a double-pass CMA (cylindrical mirror analyzer) [5].

4.2.1 Au-Diamond Interface

The electronic structure of metal-CVD diamond interfaces was investigated using EELS, AES, and XPS. Figure 4.2.1-1 shows EELS spectra presented as the negative second derivative of the electron energy distribution at primary electron energy E_p of 300 eV for CVD diamond surfaces. The spectra shown were measured for (a) an as-grown specimen, (b) after Au deposition at RT on the specimen (a), and (c) after annealing the specimen (b) at 850°C. The AES spectrum obtained for the specimen (b) is also exhibited in the inset in Figure 4.2.1-1. The estimated Au thickness, according to Chang [6], is about 0.3Å.

The characteristic loss spectrum of (a) is similar to that of the as-polished natural diamond. One can assign the 34-eV feature to the bulk plasmon excitation, the 22-eV feature to the surface plasmon excitation or interband transition, and the 15-eV feature to an interband transition. Although the 22-eV loss is not clearly assigned to the surface plasmon excitation, the interband transition or the mixture of them, it is likely to be related to the surface. This is because the relative intensity of the 22-eV structure to that of the bulk plasmon loss is getting smaller for the higher primary electron energy of which electrons can probe deeper bulk region. In any case, the assignment of the 22-eV feature does not affect later discussions, so we do not discuss about it any more. No losses originating from possible surface states in the

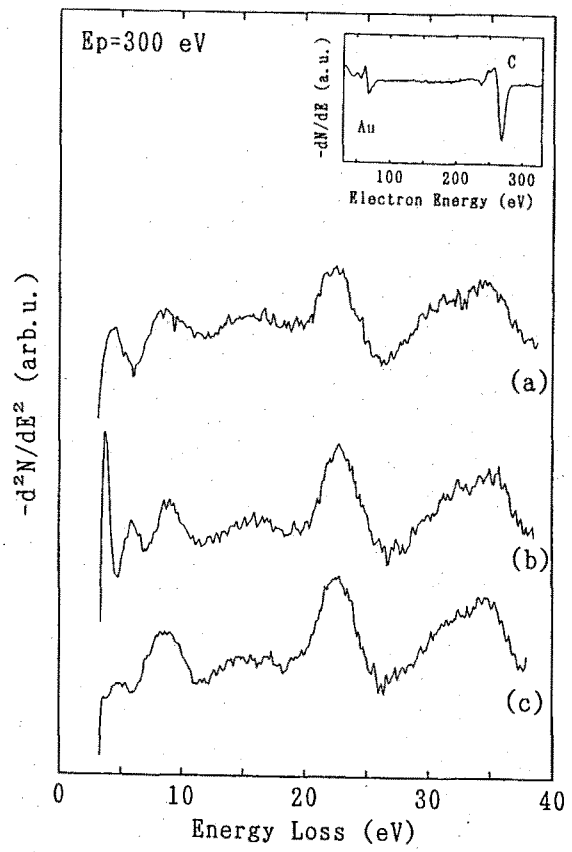

Figure 4.2.1-1. Negative second-derivative EELS pectra at E_p=300 eV for various CVD diamond surfaces: (a) as-grown, (b) after RT Au deposition, and (c) after annealing (b) to 850°C. AES spectrum obtained for the specimen (b) is also exhibited.

band gap can appear in the spectrum (a), suggesting that the as-grown CVD diamond surface is hydrogen-terminated [7].

In the spectrum (b), characteristic loss peaks originating from Au are observed around 3 and 6 eV [8]. On the other hand, the 34-, 23-, and 15-eV features in the spectrum (b) do not change with the Au adsorption onto the surface. This indicates that there is no significant chemical reaction between the Au atoms and the CVD diamond surface at RT. For the case of thick Au films (>8Å) deposited on the natural diamond surface, there is no chemical reaction, either [9]. After an in-situ heating of the Au-CVD diamond to 850°C, no change is observed in the loss features attributed to the diamond, while the 3- and 6-eV losses disappear as shown in the spectrum (c). These EELS results correspond with AES result that the Au signal at 69 eV can be observed for the specimen (b) while not for the specimen after the annealing. This indicates that on the hydrogenated CVD diamond surface Au atoms can easily migrate, even at a lower temperature than its melting point, as to diffuse to outside from the surface investigated. Therefore, it is concluded that the evaporated Au atoms cannot react with the CVD diamond surface even at 850°C.

4.2.2 Ti-Diamond Interface

Figure 4.2.2-1 shows EELS spectra for the Ti-CVD diamond system, including spectra of (a) the as-grown specimen, (b) after Ti deposition (3Å) at RT, (c) after Ti deposition (6Å) at RT, and (d) after annealing the specimen (c) at 850°C. The AES spectrum obtained for the specimen (b) is demonstrated as an inset in Figure 4.2.2-1. The Ti thickness cannot be estimated from the AES analysis due to the interfacial reaction. In this case, RBS was employed to measure the Ti thickness.

The same features for spectrum (a) were previously described in the discussion concerning Figure 4.2.2-1. After the Ti deposition (3) at RT onto the hydrogenated surface, 6-, 10- and, 23-eV features can be observed, while the features attributed to the diamond disappear after the Ti deposition as shown in the spectrum (b). Although there is stoichiometry-dependence of the electron energy loss function of TiC_x [10], one can assign the 23-eV

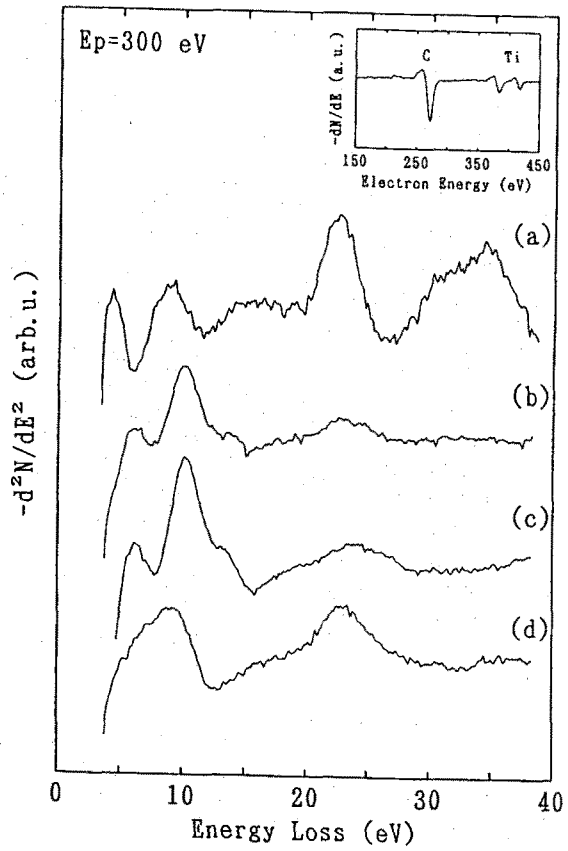

Figure 4.2.2-1. Negative second-derivative EELS spectra at E_P=300 eV for various CVD diamond surfaces: (a) as-grown, (b) after RT Ti deposition (3Å), (c) after RT Ti deposition (6Å),and (d) after annealing (c) to 850°C. AES spectrum obtained for the specimen (b) is alsoexhibited.

feature to a bulk plasmon excitation of TiC_x. The 6- and 10-eV features are also considered to come from TiC_x, although the details concerning them are not clear at present. Moreover, no feature attributed to the pure Ti metal can be observed in the spectrum (b). With increasing Ti coverage up to 6Å, there is no shift for these loss peaks, indicating that the TiC_x formation does not depend on the Ti coverage as shown in the spectrum (c). Therefore, we conclude that even at RT Ti atoms can react with C atoms on the hydrogenated CVD diamond surface, and that the TiC_x layer is formed.

After heating the CVD diamond-Ti surface to 850°C, some small changes are observed in the characteristic loss near 6~10 eV and a new weak loss feature appears around 16 eV. These modifications appear to be due to the stoichiometry-dependence of the loss function of TiC_x. The thermal annealing seems to enhance Ti-diamond reaction. However, change in the stoichiometry of TiC_x is considered to be small, because of a small shift in the bulk plasmon loss of TiC_x at 23-eV after annealing. We conclude that a very stable TiC_x phase can be formed immediately after the Ti deposition at RT.

In order to investigate deeper regions of the CVD diamond, higher primary electron energy of E_p=1 KeV was used. Figure 4.2.2-2 (a) shows an EELS spectrum obtained for the as-grown CVD diamond surface. Dominant loss features observed are the same as those shown in Figure 4.2.2-1 (a). As shown in Figure 4.2.2-2 (b), exactly the same features attributed to TiC_x are observed after the Ti deposition at RT onto the hydrogenated CVD diamond surface. Ti atoms can diffuse into bulk diamond even at RT and form an uniform TiC_x film whose stoichiometry is homogeneous from the surface. After annealing the Ti-CVD diamond to 850°C, a new loss can be observed at 16 eV with a minor change of the loss feature in the 6-10 eV region. Similar tendencies can be seen for Figure 4.2.2-1 (c), indicating that there is a homogeneous region of the TiC_x phase, at least 10Å (probing depth of 1-keV electron) from the surface due to the strong reaction between Ti and the CVD diamond.

The difference in the reaction between the Au-CVD diamond and Ti-CVD diamond interfaces cannot be explained in terms of theories, such as band-closure model [11] or screening model [12], which includes only electron-electron multibody interactions. The

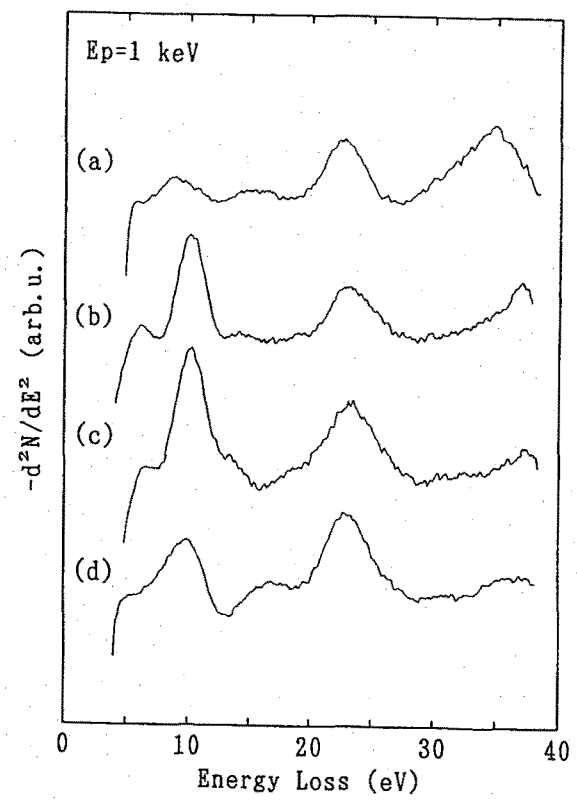

Figure 4.2.2-2. Negative second-derivative EELS spectra at E_p=1 KeV for the CVD diamond surfaces shown in Figure 4.2.2-1.

present results clearly indicate that it is necessary at least to take into account direct interactions of d-electrons of Ti atoms with s, p-electrons of C atoms at the CVD diamond surface. For high temperature devices, the electrode structure should be stable during high temperature operation. It is found that Au is not available for the electrode because of its rapid migration on the surface at high temperatures. On the other hand, Ti is a candidate for the stable electrode due to the RT formation of a stable TiC_x layer, which can be used up to at least 850°C, the highest temperature examined in the present study.

4.2.3 Ni-Diamond Interface

Figure 4.2.3-1 shows the SEM images obtained at various stages of Ni deposition on a polycrystalline diamond surface. The as-grown diamond surface is shown in Figure 4.2.3-1 (a). Evaporation of approximately 14Å of Ni onto the diamond surface at RT results in the surface morphologies shown in Figure 4.2.3-1 (b). There is little difference between the two surfaces, However, islands appear on the surface after heating to 500°C for 2 min (Figure 4.2.3-1 (c)). When a part of the island is stripped off, new diamond surfaces appear (Figure 4.2.3-1 (d)), indicating that the diamond structure remains in most parts of the substrate and that the structural change is observed only in a very shallow surface region. Since the top surface layer can be stripped off easily, the bonding between the surface layer and diamond is very weak, compared with the diamond C-C bonding.

Figure 4.2.3-2 shows various AES spectra of 25Å of Ni-deposited diamond surfaces after annealing at different temperatures from 200 to 900°C at 100°C intervals (curves (b)-(i)) as well as the spectrum of an as-Ni-deposited surface (curve (a)). The AES measurements were performed at RT after each anneal. No impurities except for a small amount of oxygen can be observed on the Ni-deposited surface. The Ni Auger signal decreases gradually with increasing annealing temperature and finally disappears after a 2 min. anneal at 900°C, where the Ni atoms diffuse strongly (to about 1 μm depth, determined by RBS) into the CVD diamond film as shown in Figure 4.2.3-3. The oxygen Auger signal also decreases with increasing specimen temperature and is absent in the top surface region after a 400°C anneal.

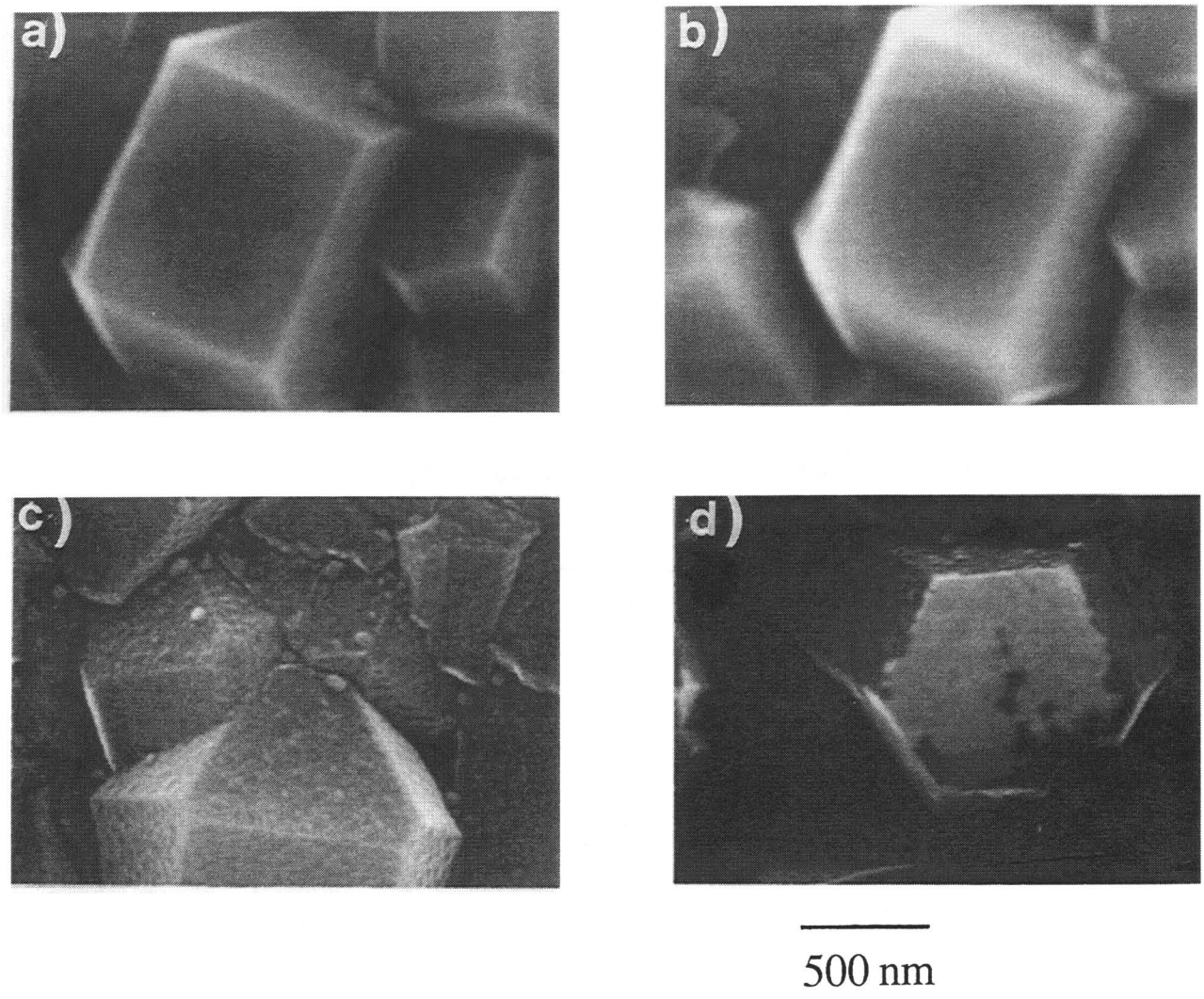

Figure 4.2.3-1. SEM images of (a) as-grown CVD diamond, (b) as-Ni-deposited diamond, (c) after annealing the sample in (b) at 500°C for 2 min and (d) the sample in (c) after the surface layer was stripped off.

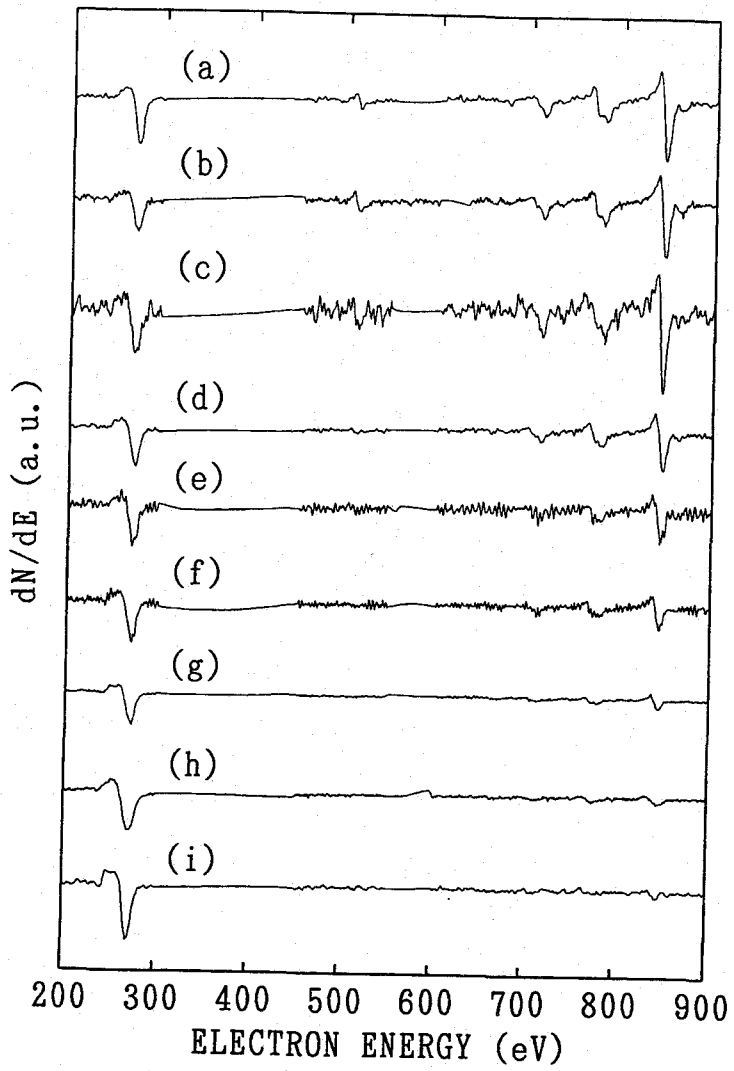

Figure 4.2.3-2. Auger electron spectra of Ni deposited diamond: (a) as-deposited, (b)-(i) after annealing at 10^{-9} Torr at temperatures ranging from 200°C to 900°C with 100°C step.

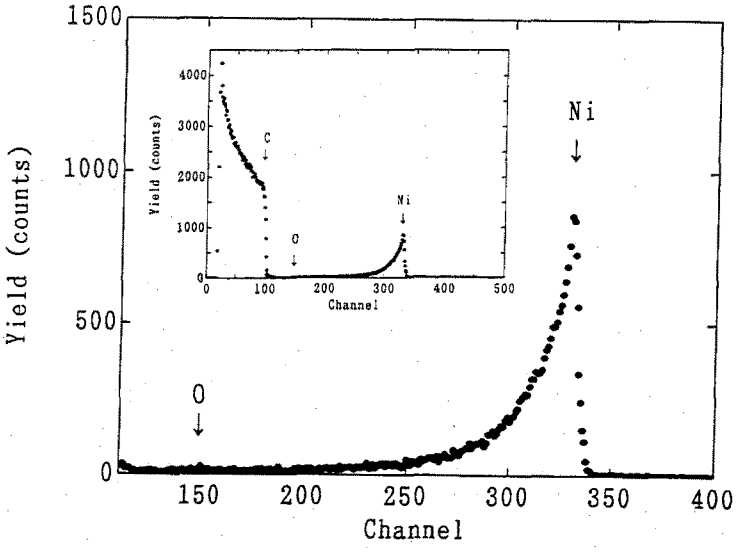

Figure 4.2.3-3. Typical backscattering spectrum for 2.1 MeV He ions incident on Ni-deposited CVD diamond after annealing at 900°C in the vacuum of 10^{-9} Torr.

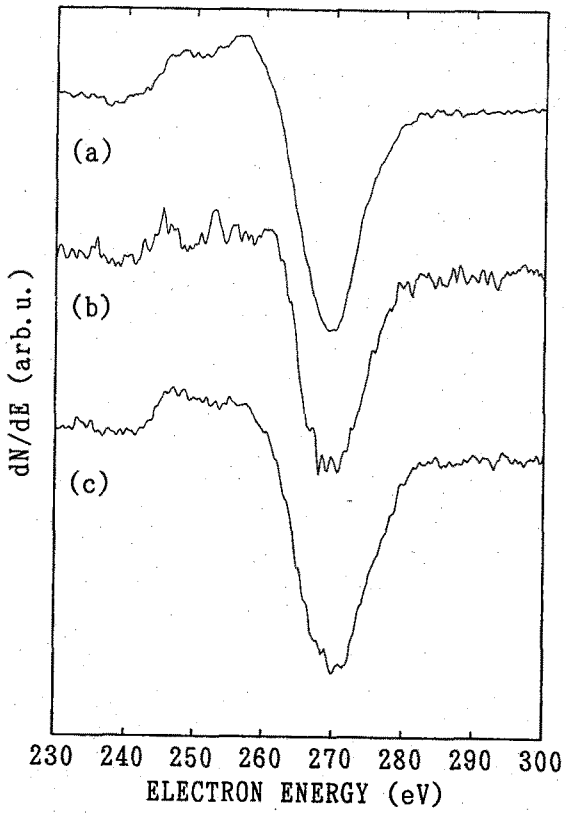

Figure 4.2.3-4. Carbon Auger structures: (a) as-grown CVD diamond, (b) as-Ni-deposited, (c) after annealing the sample in (b) at 500°C for 2 min.

Details of the carbon Auger structure are shown in Figure 4.2.3-4. The carbon Auger spectrum exhibiting the diamond structure before the Ni deposition (Figure 4.2.3-4, curve (a)) changes slightly after the Ni deposition on this surface; the carbon Auger line shape is indicative of carbidic carbon [13] (Figure 4.2.3-4, curve (b)). After a 2 min heating at 500°C the carbon Auger structure changes completely to that of graphitic carbon.

Figure 4.2.3-5, curve (a), shows a typical electron energy loss spectrum of an as-grown CVD polycrystalline diamond film. The spectrum is similar to that of as-polished natural diamond [14]; the structure is characterized mainly by two losses due to the bulk plasmon excitation (near 34 eV) and to the surface plasmon excitation (near 23 eV). An electron energy loss spectrum taken just after the Ni deposition of approximately 14Å is shown in Figure 4.2.3-5, curve (b). This spectrum is similar to that of Ni [15] or graphite (Figure 4.2.3-5, curve (d); one can assign the 6.7 eV feature to π-plasmon excitation, the 26.5 eV feature to a bulk plasmon excitation and the 11-13 eV feature to an interband transition). Electron energy loss spectra of Ni and graphite have the 6-7eV feature. So distinction between the electron energy loss spectra of Ni and graphite is difficult. A Rutherford backscattering spectrum of this specimen suggests that Ni atoms are located near the surface (Figure 4.2.3-6 (a)). In considering these results and the study of Lurie and Wilson [14], the Ni layer exists at the specimen surface and the Ni carbide layer at the Ni diamond interface. This structure does not change after annealing at 500°C.

Thus, after the Ni deposition on the diamond surface, Ni atoms may break down the electronic structure of the diamond surface, and carbon atoms at the diamond surface may be dissolved in Ni. Then, dissolved carbon atoms can form graphite or Ni carbide at the Ni diamond interface (Figure 4.2.3-5, curve (b), and Figure 4.2.3-7). The carbon atoms at the interface form more stable carbidic bonding than the diamond bonding (Figure 4.2.3-4, curve (b)). The Ni carbide (Ni_3C) structure is similar to graphite and the two structures are not distinguished clearly by EELS. After a 2min anneal at 500°C, carbon atoms located in the Ni film or near the specimen surface seem to change in electronic structure to graphite (Figure 4.2.3-4, curve (c), Figure 4.2.3-5, curve (c) and Figure 4.2.3-7). The weak nature of the Ni

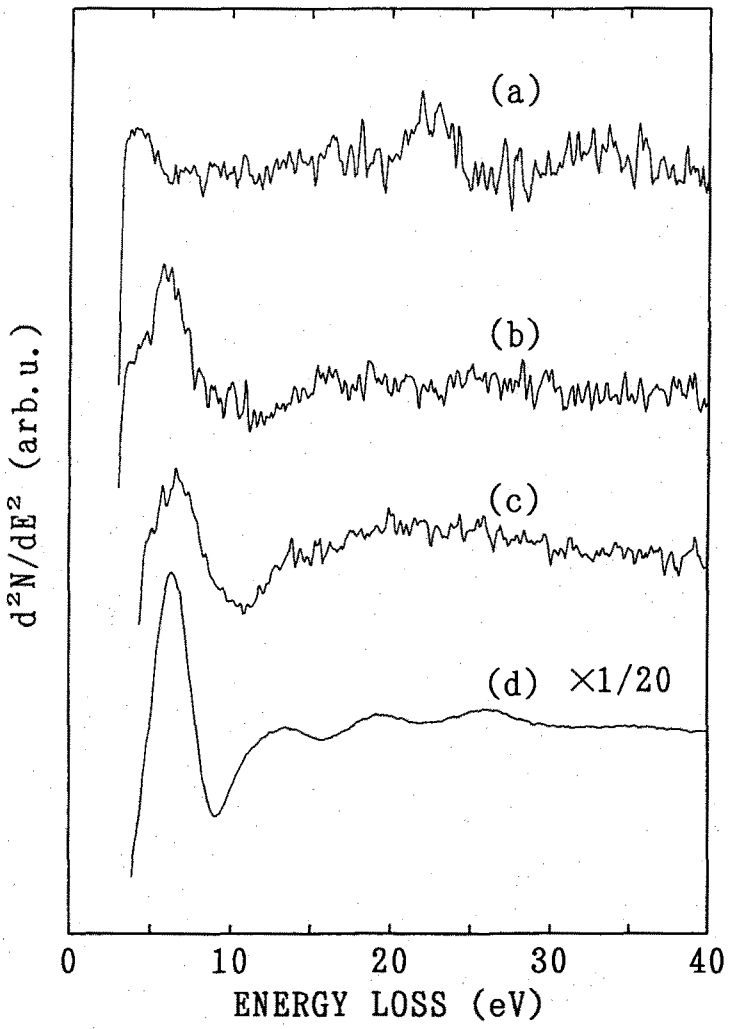

Figure 4.2.3-5. Negative second-derivative EELS spectra at E_p=300 eV for various CVD diamond surfaces: (a) as-grown, (b) after RT Ni deposition (14Å), (c) after annealing (b) to 500°C in vacuum, (d) polycrystalline graphite.

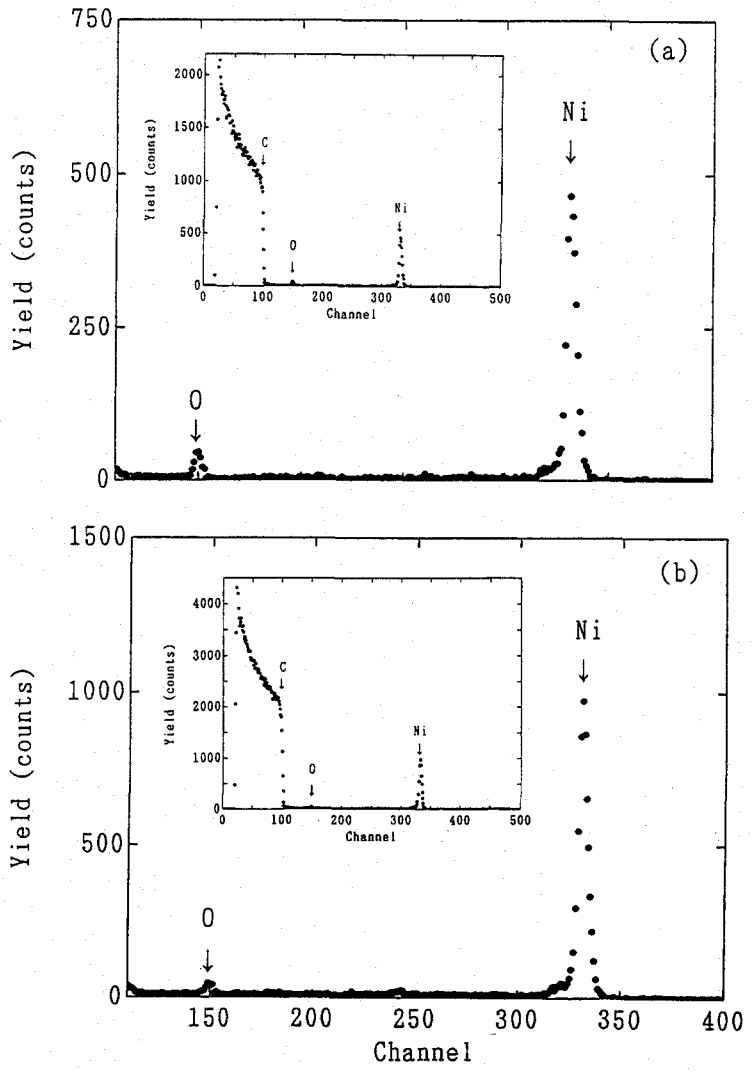

Figure 4.2.3-6. Backscattering spectra of (a) as-Ni-deposited diamond and (b) after 2 min annealing of the sample in (a) at 500°C in vacuum.

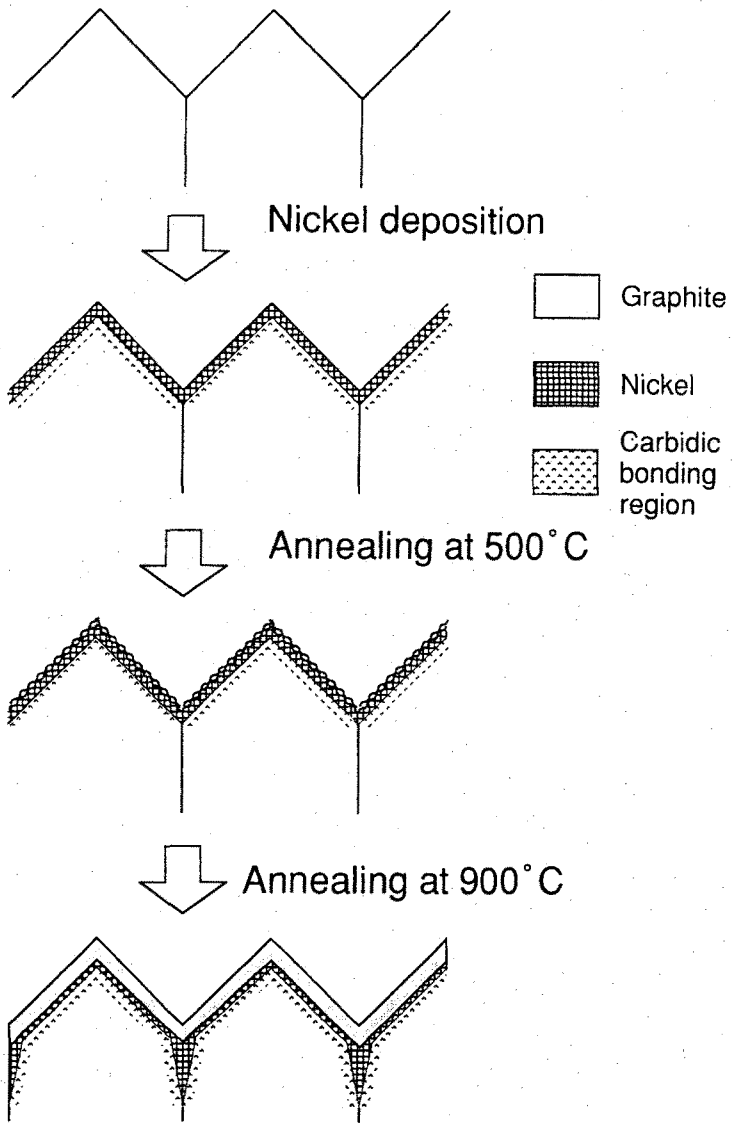

Figure 4.2.3-7. Schematic drawing of the models proposed for the Ni-CVD diamond interfacial reaction.

carbon interactions is evident from the easy exfoliation of the surface layer and from the strong diffusion of Ni atoms at high temperatures (about 900°C).

However, it cannot be determined clearly from Rutherford backscattering spectra whether the Ni atoms are present in the CVD diamond particles or at the grain boundaries of the polycrystalline specimen. The low mutual solubility between carbon and Ni suggests that most of the Ni atoms deposited diffuse into grain boundaries while only a small number of them are located in discussed above, the Ni-covered CVD diamond surface can be significantly graphitized even at temperatures as low as 500°C where no graphitization of the as-grown CVD diamond can occur, This means that the catalytic interaction between carbon and Ni plays diamond particles (Figure 4.2.3-7). As an important role in the graphitization observed. At the low temperature of 500°C, Ni atoms do not diffuse into the inside of diamond particles but remain at the diamond Ni interface to react with carbon atoms owing to the catalytic nature of Ni. As a result, graphite is formed at the specimen surface (Figure 4.2.3-7).

The number of oxygen atoms absorbed to the specimen surfaces after exposure to the air may give information on the reactivity of the top surfaces. The as-Ni-deposited specimen whose top surface was covered with Ni atoms and exposed to air had twice the amount of oxygen as those after annealing at 500 °C (Figure 4.2.3-6). In other words, the latter specimen surface is covered substantially by a carbon layer with much less reactivity to oxygen, and most of the reactive Ni atoms stay below the carbon layer. Similarly, the fact that there is little oxygen at the specimen surface after a 900 °C anneal (Figure 4.2.3-4) is evidence of the Ni diffusion from the top surface into deeper regions (Figure 4.2.3-7).

4.3 Properties of Metal-Diamond Interfaces

It has been suggested that semiconductors can be divided into two categories. Covalently bonded semiconductors like Si, Ge and GaAs have a large density of surface states in the band gap, and the Schottky barrier height in these semiconductors is pinned by the surface states [16]. For ionically bonded semiconductors there are few surface states in the band gap and the Schottky barrier height is determined by the electronegativity. Diamond

is considered as a key material in the field of Schottky barrier theory, due to its unique properties- wide band gap (5.45 eV) and small dielectric constant (5.5) but zero ionicity. In the chapter 3, the author reported that the hydrogen chemisorbed diamond surface exhibits no surface states in the band gap. Therefore, Schottky diode properties should depend on the contact metal. For the device fabrication, device performance depends on the qualities of Schottky contact and ohmic contacts. We must find out the suitable condition of metal-diamond interfaces for practical application. In this section, author reports the properties of various metal-CVD diamond interfaces and the effect of the surface treatment on the properties.

4.3.1 Dependence of Interfacial Properties on the Contact Metal

Fourteen sorts of metals were used to fabricate (point-contact method) the metal/diamond interface, and Table 4.3.1-1 shows the dependence of the I-V characteristic on metals. In most cases, except for Ag and Ni contacts, the point contact rectifying property of metal-CVD diamond interfaces is determined by work function of metal. Furthermore, accordingly to electronegativity of metal, the above two exceptions have been explained. The electronegativity which is closely related to the work function, determines the contact property more accurately without exception at present 14 metals. However, there is a study which shows that the rectifying property of point contact to natural diamond does not depend on work function of the metal [17]. Also it is reported that Schottky barrier height has been measured at Au-natural diamond interfaces [9,18], whereas we obtained ohmic behavior at Au-CVD diamond interface as shown in Table 4.3.1-1. So there should be a certain difference of the surface conditions between natural diamond and CVD diamond formed with $CO(5\%)/H_2$. This difference is discussed later. When some metals such as Ti and Ni, which shows schottky property in point contact, are evaporated on the diamond films, the contact property are observed to be ohmic. This can be explained by that Ti and Ni atoms can react with diamond surface at room temperature as reported in the previous section. On the other hand, the point contact interface of Ti-diamond, where Ti-C reaction does not occur, still has the rectifying property.

Figure 4.3.1-1 shows a schematic of metal-diamond structure used for the measurement

Table 4.3.1-1. Relationship between work function and electronegativity of metals and their contact properties with CVD diamond formed with CO/H_2

Metal	Work Function	Electronegativity	Property
Pt	5.65	2.2	Ohmic
Ni	5.15	1.8	Schottky
Au	5.1	2.4	Ohmic
C	5.0	2.5	Ohmic
Cu	4.65	1.9	Ohmic
W	4.55	1.7	Schottky
Sn	4.42	1.8	Schottky
Zn	4.33	1.6	Schottky
Ti	4.33	1.5	Schottky
Al	4.28	1.5	Schottky
Ag	4.26	1.9	Ohmic
Pb	4.25	1.7	Schottky
Ta	4.25	1.5	Schottky
In	4.12	1.7	Schottky

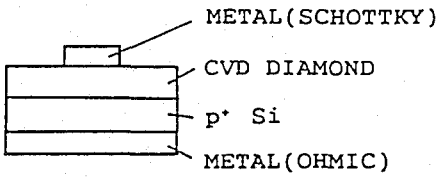

Figure 4.3.1-1. Schematics of metal-CVD diamond structutre used for I-V measurement.

of I-V characteristic. Figures 4.3.1-2 and -3 show the I-V characteristics obtained in the films formed with CO(5%)/H_2. Aluminum was evaporated as a Schottky contact. A high breakdown voltage (200 V) and a high rectification ratio (10^5) have been obtained. Almost the same property has been also observed by point contact method. It should be pointed out that the films formed with CH_4(0.5%)/H_2 shows inferior I-V characteristics as shown in Figure 4.3.1-4 compared with those obtained for the films formed with CO/H_2. From the point of Raman scattering and SEM observation, the crystal qualities of both films are in the same level.

The I-V characteristic of the film formed with 0.5% CH_4 in H_2 turn to be better like Figure 4.3.1-2 after depositing CVD diamond formed with 5% CO in H_2 about 10 min on it. Figure 4.3.1-5 shows the schematic of this structure. This results suggests that difference of these characteristics is due to surface conditions influenced by the reaction gas. Oxygen contained in CO/H_2 have the important roles to form the rectifying property. The effect of oxygen is supposed to be etching of graphite-like surface layers which degrade the rectifying property.

4.3.2 Effect of Surface Treatment on the Interfacial Properties

The author has found that metal-CVD diamond interfacial property depends on the electronegativity of the contact metals. However, a contrary result has also been reported for natural diamonds. The author tries to clarify the reason for the difference between these two results [19,20].

The surface conditions of diamond can affect interfacial property strongly. Four kinds of surface treatments have been carried out, (I) boiling in a saturated solution of CrO_3 in H_2SO_4 at 200°C followed by a rinse in a 1:1 solution of H_2O_2 (30%) and NH_4OH (70%) at 90°C (treatment-A), (II) boiling in a pure H_2SO_4 solution at 200°C (treatment-B), (III) exposing to an O_2 plasma for a few minutes (treatment-C) and (IV) exposing to a H_2 plasma for 5 minutes (treatment-D). Treatment-A is popular in cleaning diamond surfaces [20-22]. The effects of treatment-A and treatment-D on the electrical properties have been previously reported [23] and we have observed similar tendency.

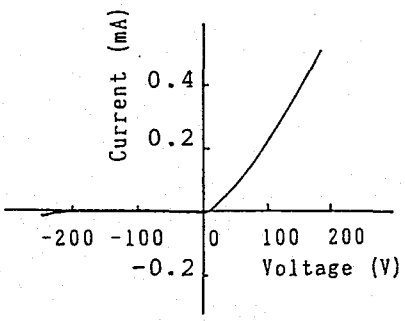

Figure 4.3.1-2. Current-voltage characteristics of Al contact to CVD diamond film formed with CO/H_2.

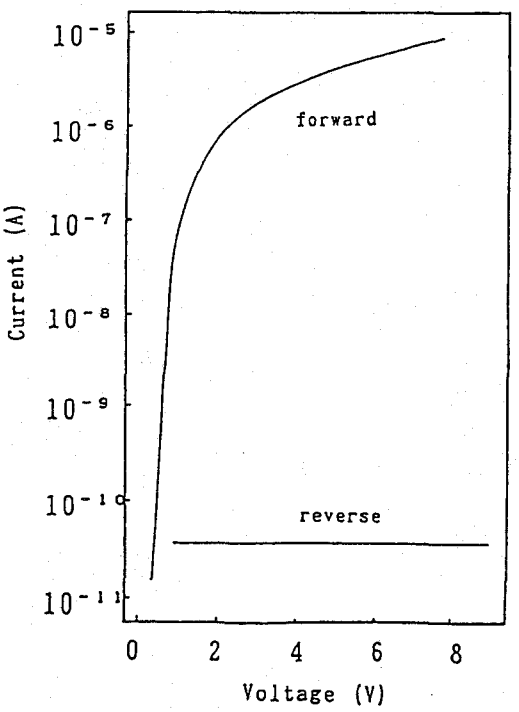

Figure 4.3.1-3. Logarismic plot of I-V characteristics of Al contact to CVD diamond film formed with CO/H_2.

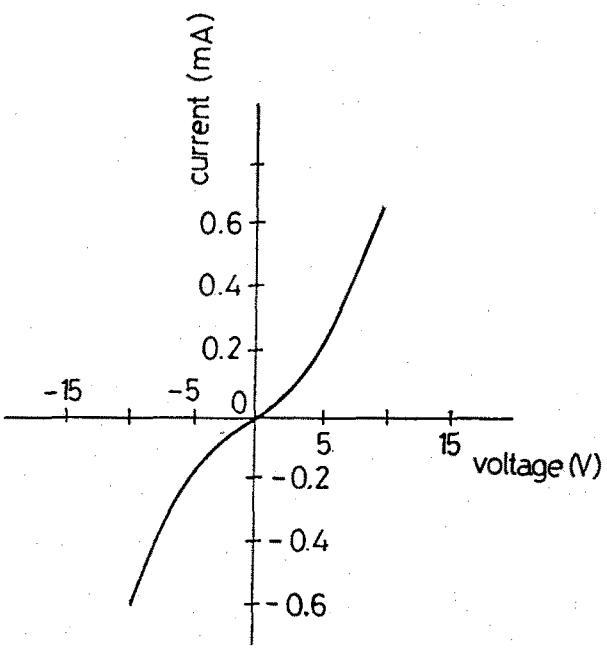

Figure 4.3.1-4. Current-voltage characteristics of Al contact to CVD diamond film formed with CH_4/H_2.

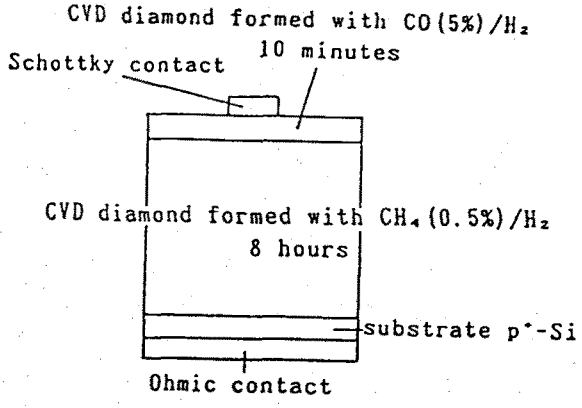

Figure 4.3.1-5. Schematics of metal-CVD diamond (CO/H_2)-CVD diamond (CH_4/H_2) structutre.

Figsures 4.3.2-1 and -2 show the I-V characteristics of evaporated gold and aluminum metal-semiconductor contacts respectively, both before and after treatment-A. The I-V characteristic changes from ohmic to rectifying after treatment-A (Figure 4.3.2-1). Table 4.3.2-1 shows the effects of treatment-A and treatment-C on I-V characteristics obtained from point-contact interfaces between CVD diamond films and 14 kinds of metals. The I-V characteristics obtained from as-grown diamond films depend on the metal, especially its electronegativity. After surface treatment, these dependences disappear and all interfaces show Schottky properties. These changes are due to the change in the surface conditions.

Figsures 4.3.2-3 and -4 show the XPS spectra of CVD diamond surfaces before and after treatment-A, respectively. Very little oxide is present on the as-grown surface of the CVD diamond films although they were formed from CO/H_2 (Figure 4.3.2-3). This result shows that diamond surfaces are stable without surface oxide layers, like other carbon phases such as graphite which also has little native oxide on its surface. Treatment-A, heavy oxidation, covers the diamond surface with oxygen (FIgure 4.3.2-4), and adsorption of oxygen must be the main reason for the change in the I-V characteristics shown in Figure 4.3.2-1.

The effects of treatment-C on I-V the characteristics are same as treatment-A, and the XPS spectra of such diamond films are the same as in Figure 4.3.2-4. However treatment-B has no effect on the I-V characteristics, because it cannot oxidize diamond. A strong oxidation ability is essential for the chemical adsorption of oxygen onto diamond surfaces. Treatment-D removes oxygen from the oxidized diamond surfaces. When the as-grown diamond films have first been subjected to treatment-A and then to treatment-D, their I-V characteristics using Pt, Au and Al as contacts metals were almost the same as those of the as-grown diamond films. From these results, it can be seen that the adsorption of oxygen has a very important role in changing electrical surface structure relating to Schottky barriers of metal-diamond interfaces. Oxygen adsorbed onto diamond surfaces is stable even after annealing at 900°C for 1 hour after treatment-A and we can also see oxygen on them using XPS. One possible explanation is that the surface states induced by oxygen adsorption pin the Fermi level.

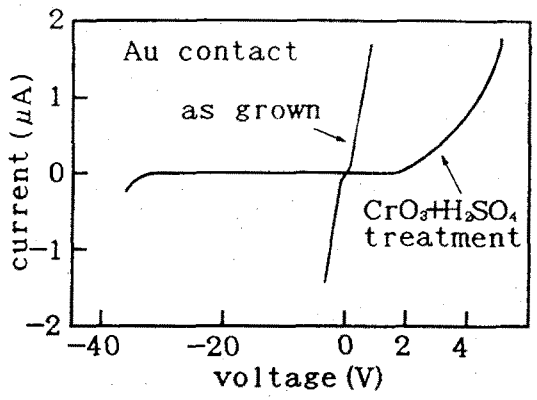

Figure 4.3.2-1. Current-voltage characteristics of a gold contact on CVD diamond with as-grown surface and after treatment-A. The characteristic of a gold to as-grown surface contact shows ohmic behaviour (dashed line). This changes to rectifying behaviour after treatment-A.

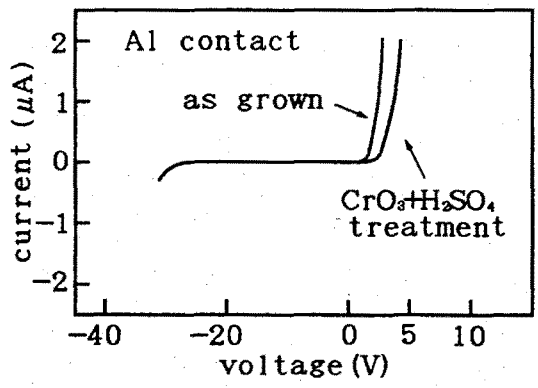

Figure 4.3.2-2. Current-voltage characteristics of an aluminum contact on CVD diamond with as-grown surface and after treatment-A. The characteristic of an aluminum to as-grown surface contact shows rectifying behaviour (dashed line). This is also the case after treatment-A.

Table 4.3.2-1. Relationship between work function (Φ_M) and electronegativity (X_M) of metals, and their contact properties with CVD diamond before (as-grown) and after treatments

Metal	Φ_M (eV)	X_M (eV)	As-grown	After treatment *A*	After treatment *C*
Pt	5.65	2.2	Ohmic	Schottky	Schottky
Ni	5.15	1.8	Schottky	Schottky	Schottky
Au	5.10	2.4	Ohmic	Schottky	Schottky
Cu	4.65	1.9	Ohmic	Schottky	Schottky
Sn	4.42	1.8	Schottky	Schottky	Schottky
Zn	4.33	1.6	Schottky	Schottky	Schottky
Ti	4.33	1.5	Schottky	Schottky	Schottky
Al	4.28	1.5	Schottky	Schottky	Schottky
Ag	4.26	1.9	Ohmic	Schottky	Schottky
Ta	4.25	1.5	Schottky	Schottky	Schottky
In	4.12	1.7	Schottky	Schottky	Schottky

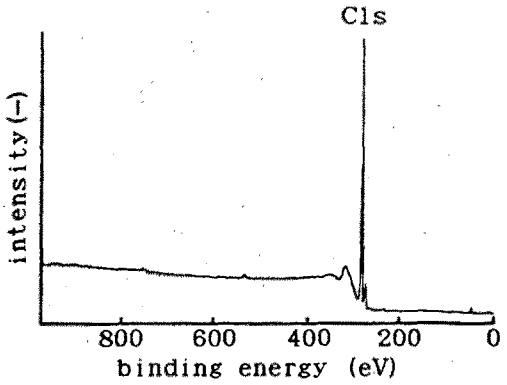

Figure 4.3.2-3. XPS study of the as-grown CVD diamond surface. Little oxide is present on the surface.

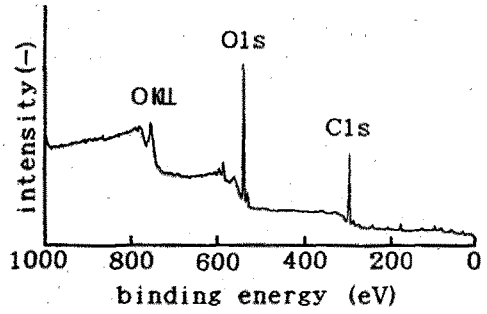

Figure 4.3.2-4. XPS study of CVD diamond surface after treatment-A. Oxygen is present to less than sub-monolayer coverage.

4.3.3 Electroluminescence from Metal-Diamond Interfaces

The electroluminescence (EL) from the Schottky diode of semiconducting diamond film has been investigated for the first time. The author has compared the EL spectra with the CL spectra. Figures 10(a) and 10(b) show EL spectra of the lightly doped and heavily doped diamond films, respectively. The EL is observable when the forward bias exceeds 25 V or the reverse bias exceeds 20 V. The EL spectra are almost the same in the forward and reverse biases. The mechanism of the forward-bias luminescence can be explained by the minority-carrier (electron) injection. The efficiency of minority-carrier injection is expected to be extremely small in the case of the Schottky diode. However, the same kind of phenomenon has been observed in the case of natural type-IIb diamond [17,23]. The reverse-bias luminescence can be explained by electron-hole generation by the avalanche break-down or microplasma breakdown [24]. In Figure 4.3.3-1 (a) , the EL spectrum has a peak at 2.35 eV and a shoulder at 2.7 eV. The CL spectrum measured at 0.2 μA/mm^2 of the same film shows almost the same nature. Also in Figure 4.3.3-1 (b) , the main peak of the EL spectrum, which is in the lower energy region than in Figure 4.3.3-1 (a), is almost equal to that of the CL measured at 2 μA/mm^2. From the correspondence between the EL and the CL in the two different samples, it can be concluded that the luminescent center of EL is equal to that of CL.

The excitations for EL in the present case, i.e., the minority-carrier injection or the generation of electron-hole pairs, are not so efficient that the emission peak occurs at the higher energy region as observed in the CL spectra [25]. However, it can be improved by suitable methods for more efficient excitation. Based on the CL measurements, it is reasonable to expect that boron-doped films as well as undoped films have the potential for far more intense and more blue EL than those obtained in Figure 4.3.3-1.

4.4 Summary

The formation of Au-, Ti- and Ni-CVD diamond interfaces have been studied mainly by EELS. Author has found that there is no chemical reaction at the Au-CVD diamond interface even at 850°C, and that the Au atoms rapidly migrate on the surface. The stable

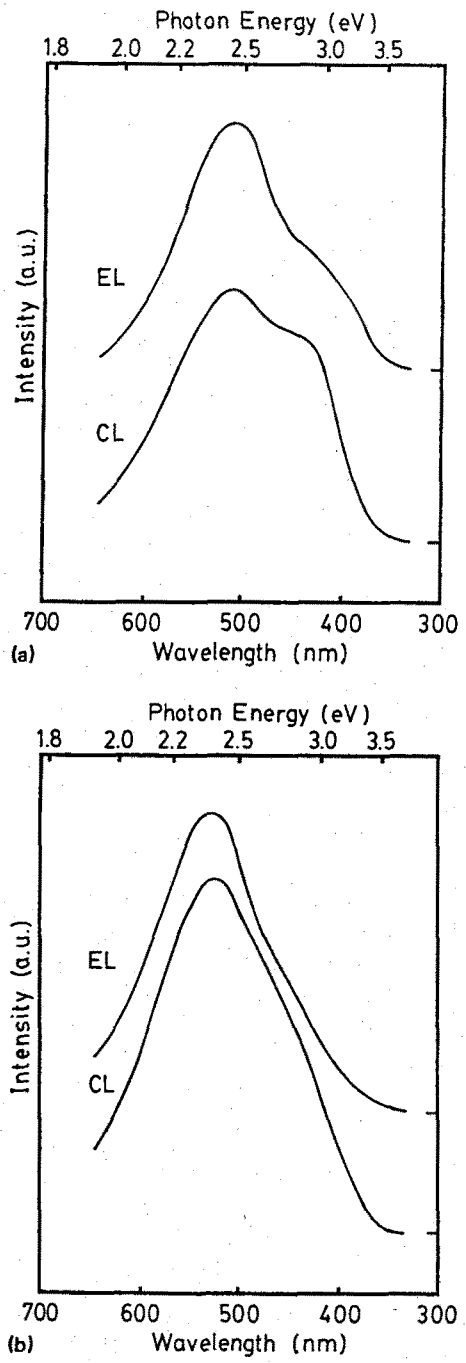

Figure 4.3.3-1. EL spectra and CL spectra of B-doped CVD diamond. EL spectra have been obtained at Schottky diodes. The bias voltages were ~30V. (a) B/C = 200 ppm. (b) B/C = 1000 ppm.

TiC_x can be formed at the Ti-CVD diamond interface immediately at RT. After Ni deposition on as-grown CVD diamond at RT, the electronic structure of specimen surface changes to carbidic and graphitic phases because of the solvent and catalytic nature of Ni. After annealing at 500°C the specimen surface is completely graphitized and, at 900°C Ni atoms diffuse into the diamond film; most of Ni atoms exist at the grain boundaries while only a few of them diffuse into diamond particles.

The interfacial property of evaporated Al contact to the diamond film formed with $CO(5\%)/H_2$ grown on p-Si substrate show a high breakdown voltage (200 V) and a high rectification ratio (10^5). The values are much better than those obtained by CH_4/H_2. At the point contact interfaces, metal-carbon reaction does not occur and the property of these interfaces depends on metals, especially on their electronegativity. Author has investigated the effects of oxidation of the surface of CVD diamond films on the electrical characteristics of Schottky diodes. The I-V characteristics obtained from CVD diamond films without oxygen on their surfaces depend on the metals, especially their electronegativities, but when oxygen is adsorbed onto the diamond surfaces, this dependence vanishes.

Electroluminescence due to the Schottky diode can be obtained at metal-diamond interfaces in the boron-doped polycrystalline diamond. The EL spectra almost coincide with those of CL.

4.5 References

[1] J.C.Phillips: Solid State Comm. 12 (1973) 861.

[2] J.C.Inkson: J. Phys. C6 (1973) 1350.

[3] W.E.Pickett and S.C.Erwin: Surperlattices and Microstructures, 7(1990)335.

[4] T.P.Humphreys, J.V.Labrasca, R.J.Nemanich, K.Das, and J.B.Posthill: Jpn. J. Appl. Phys. 30 (1991)L1409.

[5] T.Ito, M.Iwami and A.Hiraki: J. Phys. Soc. Japan 50 (1981) 2704.

[6] C.C.Chang: Sur. Sci. 48 (1975) 9.

[7] Y.Mori, N.Eimori, J.S.Ma, T.Ito and A.Hiraki: Appl. Surf. Sci. 56-58 (1991) 89.

[8] M.Creuzburg: Z. Physik 196 (1966) 433.

[9] F.J.Himpsel, P.Heimann and D.E.Eastman: Solid States Comm. 36 (1980) 631.

[10] D.W.Lynch, C.G.Olson, and D.J.Peterman: Phys. Rev. B22 (1980) 3991.

[11] P.W.Anderson, Elementary Excitations in Solids, Molecules and Atoms, Part A, Nato Advanced Study Institute Series (Plenum, New York, 1974) p.1.

[12] A.Hiraki: J. Electrochem. Soc.127(1980) 2662.

[13] L.S.Caputi, G.Chiarello and L.Papagno: Surf. Sci. 162 (1985) 259.

[14] P.G.Lurie and J.M.Wilson, Surface Sci., 65(1977)453.

[15] R.Rosei, S.Mondesti, F.Sette, C.Quaresima, A.Savoia and P.Perfetti: Phys. Rev. B29 (1984) 3416.

[16] C.A.Mead: Solid-State Electron 9 (1966) 1023.

[17] M.D.Bell and W.J.Leivo: Phys. Rev. 111 (1958) 1227.

[18] C.A.Mead and T.C.McGill: Phys. Lett. 58A (1976) 249.

[19] C.Hicks, C.R.Wronski, S.A.Grot, G.Sh.Gildenblat, A.R.Badzian, T.Badzian & R.Messier: J. Appl. Phys. 65 (1989) 2139.

[20] G.Sh.Gildenblat, S.A.Grot, C.R.Wronski, A.R.Badzian, T.Badzian and R.Messier: Appl. Phys. Lett. 53 (1988) 586.

[21] M.W.Geis, D.D.Rathman, D.J.Ehrlich, R.A.Murphy, and W.T.Lindley: IEEE Electron Device Lett. EDL-8 (1987) 341.

[22] S.A.Grot, G.Sh.Gildenblat, C.W.Hatfield, C.R.Wronski, A.R.Badzian, T.Badzian & R.Messier: IEEE Electron Device Lett. 11 (1990) 100.

[23] R.Wolfe and J.Wood: Phys. Rev. 105 (1957) 921.

[24] A.V.Bogdanov, I.M.Vikulin and T.V.Bogdanova: Sov. Phys. Semicond. 16 (1982) 720.

[25] H.Kawarada, Y.Yokota, Y.Mori, K.Nishimura and A.Hiraki: J. Appl. Phys. 67 (1990) 983.

5. ION IMPLANTATION IN DIAMOND

5.1 Introduction

One of the key problems in diamond device fabrication is the doping of electrically active n- and p-type dopants into CVD diamond. This is complicated by the extremely low solubility of most elements, except nitrogen and boron, in diamond [1]. As shown in chapter 2, doping of CVD diamond has been carried out using a mixture of the reaction gas and a dopant gas such as B_2H_6, N_2, PH_3 or P_2O_5. Boron doping gives rise to semiconducting p-type diamond with sufficiently low resistivity (~10^{-2} Ohm.cm) [2]. In the cases of nitrogen and phosphorous doping, however, the resistivity of the resulting n-type CVD diamond is too high to be of practical use [3].

Ion implantation, widely used in Si device technology, may also be a useful technique for doping diamond with the desired ions in a controlled manner. Although this method has yielded some successes [4,5], it has been found to be difficult to anneal out the implantation damage without graphitizing the diamond [6,7]. In the case of low doses (< 2 x 10^{15}/cm^2) of 100~200-keV ions of light elements, almost complete recovery of the implantation damage in the bulk region, as measured by means of the RBS/channeling technique, occurs after a suitable subsequent thermal annealing [8]. On the other hand, an increase in ion dose above a critical level, which obviously depends on the ion species and implantation conditions used, causes irreversible amorphization of diamond, leading to graphitization during subsequent annealing [7]. This is in contrast to the case of silicon where amorphous Si created during implantation can regrow epitaxially under subsequent thermal annealing. It is more difficult to anneal out the implantation damage without causing graphitization for shallower implantations, which are indispensable for thin-film device fabrication, because the graphitization of the CVD diamond film occurs from the surface during annealing due to its thermodynamical instability [9]. Accordingly, the damaged surface of diamond cannot regrow during an equilibrium processes, such as thermal annealing. One must therefore develop a new method, using non-equilibrium processes, to replace the commonly used thermal annealing

in order to overcome the graphitization problem.

In this chapter, the author reports on the ion implantation in diamond and proposes new method, a hydrogen plasma treatment, to anneal out implantation damage. The effect of hydrogen plasma treatment on implantation damage and electrical properties is also discussed.

5.2 Implantation Damage in Diamond Films

5.2.1 Hydrogen Plasma Treatment

The author proposes a hydrogen plasma treatment to anneal out implantation damage in CVD diamond. This is because hydrogen in reaction with the diamond surface induces sp^3 hybridized carbon atoms [10], which can lead to further growth of CVD diamond. In this section, the author has examined N as an implant because only N gives rise to specific groups of cathodoluminescence (CL) lines, such as the 389-nm center [11]. To clarify the effects of the ion implantation and the subsequent treatments on and near the surface region of diamond, N ions with relatively low energy (10 keV) were used. The remarkable effects of the hydrogen plasma treatment on the implantation damage are described and compared with those of the more commonly used thermal annealing process.

Diamond films were synthesized by means of a μ-wave plasma CVD method on Si substrates. A dilute B_2H_6 gas was used to synthesize semiconducting diamond to prevent charging of the specimens during electron microscopy measurements. The details of the present CVD have been described in chapter 2. Ion implantations of $10^{15}/cm^2$ were performed at room temperature using 10-keV N ions. After the implantation, some of the samples were annealed at 900°C in a vacuum (10^{-6} Torr range) and others were exposed to a hydrogen μ-wave plasma at 30 Torr. The specimen temperature measured was automatically increased to 900°C during the hydrogen plasma treatment. Samples examined in the present study are summarized in Table 5.2.1-1.

5.2.2 Effects of Hydrogen Plasma Treatment on Implantation Damage

Figure 5.2.2-1 shows EELS spectra of samples 1-4 presented as the negative second derivative of the electron energy distribution at a primary electron energy E_p of 300 eV. The characteristic losses of as-deposited diamond (sample 1) are similar to those of the as-polished natural diamond [12]. One can assign the 34, 22 and 15-eV features to bulk plasmon excitation, surface plasmon excitation and an interband transition, respectively [12]. For as-implanted CVD diamond (sample 2), obvious implantation-induced amorphization was observed in the surface region of the specimen, occurring even for a low ion dose (10^{15} ions/cm^2). This is indicated by the fact that the characteristic losses changed from those of sample 1 after the implantation. For CVD diamond annealed thermally after the implantation (sample 3), loss features due to the p-plasmon loss and the interband transition of graphite appear at 6.7 and 13 eV [12], respectively, while the losses originating from diamond, such as 34 and 15-eV features, disappear in the EELS spectrum. This indicates that it is difficult to avoid the anneal-induced surface graphitization of the implanted CVD diamond even for such low doses. In contrast, the same loss spectrum as that of as-deposited diamond (sample 1) was obtained from CVD diamond treated by hydrogen plasma after the implantation (sample 4), indicating that the damaged layer may be removed and/or be reconverted to the diamond structure by the hydrogen plasma treatment.

Figure 5.2.2-2 shows SIMS depth profiles of N obtained from samples 1 and 4. The peak concentration (4 x 10^{20} /cm^3) of the N profile of sample 1, called the projectile range RP, is located at ~20 nm below the surface. After the hydrogen plasma treatment, the peak concentration of N atoms (>10^{20} /cm^3) corresponds to the surface region (sample 4). This indicates that the hydrogen plasma treatment can remove damaged layers between the original specimen surface and the RP region. The new surface, which was buried near the RP region before the hydrogen plasma treatment, is considered to be free from the damage since both EELS spectra for sample 1 and 4 are identical. Note that substantial radiation damage always exists around the RP region after an implantation. These facts imply that the hydrogen plasma cannot remove the whole of the damaged layer and therefore that the residual damaged

Table 5.2.1-1. Summary of the specimens examined in the present Study

Sample	Implantation of nitrogen ions	Subsequent treatment
1	No	No
2	Yes	No
3	Yes	TA
4	Yes	HPT

TA: thermal annealing at 900°C.
HPT: hydrogen plasma treatment at 900°C.

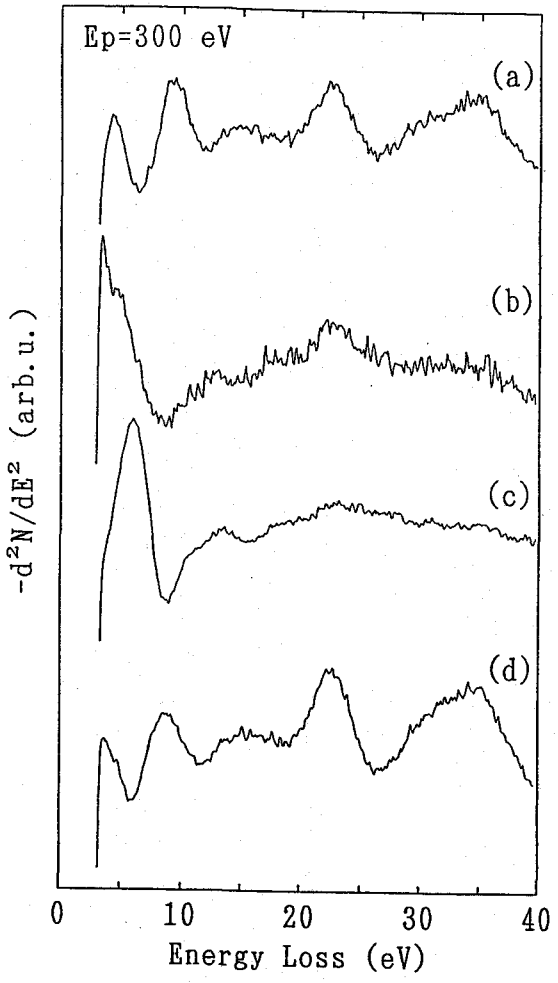

Figure 5.2.2-1. Negative second-derivative EELS spectra at E_p=300 eV for different samples. Curves (a)-(d) were measured for samples 1-4, respectively. The details of the specimens are listed in Table 5.2.1-1.

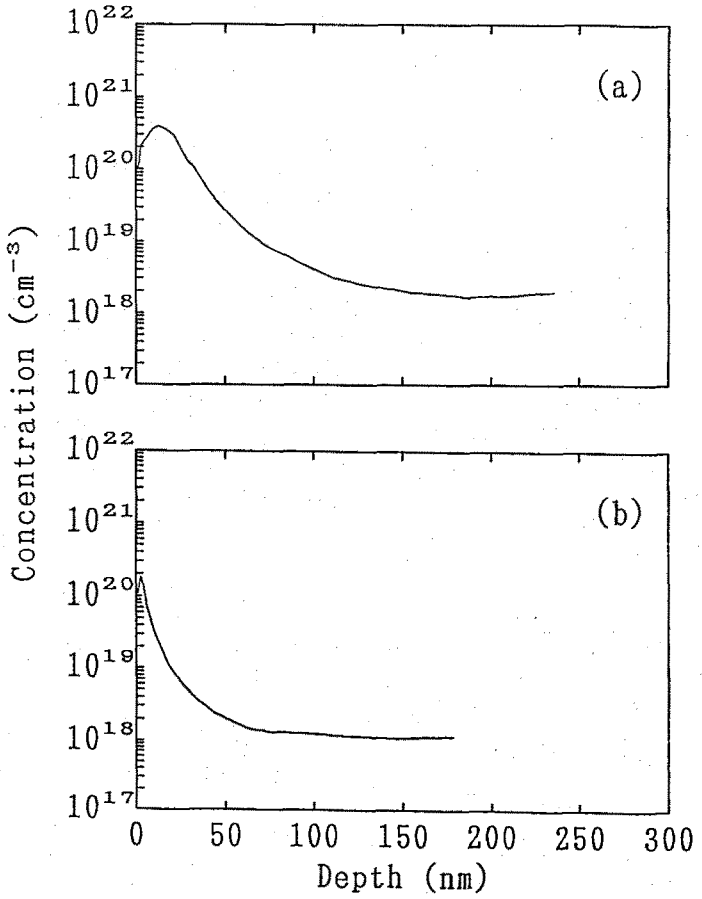

Figure 5.2.2-2. SIMS depth profiles of nitrogen measured for (a) sample 1 and (b) sample 4 shown in Figure 5.2.2-1.

layers containing a large concentration of implants recover the original crystal structure during exposure to the hydrogen plasma.

Figure 5.2.2-3 shows the CL spectra taken for samples 1 and 4. CL is a powerful technique for investigating crystallinity, impurities, and defects in a region of a several tens of nm below the specimen surface [13]. Accordingly the present CL measurements probe the RP region. The spectrum of sample 1 is composed of two components, a broadband luminescence, called band A, with its peak at 425 nm and the shoulder around 520 nm attributed to the doped B atoms [14].

No emissions can be observed from samples 2 and 3, implying that the diamond layers between the surface and the RP region are too damaged to emit luminescence and cannot be recovered by means of the thermal annealing. On the other hand, strong emissions with a clear structure of a zero-phonon line at 389 nm and phonon replicas were observed for sample 4. The color center attributed to the 389-nm emission is due to implanted N interstitial or their complexes with defects [15]. The emission of band A is reduced in intensity by the ion implantation, while a broadband luminescence at 500 nm, attributed to doped B, is still intense in the spectrum of sample 4. Similar results have been reported for the B-doped CVD diamond after 20-MeV electron irradiation followed by a thermal annealing at 900°C [16].

The SIMS result suggests that the damaged layers between the surface and the RP region are etched away during the hydrogen plasma treatment. Moreover, there is a possibility that the remaining damaged layers which escaped from the hydrogen plasma etching may somehow be reconverted to the crystalline diamond structure by the hydrogen plasma. Hydrogen atoms may possibly penetrate into the damaged region to induce rehybridization of distorted bonding orbitals of the damaged carbon atoms and so complete sp^3-orbitals during a hydrogen plasma treatment. Similar effects may be expected in a hydrogen ambient containing radical hydrogen atoms, which are consider to be essential.

5.3 Electrical Doping of Diamond Films by Ion Implantation

The electrical properties of homoepitaxial diamond films implanted with B and P ions

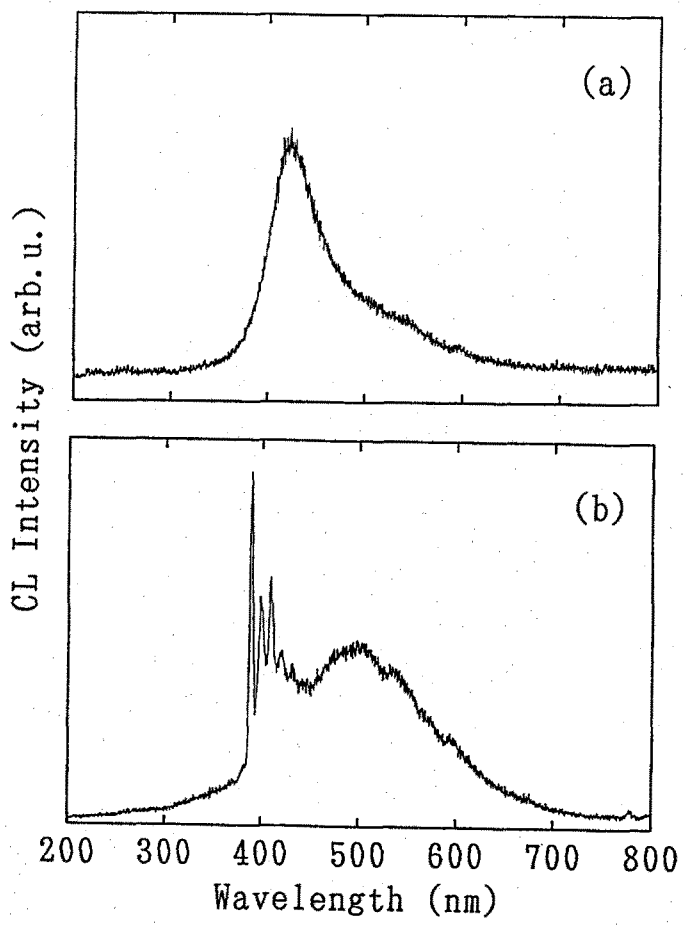

Figure 5.2.2-3. CL spectra at room temperature, aquired with a 5-keV electron beam from (a) sample 1 and (b) sample 4 shown in Figure 5.2.2-1.

have been examined by measuring resistance as a function of temperature. Ion implantations of 10^{15} /cm^2 were performed at room temperature using 100-keV B ions. A Monte Carlo simulation for this implantation energy gave a projected range of ~1800 with the peak concentration of ~10^{20} /cm^3. After implantation, some of the samples were annealed at 900°C in a vacuum (10^{-6} Torr range) and others were exposed to a hydrogen microwave plasma at 30 Torr. Hydrogen plasma treatment caused the temperatures of these specimens to rise to 900°C, the same level as the other samples during annealing. Samples examined in the present study are summarized in Table 5.3-1. After the thermal annealing or hydrogen plasma treatment, specimens were exposed to air when they were at high temperature to remove the surface conductive layer by reaction with oxygen [17]. Therefore, resistivity of HPHT synthesized and CVD diamonds without implantation could not decrease after these treatments. This indicates that the conductive mechanism examined in this paper is caused not by surface graphitization or hydrogenation but by ion implantation. Electrical contacts to the samples were made by evaporation of Ti dots, previously shown in chapter 3 to make ohmic contacts.1 The contact area and the separation distance between electrodes were about ~1 mm and ~1 mm, respectively. For resistance measurements, the two-point probe technique was used. The current-voltage characteristics were measured using a Keithly 237 high-voltage source measurement unit. Care was taken to ensure that samples were exposed to N gas during measurement.

5.3.1 Electrical Properties of Ion Implanted Diamond Films

Figure 5.3.1-1 shows the resistance versus reciprocal temperature measured for the B-implanted (111) HPHT synthesized and (111) and (100) homoepitaxial diamond with subsequent thermal annealing. For sample 1, the resistance is low and does not change much with increasing temperature. The activation energy (Ea) estimated from the slope of the R-1/T curves is ~0.046 eV. Similar results have been reported for the case of B-implanted natural diamond after a subsequent thermal annealing [5]. Sample 1 is light brown, differing from the specimens before implantation which are yellow. These results indicate that sample

Table 5.3-1. Summary of the subsequent treatments of B-implanted diamonds and their electrical properties

Sample	Diamond	Subsequent treatment	Resistance at 300 K (Ω)	Activation energy (eV)
1	HPS(111)	TA	2.2×10^{4}	~0.046
2	CVD(111)	TA	7.8×10^{10}	~0.23
3	CVD(100)	TA	7.9×10^{9}	0.25~0.18
4	HPS(111)	HPT	1.4×10^{11}	0.45~0.27
5	CVD(111)	HPT	9.4×10^{9}	~0.27
6	CVD(100)	HPT	8.9×10^{8}	0.35~0.28

HPS: high-pressure synthesized diamond.
CVD: homoepitaxial CVD diamond on HPS diamond.
TA: thermal annealing at 900°C for 30 min.
HPT: hydrogen plasma treatment at 900°C for 30 min.

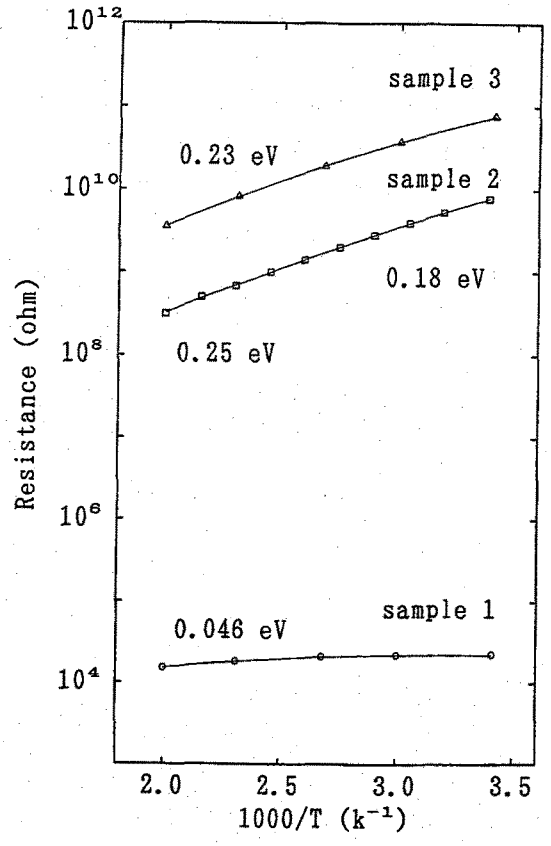

Figure 5.3.1-1. Electrical resistance as a function of inverse absolute temperature for samples 1-3. See Table 5.3-1 for the treatments of individual samples.

1 contains significant conductive damaged layers. These layers are not removed by the thermal annealing at 900°C. Although samples 2 and 3 underwent the same annealing process as sample 1, they exhibit higher resistance and Ea than sample 1, as shown in Figure 5.3.1-1. This means that a conductive damaged layer, such as a graphitic phase, exists only in a small amount in samples 2 and 3. This result suggest that resistance against radiation damage of the CVD diamond is better than that of the HPHT synthesized diamond. Additionally, Raman scattering study provided indirect support for the strong resistance against radiation damage of CVD diamond [18]. The 1332 cm^{-1} peak decreased significantly in the HPHT synthesized case compared with the CVD case after ion implantation. Although the reason for this difference remains unclear, it seems to be a higher hydrogen concentration in CVD diamond. These results suggest the substantial advantages of CVD diamond for ion implantation.

Figure 5.3.1-2 shows the electrical resistance as a function of inverse temperature for the HPHT synthesized, (111) and (100) films after B implantation followed by hydrogen plasma treatment. Compared to sample 1, sample 4 shows a higher resistance and Ea. This suggests that only a small amount of damage remains in the implanted diamond layer after exposure to the hydrogen plasma. For B-implanted (111) and (100) films, better electrical properties were observed after the hydrogen plasma treatment compared with the thermal annealing case. Samples 5 and 6 exhibit lower resistance and an Ea nearer the reported value of 0.37 eV for natural-type IIb diamond compared with samples 1 and 2, respectively. Hence, hydrogen plasma treatment seems to have a more positive effect on electrical activation of implanted dopants and/or passivation of electrically active defects produced by implantation in the CVD diamond. The Ea of sample 6 is 0.35 eV at higher temperatures, which is in close agreement with the value of 0.37 eV, indicating a high rate of substitution of B atoms. The resistance of the (100) films is about one order of magnitude less than that of the (111) films for both thermal annealing and hydrogen plasma treatment cases, and sample 5 exhibits a lower Ea of 0.27 eV than that of sample 6. Although the reason for this difference remains unclear, it seems that the electrical properties of B-implanted CVD diamonds depend upon their own crystallinity. Here we note that the (100) film has a better crystallinity than the

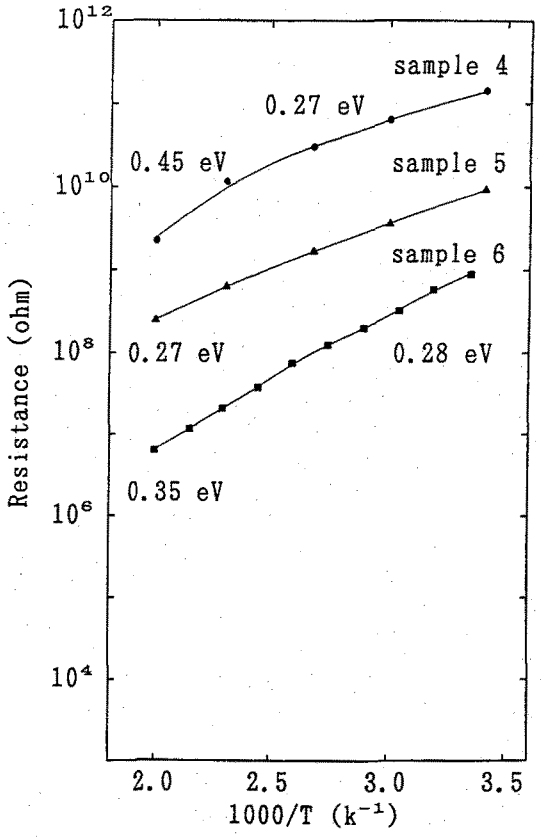

Figure 5.3.1-2. Electrical resistance as a function of inverse absolute temperature for samples 4-6. Details of sample treatment are given in Table 5.3-1.

(111) film. The slightly lower Ea values of samples 5 and 6 at lower temperatures appear to contribute to conduction though variable range hopping between acceptor centers produced by substituted B atoms and defects. The type of hydrogen which affects electrical properties is unknown at present; therefore, the diffusion rate in diamond during hydrogen plasma treatment cannot be determined because it is complicated by the existence of several charge states of hydrogen, and by the fact that hydrogen is present in a number of different forms [19].

In order to attempt to obtain n-type conductivity, P ions were introduced into HPHT synthesized and CVD diamond (100) films by ion implantation. Ion implantations of 10^{14} /cm^2 were performed at room temperature using 170-keV P ions. The fluence of P ions is one order of magnitude smaller than that of B ions because heavier ions induce greater implantation damages in diamond. After implantation, some of the samples were annealed at 900°C in a vacuum (10^{-6} Torr range) and others were exposed to a hydrogen μ-wave plasma at 30 Torr. Diamond films exhibited a substantial difference in electrical properties compared to HPHT synthesized diamond after P implantation followed by thermal annealing. This result corresponds well with that obtained for B implantation. The resistance of P-implanted HPHT synthesis diamond was low, ~10^5 Ohm, and does not change with increasing temperature. On the other hand, P-implanted CVD diamond (100) film showed high resistance over 10^{13} Ohm. In case of hydrogen plasma treatment, P-implanted diamond films also exhibited high resistance over 10^{13} Ohm. It is difficult to introduce electrically active P by ion implantation method.

5.4 Summary

The effect of thermal annealing and hydrogen plasma treatment of CVD diamond layers implanted with 10-keV N ions to 10^{15} /cm^2 have been characterized using EELS, SIMS and CL. The damaged layers produced by the implantation are subjected to significant graphitization during conventional thermal annealing even for low dose implantations (>10^{15} /cm^2). In contrast, after exposure to a hydrogen plasma, the damaged layers of CVD diamond can be at least partially removed without leaving any graphitic phase in the specimen, and

furthermore, material containing a large concentration of implanted N atoms may be obtained.

Homoepitaxial diamond films exhibited a substantial difference in electrical properties compared to HPHT synthesized diamond after B and P implantations followed by thermal annealing. The resistance and Ea observed for the homoepitaxial diamond films were much higher than those for the HPHT synthesized diamonds, indicating a better resistance against radiation damage. The hydrogen plasma treatment produced lower resistance in B-implanted homoepitaxial films compared to the thermal annealing. Moreover, the activation energy of ~0.35 eV, which is near the energy expected for the substitutional B acceptor in diamond, was observed for the (100) films after B implantation followed by hydrogen plasma treatment. The P-implanted diamond films both followed by thermal annealing and hydrogen plasma treatment were highly electrically resistive, with resistance of over 10^{13} Ohm.

5.5 References

[1] J.E.Field: The Properties of Diamond (Academic Press, New York, 1979).

[2] A.T.Collins: Proc. Mater. Res. Soc.162 (1990) 3.

[3] N.Fujimori, T.Imai and A.Doi: Vacuum 36 (1986) 99.

[4] G.Braunstein and R.Kalish: J. Appl. Phys. 54 (1983) 2106.

[5] J.F.Prins: Phys.Rev.B 38 (1988) 5576.

[6] G.Braunstein, A.Talmi, R.Kalish, T.Bernstein and R.Baserman: Radiat. Eff. 48 (1980) 138.

[7] R.Kalish, T.Bernstein, B.Shapiro and A.Talmi: Radiat. Eff. 52 (1980) 153.

[8] G.S.Sandhu, B.Liu, N.R.Parikh, J.D.Hunn, M.L.Swanson, Th.Wichert, M.Deicher, H.Skudik, W.N.Lennard and I.V.Mitchell: Proc. Mater. Res. Soc.162 (1990) 189.

[9] Y.Mori, N.Eimori, J.S.Ma, T.Ito and A.Hiraki: Appl. Surf. Sci. 56-58 (1992) 89.

[10] B.B.Pate: Surf. Sci. 165 (1986) 83.

[11] P.J.Dean: Phys. Rev.139A (1965) 588.

[12] P.G.Lurie and J.M.Wilson: Surf. Sci. 65 (1977) 476.

[13] J.Christen, M.Grundmann and D.Bimberg: Appl .Surf. Sci. 41-42 (1989) 329.

[14] H.Kawarada, Y.Yokota, Y.Mori, K.Nishimura and A.Hiraki: J. Appl .Phys. 67 (1990) 983.

[15] A.M.Zaitsev, A.A.Gippius and V.S.Vavilov: Sov. Phys. Semicond. 16 (1982) 252.

[16] Y.Yokota, H.Kotsuka, T.Sogi, J.S.Ma, H.Kawarada, K.Matsuda, M.Hatada and A.Hiraki: Diamond & Related Matr.

[17] Y.Mori, A.Hatta, T.Ito and A.Hiraki: Jpn. J. Appl. Phys. 31 (1992) L1718. [18] Y.Mori: unpublished.

[19] S.J.Pearton, J.W.Corbett and J.T.Borenstein: in Proc. 6th ICTP-IUPAP Semiconductor Symp. on Hydrogen in Semiconductors, eds. M.Stutzmann and J.Chevallier (North-Holland, Netherlands, 1991), pp. 85-97.

6. HYDROGEN ENHANCED OXYGEN DIFFUSION IN DIAMOND

6.1 Introduction

Ion implantation method and mixing method of dopant gas into reaction source gas during crystal growth show difficulty in introducing n-type dopant, such as P, into diamond as discussed in chapter 2 and 5. The another method to dope diamond is to use a diffusion process. Diffusion of impurities into semiconductors exhibits an advantage that it causes less structural defects compared with ion implantation. Therefore, the subsequent annealing is not requested for impurity diffusion process. The strong covalent bond and small lattice constant of diamond, however, make solubility and diffusivity of the most elements extremely small. An ultrashallow boron-doped layer has been created by the rapid thermal processing (RTP) solid-state diffusion using boron nitride as the dopant source [1]. The RTP condition, however, requested annealing temperature of ~1400°C which is too high for the practical application. It is difficult to introduce impurities, except B and N, into diamond by RTP. We need to develop a new method instead of thermal diffusion in order to utilize diffusion process for doping of diamond.

In this chapter, a hydrogen enhanced oxygen diffusion in diamond discovered by the present author are reported. The process contains a CrO_3 treatment followed by an exposure to a hydrogen plasma. The results of Raman scattering spectroscopy reveal that the present process does not induce any detectable damages. It is found that the doped oxygen atoms induce new cathodoluminescence (CL) centers in the band gap of the diamond.

6.2 Oxygen Diffusion into Diamond Induced by Hydrogen μ-wave Plasma

High-pressure high-temperature (HPHT) synthesized diamond, and homoepitaxial single-crystalline and polycrystalline CVD diamond films were used in this study. Oxygen atoms were diffused into the CVD diamond by the following process (called treatment-A): boiling in a saturated solution of CrO_3 in H_2SO_4 at 200°C, followed by a rinse of hot (90°C) solution of H_2O_2 (30%) and NH_4OH (70%); then, the specimens were finally exposed to a

hydrogen microwave plasma in 10 Torr for 45 min. The specimen temperature was increased up to 800°C. For Rutherford backscattering spectrometry (RBS) measurements, we employed a Pelletron accelerator (NEC: model 3S-10R) equipped with a computer-controlled precise goniometer having two-angular and two-translational motions. All the present RBS data were taken using 1.0-MeV He ions. For CL experiments, a scanning electron microscope (SEM) apparatus (JEOL :model JSM-840) equipped with a parabolic mirror, a monochromator, and a photomultiplier suitable for photons with energy of 2.0~6.0 eV was used. Typical accelerating voltages of the incident electrons ranged from 5 to 10 keV. The electron beam currents used were 1~3 x 10^{-8} A. All the CL measurements were performed at room temperature (RT).

Figures 6.2-1 show RBS spectra measured for the homoepitaxial CVD diamond of as-grown (a), after CrO_3 treatment (b), and after treatment-A (c). The concentrations of impurities such as nitrogen in the specimen whose atomic numbers are greater than that of the host carbon atoms can be easily evaluated from the RBS data. The values obtained for the as-grown CVD diamond were less than 10^{15} atoms/cm^3. After the CrO_3 treatment, oxygen, sulfur, and chromium remain on the surface of the CVD diamonds (Figure 6.2-1 (b)). Since the effects of the CrO_3 treatment on the interfacial properties of metal-CVD diamonds and on the stabilization of diamond surfaces have already been reported by the authors [2,3].

The author has found a very interesting phenomenon in which a suitable hydrogen plasma can induce substantial diffusion of the oxygen atoms into the CVD diamond, as shown in Figure 6.2-1 (c). This is also the case for the HPHT synthesized diamond. On the other hand, the sulfur and chromium atoms deposited can be simply removed from the specimen surface without detectable diffusion into the bulk after the exposure to the hydrogen plasma. From the RBS spectrum shown in Figure 6.2-1 (c), we can see that the oxygen atoms of about 10^{20} atoms/cm^3 distribute homogeneously in the diamond to the depth of at least 300 nm from the specimen surface. Figure 6.2-2 shows the Raman spectrum obtained from a polycrystalline CVD diamond after treatment-A. The only clear in the figure observed is the peak located at 1333 cm^{-1} which is related to the sp^3 hybrid orbitals of the carbon atoms. No noticeable change of the Raman peak intensity was observed between the specimens before

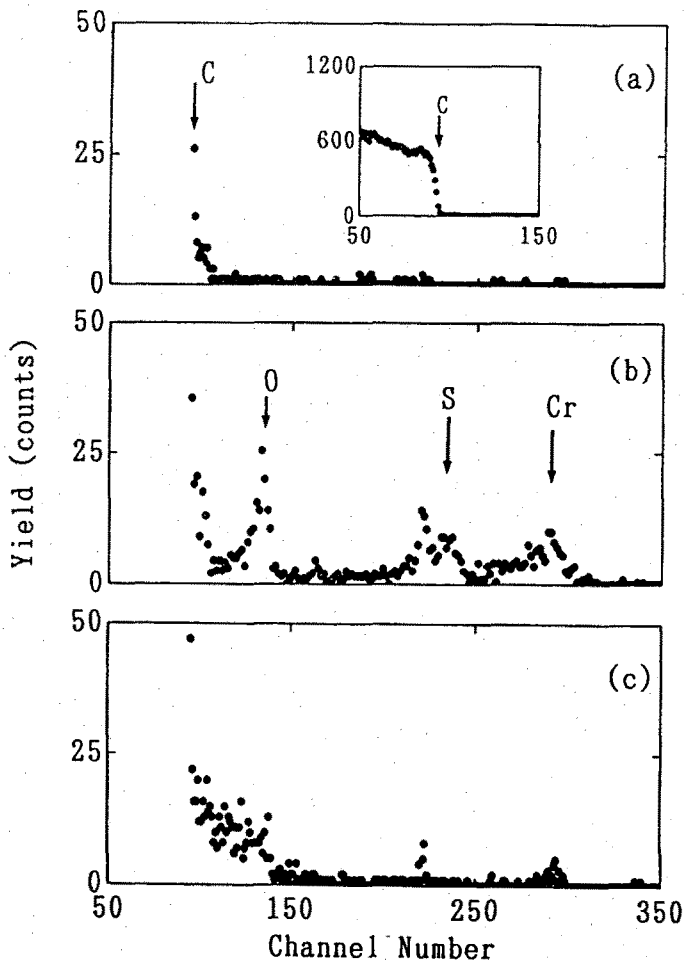

Figure 6.2-1. Backscattering spectra for 1.0-MeV He ions incident on a samples of (a) the as-grown CVD diamond, (b) the CVD diamond after CrO_3-treatment, and (c) the CVD diamond after treatment-A.

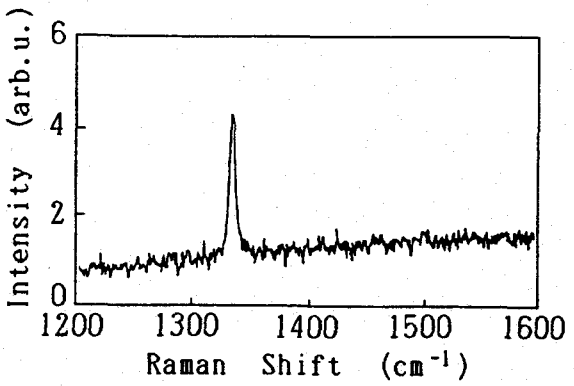

Figure 6.2-2. Raman spectrum of the CVD diamond after treatment-A.

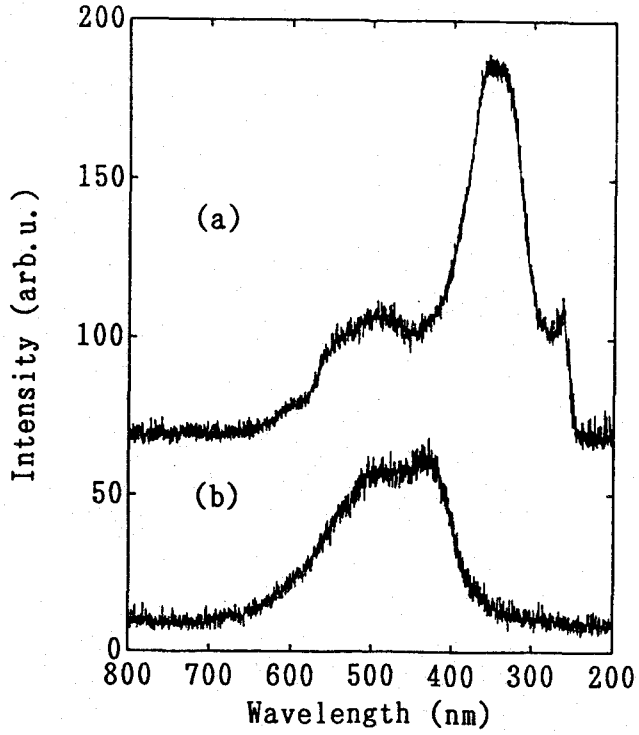

Figure 6.3-1. CL spectra of (a) the CVD diamond after treatment-A and (b) the as-grown CVD diamond.

and after treatment-A. However, note that the Raman scattering investigation of diamond is not always very sensitive to damages in the specimen. For example, clear Raman peaks at 1333 cm^{-1} can be observed for CVD diamond films even after ion implantation using 100-keV nitrogen ions $<10^{15}$ $/cm^2$, while further dosage of N ions decreases the Raman intensity. Thus, treatment-A might induce damages in the specimen less than that for detectable amounts of the Raman scattering technique.

Although a reason of this enhanced oxygen diffusion is not cleared yet, it seems to be catalysed by diffusing hydrogen into diamond during hydrogen plasma treatment.

6.3 Cathodoluminescence of Oxygen Diffused Diamond

The information concerning impurity-induced electronic states in the band gap can be obtained by CL measurements. For example, nitrogen, the most common impurity in the diamond, can be induced to various luminescence centers, such as the H3 or N3 center. Their energy levels are located at 2.985 eV and 2.45 eV in the CL spectra, respectively [4]. However, oxygen is a rare impurity in diamond and has not yet been reported to produce a luminescence center in diamond.

For the first time, the author found new luminescence centers attributed to oxygen. Figures 6.3-1 (a) and (b) show typical CL spectra observed at RT for the specimen after treatment-A and as-grown specimen, respectively. A new feature observed is characterized by two peaks located at 4.64 and 3.75 eV (Figure 6.3-1 (a)). The CL spectrum observed for the CVD diamond after an exposure to the hydrogen plasma is, however, essentially the same as that for the as-grown CVD diamond. This is also the case for the CVD diamond after the CrO_3 treatment without a hydrogen plasma treatment. Therefore, the new features could not have originated from hydrogen atoms possibly introduced into the diamond during the plasma treatment.

The author considers effects of the doped oxygen on the CL centers. In this case, it is important to compare the probing depth for the CL experiments with that of the RBS measurements. In order to estimate the penetration depth of incident electron beam, Kanayama's

equation [5] was applied to the case for diamond. The estimated penetration depth in the diamond is about 280 nm for the electron beam with 5-keV energy. Thus, the depth region examined in the CL measurements corresponds well to that examined in the RBS measurements. Therefore, the feature near 3.75 eV should be attributed to the doped oxygen atoms since no previous reports about such a feature attributed to other impurities. Although the feature near 4.64 eV may appear to come from the 5RL center (4.581 eV), which originates from interstitial carbon atoms, the CL intensity observed at RT is too strong compared to that of the typical 5RL center. Furthermore, its peak position (4.64 eV) is different from a value (4.581 eV) reported for the 5RL center. Therefore, the feature near 4.64 eV should also be attributed to the doped oxygen atoms or a possible complex of the oxygen and defects such as interstitial carbon atoms.

6-4. Summary.

It is found that hydrogen can enhance oxygen diffusion into diamond. Oxygen can easily be introduced into both the CVD diamond and HPHT synthesized diamond by a CrO_3 treatment followed by an exposure to a hydrogen plasma. The resultant depth distribution of the doped oxygen atoms is homogeneous and the concentration is typically about 10^{20} atoms/cm^3. The doped oxygen atoms can produce new CL centers giving two luminescence peaks at 3.75 and 4.64 eV.

6.5 References

[1] W.Tsai, M.Delfino, D.Hodul, M.Riaziat, L.Y.Ching, G.Reynolds and C.B.Cooper, IEEE Electron Device Lett. 12 (1991) 157.

[2] Y.Mori, H.Kawarada and A.Hiraki: Appl. Phys. Lett. 58 (1991) 940.

[3] Y.Mori, N.Eimori, J.S.Ma, T.Ito and A.Hiraki: Appl. Surf. Sci. 56-58 (1992) 89.

[4] J.Walker: Rep. Prog. Phys. 42 (1979) 1605.

[5] K.Kanaya and S.Okayama: J. Phys. D5 (1972) 43.

7. CONCLUSIONS

7.1 Summary

The synthesis and doping of diamond films, characteristics of diamond surface, and formation and properties of metal-diamond interfaces have been investigated. The high quality diamond films have been grown on both HPHT synthesis diamond and Si substrates from carbon monoxide by using μ-wave plasma CVD. In deposited diamond, doping has been performed as growth proceeds by using B_2H_6 for p-type dopant and $(CH_3O)_3P$ for n-type dopant, respectively. The B doping of diamond could realize p-type conductivity with low resistivity of 7.26 Ohm.cm and high mobility of 451 cm/Vsec at room temperature in the case of the homoepiaxial (100) film. On the other hand, P-doped diamond films showed the high resistivity of ~10^7 Ohm.cm. Ion implantation has been attempted as a means of forcing the desired impurities, such as B and P, into the diamond. The author has developed a hydrogen plasma treatment instead of commonly used thermal annealing method in order to anneal out the implantation damage. The n-type doping, however, could not be succeeded in this work. Concerning impurity diffusion process, the author has found that hydrogen plasma can enhance oxygen diffusion in diamond despite the extremely low diffusivity of most elements in diamond.

The surface of as-grown CVD diamond formed from CO has been shown to be hydrogen-terminated and there were no surface states in the band gap. Insulating diamond film, which is important for fabrication of diamond-based electronic devices, has found to be obtained by cooling in an oxygen ambient after deposition. Although the graphitization of the as-grown CVD diamond surface was induced by heating at 900°C in a low vacuum (~10^{-7} Torr), it could be restrained by the CrO_3 surface treatment. Studies on metal-diamond interfaces have shown that there is the difference in reaction between the CVD diamond surface with Au, Ti and Ni. It was found that Ti is the most available element for the stable ohmic electrode due to the formation of a stable TiC_x layer. It has been shown that the interfacial properties depend on the electronegativity of the contact metal and the surface oxidation

treatments change the interfacial properties from ohmic to Schottky. The Schottky property with high breakdown voltage ~200V was obtained in the case for Al contact. Additionally, the electroluminescence in the blue spectrum region has been obtained at metal-diamond interfaces.

With these results, the author believes that a metal-semiconductor field-effect transistor (MESFET) and a metal-insulator-semiconductor field-effect transistor (MISFET) can be realized on boron-doped p-type diamond films as high power and high temperature devices. The most interesting application for diamond, however, seems to be a cold cathode device because of the recent successes of SiC power devices and GaN blue LED. The lack of n-type donor has to be overcome before realization of diamond cold cathode. After all, the difficulty in n-type doping hinders development of diamond devices.

7.1.1 Summaries in detail

The detailed results obtained in this work are summarized as follows.

Chapter 2.

Homoepitaxial diamond films grown from CO by using μ-wave plasma CVD have been characterized. The (100) 2 x 1 surface was smooth, whereas the (111) surface was rough with triangular microstructures. The growth rate on the (111) substrate was about one order of magnitude greater than that on the (100) substrate.

The resistivity, Hall mobility and corresponding B activation energy measured for the B-doped (100) film were 7.26 Ohm.cm, 451 cm/Vsec and 0.38 eV at RT, respectively. The transverse magnetoresistance has been observed to be 0.2 at 5 Tesla at RT. The P-doped CVD diamond films have grown on Si substrate by using $(CH_3O)_3P$ as a dopant. These films showed the high resistivity of ~10^7 Ohm.cm at RT.

Chapter 3.

The surface of as-grown CVD diamond formed from CO has been shown to be

hydrogen-terminated and there were no surface states in the band gap. The diamond films cooled slowly until room temperature in the 10^{-3} Torr range after deposition showed relatively low resistances in the range of 10^{6}~10^{7} Ohm. The electron energy loss spectroscopy study showed that the surfaces of these films seem to contain a small amount of a-C:H and/or a-C phase, which may act as a electrically active p-type dopant in the surface layers. On the other hand, high resistances over 10^{13} Ohm were obtained for the films after cooling in an oxygen or an air ambient at atmospheric pressure.

The characteristics and dynamics of CVD diamond surfaces have been studied. The graphitization of the as-grown CVD diamond surface is induced by heating at 900°C in a low vacuum (~10^{-7} Torr), while such graphitization can be restrained by the CrO_3 treatment which chemisorb oxygen and chromium atoms onto the diamond surface as a complex to form stable states.

Chapter 4.

The formation of Au-, Ti- and Ni-diamond films interfaces have been studied. It has found that there is no chemical reaction at the Au-diamond interface even at 850°C, and that the Au atoms rapidly migrate on the surface. The stable TiC_x can be formed at the Ti-diamond interfaces immediately at RT. After Ni deposition on as-grown CVD diamond at RT, the electronic structure of specimen surface changes to carbidic and graphitic phases because of the solvent and catalytic nature of Ni. After annealing at 500°C the specimen surface is completely graphitized and, at 900°C Ni atoms diffuse into the diamond film; most of Ni atoms exist at the grain boundaries while only a few of them diffuse into diamond particles.

The interfacial property of evaporated Al contact to the diamond film formed with CO/H_2 grown on Si substrate showed a high breakdown voltage (200 V) and a high rectification ratio (10^{5}). The values are much better than those obtained by CH_4/H_2. At the point contact interfaces, metal-carbon reaction does not occur and the property of these interfaces depends on metals, especially on their electronegativity. The author has investigated the effects of oxidation of the surface of CVD diamond films on the electrical characteristics of Schottky

diodes. The I-V characteristics obtained from CVD diamond films without oxygen on their surfaces depend on the metals, especially their electronegativities, but when oxygen is adsorbed onto the diamond surfaces, this dependence vanishes.

Electroluminescence due to the Schottky diode can be obtained at metal-diamond interfaces in the boron-doped polycrystalline diamond. The EL spectra almost coincide with those of CL.

Chapter 5.

The effect of thermal annealing and hydrogen plasma treatment of CVD diamond layers implanted with 10-keV N ions to 10^{15} /cm^2 have been characterized using EELS, SIMS and CL. The damaged layers produced by the implantation are subjected to significant graphitization during conventional thermal annealing even for low dose implantations (>10^{15} /cm^2). In contrast, after exposure to a hydrogen plasma, the damaged layers of CVD diamond can be at least partially removed without leaving any graphitic phase in the specimen, and furthermore, material containing a large concentration of implanted N atoms can be obtained.

Homoepitaxial diamond films exhibited a substantial difference in electrical properties compared to HPHT synthesized diamond after B and P implantations followed by thermal annealing. The resistance and Ea observed for the homoepitaxial diamond films were much higher than those for the HPHT synthesized diamonds, indicating a better resistance against radiation damage. The hydrogen plasma treatment produced lower resistance in B-implanted homoepitaxial films compared to the thermal annealing. Moreover, the activation energy of ~0.35 eV, which is near the energy expected for the substitutional B acceptor in diamond, was observed for the (100) films after B implantation followed by hydrogen plasma treatment. The P-implanted diamond films followed by thermal annealing and hydrogen plasma treatment were highly electrically resistive, with resistance of over 10^{13} Ohm.

Chapter 6.

It is found that hydrogen can enhance oxygen diffusion into diamond. Oxygen can

easily be introduced into both the CVD diamond and HPHT synthesized diamond by a CrO_3 treatment followed by an exposure to a hydrogen plasma at high temperature. The resultant depth distribution of the doped oxygen atoms is homogeneous and the concentration is typically about 10^{20} atoms/cm^3. The doped oxygen atoms can produce new cathodoluminescence centers giving two luminescence peaks at 3.75 and 4.64 eV.

7.2 Direction of Future Work

An application of diamond for semiconductor devices will not be realized before the successes of heteroepitaxy and n-type doping of diamond. Recently a clue to diamond heteroepitaxy on Si or SiC has been found. However, n-type doping of diamond have never been succeeded despite much efforts. The future research, therefore, should aim to develop wide gap nitrides, such as AlN, high Al mole fraction of AlGaN and cubic BN (cBN) films because of their possibility of achieving n-type doping. The wide gap pn junction will be realized by the heterostructures between p-type diamond and n-type nitrides, AIN, AlGaN or cBN. Additionally, the lattice constant of cBN is close to that of diamond, so that the diamond heteroepitaxy can be realized on cBN films. It is, however, extremely difficult to grow cBN in large single-crystal form. On the other hand, it is relatively easy to obtain single-crystalline AlN films on Al_2O_3. Accordingly, single crystalline pn junction might be achieved by a multi-heterostructures of Al_2O_3 - AlN - $B_xAl_{1-x}N$ - cBN - diamond, if the $B_xAl_{1-x}N$ alloys could be available.

Since the recent successes of SiC power devices and GaN blue LED, the most interesting application left for diamond seems to be a cold cathode device. Flat panel, full-color, high-resolution display technology will benefit considerably from diamond electron emitter. Success of the heterostructures between diamond and wide gap nitrides will realize a high efficient cold cathode device. Additionally, these pn heterojunctions can be used as a superior high-temperature operating and high power electronic devices compared with those made of SiC.

LIST OF PUBLICATIONS

(1) **Y.Mori**, H.Yagi, M.Deguchi, H.Makita, H.Yagyu, T.Okada, N.Eimori, M.Kitabatake, K.Nishimura, T.Ito, T.Hirao, T.Sasaki and A.Hiraki, "Electrical Properties of Phosphorous-Implanted Homoepitaxial Diamond Films", Trans. Mater. Res. Soc.**14B** 1567-1569 (1994).

(2) **Y.Mori**, H.Yagi, M.Deguchi, T.Sogi, Y.Yokota, N.Eimori, H.Yagyu, H.Ohnishi, M.Kitabatake, K.Nishimura, A.Hatta, T.Ito, T.Hirao, T.Sasaki and A.Hiraki, "Characterization of Homoepitaxial Diamond Films Grown from Carbon Monoxide", Jpn. J. Appl. Phys. **32** 4661-4668 (1993).

(3) **Y.Mori**, Y.Show, H.Yagi, M.Deguchi, N.Eimori, H.Yagyu, M.Kitabatake, A.Hatta, T.Ito, T.Izumi, T.Hirao, T.Sasaki and A.Hiraki, "Characterization of Surface Conductive Layers Formed on Diamond Films Grown by Microwave Plasma CVD", Jpn. J. Appl. Phys. **32** L987-989 (1993).

(4) **Y.Mori**, T.Okada, M.Deguchi, N.Eimori, M.Kitabatake, K.Nishimura, A.Hatta, T.Ito, T.Hirao, T.Sasaki and A.Hiraki, "Electrical Properties of Boron-Implanted Homoepitaxial Diamond Film", Jpn. J. Appl. Phys. **32** L601-603 (1993).

(5) **Y.Mori**, F.Sivazlian, H.Yagi, Y.Show, M.Deguchi, N.Eimori, H.Yagyu, T.Okada, M.Kitabatake, A.Hatta, T.Ito, T.Izumi, T.Hirao, T.Sasaki and A.Hiraki, "Characterization of Surface Conductive Layers of Diamond Films", Proc. 3rd Int. Symp. Diamond Materials. 706-712 (1993).

(6) **Y.Mori**, H.Yagi, M.Deguchi, M.Kitabatake, K.Nishimura, A.Hatta, T.Ito,

T.Hirao, T.Sasaki and A.Hiraki, "Crystallinities and Electrical properties of Homoepitaxial Diamond Films Grown from Carbon Monoxide", Proc. 2nd Int. Conf. Appl. of Diamond Films and Related Materials. p.393-398 (1993).

(7) **Y.Mori**, N.Eimori, A.Hatta, T.Ito, and A.Hiraki, "Effect of Ambient on the Surface Resistance of Diamond Films during Cooling after Deposition", Jpn. J. Appl. Phys. **31** L1718-1720 (1993).

(8) **Y.Mori**, M.Deguchi, N.Eimori, J.S.Ma, A.Hatta, M.Kitabatake, K.Nishimura, T.Ito, T.Hirao and A.Hiraki, "Radiation Damage and Electrical Properties of Ion Implanted CVD Diamond", Diamond and Related Materials. **2** 634-639 (1993).

(9) **Y.Mori**, M.Deguchi, N.Eimori, J.S.Ma, M.Kitabatake, K.Nishimura, T.Ito, T.Hirao and A.Hiraki, "Effect of Hydrogen Plasma Treatment on Implantation Damage in Diamond Films Grown by CVD", Jpn. J. Appl. Phys. **31** L1191-1194 (1993).

(10) **Y.Mori**, M.Deguchi, M.Kitabatake, H.Yagi, A.Hatta, T.Ito, T.Hirao and A.Hiraki, "Ion-Induced Fabrication of High-Quality Diamond Particles on Various Substrates", Proc. SPIE. **1759** 18 (1992).

(11) **Y.Mori**, N.Eimori, J.S.Ma, T.Ito, and A.Hiraki, "Characterization of Metal/CVD Diamond Interface Formation", Appl. Surf. Sci. **60-61** 296-300 (1992).

(12) **Y.Mori**, N.Eimori, H.Kozuka, Y.Yokota, J.Moon, J.S.Ma, T.Ito, and A.Hiraki, "Oxygen Diffusion into Diamond Induced by Hydrogen Microwave Plasma", Appl. Phys. Lett. **60** 47-49 (1992).

(13) **Y.Mori**, Y.Yokota, J.S.Ma, H.Kawarada, T.Ito and A.Hiraki, "Recent Studies of Semiconducting CVD Diamond Films", Diamond Films and Technology. **1** 93-107 (1992).

(14) **Y.Mori**, N.Eimori, J.S.Ma, T.Ito and A.Hiraki, "Surface Characteristics of Synthesized Diamond and the Effect of Surface Treatment on Surface Transformations", Appl. Surf. Sci. **56-58** 89-93 (1992).

(15) **Y.Mori**, H.Kawarada and A.Hiraki, "Properties of Metal/Diamond Interfaces and Effects of Oxygen Adsorbed onto Diamond Surface", Appl. Phys. Lett. **58** 940-941 (1991).

(16) **Y.Mori**, H.Kawarada and A.Hiraki, "Properties of CVD Diamond/Metal Interface", Proc. Material Research Society. **162** 353-358 (1990).

(17) K.Bekku, **Y.Mori**, N.Eimori, H.Makita, A.Hatta, T.Ito, T.Hirao, T.Sasaki and A.Hiraki, "Growth and Characterization of CVD Diamond Films Doped with Phosphorous", Proc. 4th Int. Conf. New Diamond Science & Technology. 701-704 (1994).

(18) N.Eimori, **Y.Mori**, J.Moon, A.Hatta, J.S.Ma, T.Ito and A.Hiraki, "Nickel/CVD Diamond Interface Studied by Electron Energy Loss Spectroscopy", Diamond and Related Materials. **2** 537-541 (1993).

(19) H.Kawarada, Y.Yokota, **Y.Mori**, K.Nishimura and A.Hiraki, "Cathodoluminescence and Electroluminescence of Undoped and Boron-doped Diamond Formed with Plasma CVD", J. Appl. Phys. **67** 983-989 (1990).

PRESENTATIONS AT INTERNATIONAL CONFERENCE

(1) "CVD Diamond Films Doped with Phosphorous, Nitrogen and Boron", 2nd Korea-Japan Workshop on Diamond Thin Film Growth Technology, Pohang-Korea, Aug. 1994. **(Oral presentation)**

(2) "Ion Implantation to Diamond with Hydrogen Treatment", 10th Int. Conf. Ion Implantation Technology, Catania-Italy, June 1994. **(Oral presentation)**

(3) "Interfacial Reaction of Various Metal/CVD Diamond Systems", 1st Int. Symp. Control of Semiconductor Interface, Karuizawa-Japan, Nov. 1993. **(Oral presentation)**

(4) "Electrical Properties of Phosphorous-Implanted Homoepitaxial Diamond Films", 3rd IUMRS Int. Conf. Advanced Materials, Tokyo-Japan, Sept. 1993. **(Oral presentation)**

(5) "Crystallinities and Electrical properties of Homoepitaxial Diamond Films Grown from Carbon Monoxide", 2nd Int. Conf. Appl. of Diamond Films and Related Materials, Saitama-Japan, Aug. 1993. (Poster session)

(6) "Characterization of Surface Conductive Layers of Diamond Films", 3rd Int. Symp. Diamond Materials, Honolulu-U.S.A., May 1993. (Poster session)

(7) "Radiation Damage and Electrical Properties of Ion Implanted CVD Diamond", Diamond 1992, Heidelberg-Germany, Sept. 1992. **(Oral presentation)**

(8) "Ion-Induced Fabrication of High-Quality Diamond Particles on Various Substrates", Diamond Optics V, San Diego-U.S.A., July 1992. **(Oral presentation)**

(9) "Characterization of Metal/CVD Diamond Interface Formation", 1st. Int. Conf. Atomically Controlled Surface and Interface, Tokyo-Japan, Nov. 1991. **(Oral presentation)**

(10) "Surface Characteristics of Synthesized Diamond and the Effect of Surface Treatment on Surface Transformations", 3rd. Int. Conf. Formation of Semiconductor Interfaces, Rome-Italy, May 1991. (Poster session)

(11) "Properties of CVD Diamond/Metal Interface", Material Research Society Meeting, Boston-U.S.A., Nov. 1989. **(Oral presentation)**